MODELING INFRARED AND COMBINATION INFRARED-MICROWAVE HEATING OF FOODS IN AN OVEN

A Dissertation

Presented to the Faculty of the Graduate School

of Cornell University

in Partial Fulfillment of the Requirements for the Degree of

Doctor of Philosophy

by

Marialuci Frangipani Almeida

January 2005

MODELING INFRARED AND COMBINATION INFRARED-MICROWAVE HEATING OF FOODS IN AN OVEN

Marialuci Frangipani Almeida, Ph.D.

Cornell University 2005

A quantitative, model-based understanding of heat exchange in infrared and combined infrared-microwave heating of food inside an oven is developed. The research is divided into three parts: measurement of optical properties, radiative heat transfer analysis and combined microwave-radiative heat transfer analysis. Optical properties of reflectance, absorptance and transmittance in a potato tissue are measured as a function of wavelength, using a spectroradiometer. Penetration of energy is higher for halogen lamps that emit in the near- and mid-infrared range, compared to ceramic rods that emit mostly in the far infrared range. Reflectance in the near infrared range increases with moisture content of the food, thus decreasing the energy coupled. Surface structure has significant influence on the optical properties. A 3-D radiative heat exchange model of an oven-food system is developed using a commercial finite-element package. The air in the oven is assumed transparent to the radiation. Heat conduction is assumed in the entire oven (food and air) for the short duration. The wavelength dependence of emissivity (non-gray surface)

is found to significantly affect the surface radiative flux and the use of a non-gray model is recommended for such materials, although simplification of the emissivity variation is required to keep the computation time reasonable. Lowering food surface emissivity reduces the radiative flux that is absorbed by the food surface. Reducing oven wall emissivities increase the radiative flux on the food surface. The location of the radiative heat source in the oven as well as placement of the food relative to the heat source were found to have significant influence on the radiative heat flux over the food surface. To add microwave heating, Maxwell's equations of electromagnetics were solved for the same cavity using separate finite element software and the volumetric heat generation, in the food, obtained from this model was input to the radiative heat transfer model, thus coupling them. Using measures such as mean temperature rise and the standard deviation of temperatures, it was demonstrated that combination heating leads to more uniform heating, without compromising the speed of heating.

BIOGRAPHICAL SKETCH

The author was born in São Paulo, Brazil. In 1982, she was admitted to UNICAMP, the State University of São Paulo, Campinas campus. She earned her Bachelor's and Master's degrees in 1987 and 1999, respectively, both from the Department of Food Engineering, at UNICAMP. She had experiences in the meat, spices and food service industry while still in Brazil. In December of 1998, she received a fellowship from the United States Department of Agriculture to pursue her Ph.D. in the subject of Food Engineering, at Cornell University. She joined the field of Food Science and Technology in September 1999, having Professor Ashim K. Datta, as her advisor. In March of 2003, she began to work in the Bunge Oil Center of Excellence as a Senior Innovation Research Scientist while continuing to work on her dissertation.

To my love, partner and friend, Cesar, for your wonderful presence in my life

To George, Louise and Thomas, for your purest smiles

To my beloved father, in memoriam, and mother, for your superb lessons of dedication

ACKNOWLEDGEMENTS

I would like to express my sincere gratitude to Professor Ashim K. Datta. For the past few years, he taught me technical knowledge, showed me the way of scientific thinking, helped me in life and gave me important instructions on career. I would also like to thank Professor Kenneth E. Torrance. His time, patience and encouragement are greatly appreciated. My sincere gratitude also goes to Professor William L. Olbricht, for his questioning and input.

I want to express special thanks to Professor Kenneth E. Torrance and all the Rhodes Hall staff for the access to the Light Instrumentation Laboratory, at Cornell University. Professors Dennis Miller and Joseph Hotchkiss showed their support on my study, life and career. Finally I would like to thank my friends Srikanth Geedipalli (also co-author in my last chapter), Valeria Acquarone, Natalia dos Santos, Jifeng Zhang, and Seung-Hwan Lee, as well as the departmental staff from the Riley-Robb and Stocking Halls for their help and friendship.

Table of Contents

1 GENERAL INTRODUCTION **1**
- 1.1 Outline . . . 1
- 1.2 Motivation . . . 2
- 1.3 Thesis Objectives . . . 6

2 MEASUREMENT OF OPTICAL PROPERTIES OF FOODS IN NEAR AND MID-INFRARED RADIATION **7**
- 2.1 Introduction . . . 7
- 2.2 Definition of Terms . . . 11
- 2.3 Objectives . . . 14
- 2.4 Methodology . . . 14
  - 2.4.1 Spectroradiometer . . . 16
  - 2.4.2 Measurement Process . . . 19
  - 2.4.3 Sample Preparation . . . 20
  - 2.4.4 Calculation of Penetration Depth . . . 24
- 2.5 Results and Discussion . . . 25
  - 2.5.1 Detector Sensitivity: Signal to Noise Ratio in the 0.85-1.15 μm Range . . . 25
  - 2.5.2 Effect of the Source of Radiation (Ceramic Rod and Halogen Lamp) . . . 26
  - 2.5.3 Variation of Spectral Reflectance with Moisture Content . . . 27
  - 2.5.4 Spectral Variation of Penetration Depth with Moisture Content 28
  - 2.5.5 Penetration Depth for Near-Infrared Heating and Microwave Heating Compared . . . 30
- 2.6 Conclusions . . . 32

3 RADIATIVE HEAT TRANSPORT MODELING INSIDE AN OVEN: PROBLEM FORMULATION AND EXPERIMENTAL SETUP **34**
- 3.1 Introduction . . . 37
- 3.2 Objectives . . . 40

3.3 Problem Formulation 41
3.3.1 Assumptions for the Enclosure Model 42
3.3.2 Radiative Heat Transfer Equation 42
3.3.3 Governing Equations and Boundary Conditions for Heat Conduction 45
3.4 Methodology 49
3.4.1 Numerical Solution 49
3.4.2 The Macro-surface Concept for Radiation Calculations . . . 49
3.4.3 Numerical Implementation of the Radiative Exchange in an Enclosure 51
3.4.4 Solution Parameters 53
3.4.5 Input Parameters 54
3.4.6 Cycling Boundary Condition for Infrared Source 57
3.4.7 Surface Convection Coefficient 63
3.4.8 Temperature Measurements 68
3.4.9 Heat Flux Measurements 70

4 RADIATIVE HEAT TRANSPORT MODELING INSIDE AN OVEN: Effect of Oven and Food Parameters 74
4.1 Introduction 74
4.2 Objectives 78
4.3 Problem Schematic, Solution and Input Parameters 78
4.4 Results and Discussion 82
4.4.1 Mesh Convergence 82
4.4.2 Gray versus Non-gray Behavior of Food Surfaces 87
4.4.3 Comparison with Experiments 89
4.4.4 Global Energy Balance in the Oven 96
4.4.5 Effect of Different Infrared Power Levels 98
4.4.6 Effect of Different Food Emissivities 99
4.4.7 Effect of Different Wall Surface Emissivities 100
4.4.8 Effect of Different Food Positions 102
4.4.9 Effect of Changing Lamp Positions 102
4.5 Conclusions 105

5 COMBINED MICROWAVE AND INFRARED HEATING OF FOODS IN AN OVEN 107
5.1 Introduction 111
5.2 Literature Studies Modeling of Combination Microwave and Infrared Heating 112
5.3 Objectives 113

5.4 Problem Formulation 113
5.4.1 Governing Equations, Boundary Conditions and Input Parameters for Microwave Heating 115
5.4.2 Governing Equations, Boundary Conditions and Input Parameters for Infrared Heat Exchange 120
5.4.3 Governing Equations, Boundary Conditions and Input Parameters for Conduction Heating in the Food 127
5.5 Methodology 129
5.5.1 Numerical Solution of the Electromagnetics and Heat Transfer Equations 129
5.5.2 Coupling of Electromagnetics and Heat Transfer Simulations 130
5.5.3 Experimental Set-up 131
5.6 Results 133
5.6.1 Experimental Results 133
5.6.2 Experimental Validation of Model 133
5.6.3 Uniformity of Infrared, Microwave and Combination Heating, Described Using Contour Plots 134
5.6.4 Statistical Analysis of the Uniformity of the Three Modes of Heating 139
5.6.5 Effect of Different Microwave Power Levels on the Uniformity of Combination Heating 145
5.6.6 Manipulation of Surface Heating Using Combination Heating 148
5.7 Conclusions 149

6 CONCLUSIONS **151**

A **155**

Bibliography **161**

List of Tables

3.1 Input Parameters 56
3.2 Parameter Values Used in Calculating Heat Transfer Coefficient, h_c 66
3.3 Nusselt numbers and heat transfer coefficients calculated using Eq. 3.16 67

5.1 Input Parameters 125
5.2 Non-uniformity in Temperature Distribution 144
5.3 Non-uniformity in Temperature Distribution 147
5.4 Non-uniformity in Temperature Distribution 148
5.5 Non-uniformity in Temperature Distribution 150

A.1 Results from least square approximations: Penetration Depth (mm), T_0 and R^2 - 82 and 77% moisture content samples 156
A.2 Results from least square approximations: Penetration Depth (mm), T_0 and R^2- 72 and 70% moisture content samples 157
A.3 Results from least square approximations: Penetration Depth (mm), T_0 and R^2- 67% moisture content samples 158

List of Figures

2.1 Direct transmitted fraction concept 13
2.2 Diffuse reflectance and transmittance measurement system layout (Top view) [20]. 16
2.3 An schematic view of the integrating sphere attachment to the spectroradiometer [20]. 17
2.4 Spectral emissive power (W/(m.m^2)). 18
2.5 Spectral reflectance (Re) and spectral transmittance (T(s)) with $s =$ 1 cm or $s = 3$ cm, with near-infrared source. 21
2.6 Variation of spectral reflectance with potato samples of different heat treatments and raw samples. 21
2.7 Pictures of (a) raw potato sample, (b) same potato sample after 10 minutes of cooking in boiling water and (c) an enlargement (three times) of detail in (b). Pictures taken with Metallurgical microscope, Model ML-MET (Meiji Labax Co. Ltd, Tokyo, Japan). 23
2.8 Variation in the reflectance measurement due to the two sources (ceramic rod and halogen lamp) for potato of high moisture content ($83 \pm 2\%$). The error bars show the range from one source to the other and the mean values are denoted by the triangle. 26
2.9 Variation of spectral reflectance in potato tissue of 1 cm thickness at moisture content levels of $83 \pm 2\%, 52 \pm 2\%$ and $31 \pm 2\%$. 27
2.10 Transmitted energy, *T(s)*, at $s = 1$ cm in the 0.7 - 2.5 μm range. . 29
2.11 Spectral variation of penetration depth of potato tissue at various moisture contents in near-infrared heating. 30
2.12 Spectral variation of coefficient T_0 with moisture content, in near-infrared heating. 31
2.13 Spectral absorptance in near-infared heating, calculated using Equation 2.2. 32

3.1 Schematic of the radiation dominant problem. The geometry of the oven is rectangular, of size 0.470 m × 0.356 m × 0.215 m. The food inside the oven is a potato slab of geometry 0.0470 m × 0.0356 m × 0.0215 m that has a volume of 3.6 $\times 10^{-5}$ m^3. Food is placed at 2.5 cm above the geometric center of the oven's bottom surface, resting on a quartz glass tray, parallel to the 0.470 m × 0.356 m oven surface. 43
3.2 Radiative exchange in a gray diffuse enclosure and the principle of a surface energy balance. 47
3.3 Spectral absorptance of potatoes in the near and mid-infrared range. See Section 2.5.4. 48
3.4 Schematic showing a) the bottom face of the lamp glass cover and thermocouple positions, A-E, and b) lamp case, showing the halogen bulb and the lamp glass cover. 50
3.5 Mesh used in the model, with 50000 hexahedral elements for the oven system, including the 360 hexahedral elements for the food volume. 59
3.6 Temperature measured at the center position below the top lamp surface (Figure 3.4) during one minute heating for three different infrared setting levels (Levels I, V and X) in the Advantium ^{TM} oven. 60
3.7 Temperature measured at center position below the top lamp surface (Figure 3.4) during one minute heating for three different infrared oven setting levels in the Advantium^{TM} oven - levels I, V and X. Only level I was used to find the right parameters of the heat source time function in the model. 61
3.8 Effect of parameters t_{max}, (a) and c, (b), on the shape of time function for source boundary condition - in the limit of $c \rightarrow \infty$ the function approximates the decay of a step function. 62
3.9 Time function used in the model for different level settings in the oven, I, V and X. The value for parameter c was kept as 0.5, but t_{max} had values of 0.06981, 0.04761 and 0.03704 respectively for oven infrared settings levels I, V and X. 64
3.10 Approximate trends in convection transients for various scenarios. . 69
3.11 Temperature probes location over the top food surface and general experimental set-up. 72
3.12 Schematic of heat flux data acquisition set up, using FLUKE Data acquisition Bucket^{TM}, Fluke Co., Washington, U.S. 73

4.1 Schematic of the radiation dominant problem. The geometry of the oven is rectangular, of size 0.470 m × 0.356 m × 0.215 m. The food inside the oven is a potato slab of geometry 0.0470 m × 0.0356 m × 0.0215 m that has a volume of 3.6 $\times 10^{-5} m^3$. Food is placed at 2.54 cm above the geometric center of the bottom surface oven, resting on a quartz tray parallel to the 0.470 m × 0.356 m oven's surface. . 81
4.2 Mesh used in the model with 50000 hexahedral elements. 83
4.3 Computation time as a function of number of elements in mesh. . 84
4.4 Temperatures calculated at the center node of food element (Figure 4.1) for different mesh sizes. 85
4.5 Cross-section of mesh showing the region around food geometry. Food volume meshed with 360 hexahedral elements. 86
4.6 Surface temperature contour plots obtained for 10,000 W/m^2 energy output from the source, with input properties as shown in Table 3.1, and different mesh densities. 88
4.7 Computed temperature at the center node on the top food surface (Figure 3.11) during one minute heating for gray ($\epsilon = 0.67$ up to 1.3 and 0.96 above 1.3) and non-gray assumptions ($\epsilon = 0.88$) of food surface. 91
4.8 Experimental temperatures at the center of top food surface (see Section 3.4.8) for heating at three different intensity levels (I, V and X) of the Advantium^{TM} oven. 92
4.9 Computed and experimental results for level I intensity of the halogen lamp, at the center of top food surface (Figure 4.1), using top lamp only: a) radiative flux and b) temperature profiles. 93
4.10 Temperature at the center of glass lamp cover (Figure 3.4) for level I, using top lamp only. 94
4.11 Computed and experimental results for level V intensity of the halogen lamp, at the center of top food surface (Figure 4.1), using top lamp only: a) radiative flux and b) temperature profiles. 95
4.12 Computed and experimental results for level X intensity of the halogen lamp, at the center of top food surface (Figure 4.1), using top lamp only: a) radiative flux and b) temperature profiles. 97
4.13 Computed radiative flux, (a), and temperature, (b), at the center of top food surface (Figure 4.1) for level X, using top lamp only - changing food emissivities. 101
4.14 Computed radiative flux, (a), and temperature, (b), at the center of top food surface (Figure 4.1) for level X, using top lamp only - changing wall emissivities. 103

4.15 Computed radiative flux, (a), and temperature, (b), at the center of top food surface (Figure 4.1) for level X, using top lamp only - changing food position. 104
4.16 Temperature contour plots for the food, heated by central and skewed top lamp positions, showing the variation on heating pattern for the lateral food surface. 106

5.1 Schematic of the combination heating oven that includes microwave plus infrared (halogen) heating. The geometry of the oven is rectangular, of size 0.470 m × 0.356 m × 0.215 m. The food inside the oven is a potato slab of geometry 0.0470 m × 0.0356 m × 0.0215 m, with a total volume of 0.00003 m^3. Food is placed at 2.5 cm above the geometric center of the bottom surface in the oven. 116
5.2 Radiative exchange in a gray diffuse enclosure and the principle of a surface energy balance, used in the infrared model. 123
5.3 Spectral absorptance of potato used in the computation of infrared heating (see Section 2.5.4). 126
5.4 Finite element mesh used in the computation of infrared heating, with 50000 hexahedral elements for the oven system, (a); Finite element mesh used in the computation of electromagnetic field in the entire oven tetrahedral elements with 110000 nodes (b). 128
5.5 Flow chart showing the coupling of the electromagnetic and the heat transfer (including the infrared radiation) model. 132
5.6 Cycling of infrared and different microwave power levels as used in this model. 135
5.7 Schematic of data acquisition set up (temperature and flux) and probes location over the top food surface. 136
5.8 Experimentally measured temperatures at the top food surface for a) infrared only heating, b) microwave only heating , and c) combined infrared-microwave heating. Level I, intensity and power level, was used for both infrared and microwave. 137
5.9 Temperature profile at the top central food surface (Figure 5.7) for a) infrared only, oven setting Level I heating, b) microwave only, power level 1 heating and c) combined microwave-infrared heating. 138
5.10 Computed temperature profiles showing the food surface for a) infrared oven setting Level I only, b) microwave power level 1 only and c) combined microwave power level 1 and infrared level I heating. . 140
5.11 Computed surface temperature contours, a-f, for combined microwave and infrared heating for level I at 7, 16.5, 33, 40, 47.5 and 60 seconds of heating, respectively. 143

5.12 Computed temperature profiles, showing the 90^{th} and 10^{th} percentiles, for a) infrared only intensity level I, b) microwave only, power level 1 and c) combined microwave-infrared heating. 146

A.1 Energy transmitted for various sample thicknesses of potato at 82 +/- 2% moisture content. Lines are fitted through data points. . . 155
A.2 Energy transmitted for various sample thicknesses of potato at 77 +/- 2% moisture content. Lines are fitted through data points. . . 159
A.3 Energy transmitted for various sample thicknesses of potato at 72 +/- 2% moisture content. Lines are fitted through data points. . . 159
A.4 Energy transmitted for various sample thicknesses of potato at 70 +/- 2% moisture content. Lines are fitted through data points. . . 160
A.5 Energy transmitted for various sample thicknesses of potato at 67 +/- 2% moisture content. Lines are fitted through data points. . . 160

Chapter 1

GENERAL INTRODUCTION

1.1 Outline

This thesis addresses the general problem of cooking food by electromagnetic waves in an oven. The heating can be either by thermal radiation from radiant heaters in the roof of the oven, or by microwaves generated by a microwave generator in the oven. The two modes of heating can be separate or simultaneous.

The thesis is organized into three separate, but related, studies. Each study is written as an individual research paper, with its own introduction, problem description, results section, and discussion.

In the first study, entitled "Measurement of Optical Properties of Foods in Near and Mid-Infrared Radiation", included as chapter 2, optical properties of reflectance, absorptance and transmittance in a potato tissue are measured as a function of wavelength, using a spectroradiometer.

Second study, "Radiative Heat Transport Modeling Inside an Oven: Problem Formulation and Experimental Set-up", included as chapter 3, develops a 3-D radiative heat exchange model of an oven-food system, using a commercial finite-element package. The air in the oven is assumed transparent to the radiation. Heat conduction is assumed in the entire oven (food and air) for the short duration.

It is followed by the third study, 'Radiative Heat Transport Modeling Inside an Oven: Effect of Oven and Food Parameters", included as chapter 4, where results for the model are shown. Wavelength dependence of emissivity (non-gray surface), food surface and oven wall emissivities effects are described.

Last study, "Combined Microwave and Infrared Heating of Foods in an Oven", included as chapter 5, was a joint effort with Srikanth S. Reddy Geedipalli. I was able to provide the experimental work and radiative model (using FIDAP software) for the chapter while Mr. Geedipalli worked on the electromagnetic model using ANSYS commercial software. We both worked on coupling both software for the results. This study is also part of Mr. Geedipalli's M.S. thesis. In this study, Maxwell's equations of electromagnetics were solved for the same cavity using separate finite element software and the volumetric heat generation in the food, obtained from this model, was input to the radiative heat transfer model, thus coupling them.

1.2 Motivation

As new appliances are being developed constantly to satisfy the need for easier food preparation with improved quality and increased energy efficiency, new heating

modes have been investigated. The use of infrared heating in domestic ovens is old and comes back and forth according to the availability and pricing of the electrical energy compared with gas in different countries.

The enhancement of new appliances for food preparation with efficiency and better food quality with less time has demanded that the scientific society put a focus to study in a fundamental level the new heating methods that the appliance industry invented or developed. The overall quality of prepared foods depends on the different modes of heat exchange because of the dissimilar internal and surface properties of foods, resulting in different rates of crust formation and color development, among others. These properties vary as a function of convective or radiative heating. This was experimentally investigated by [7] and [32].

The change of evaporation rate with these two heating modes - convective and radiative heating - was also investigated experimentally by [22] and [31]. The food surface texture in baking under convective heating and infrared heating was investigated by [34]. Almost all of these studies report the same trend of more intense and rapid changing in food characteristics with infrared heating. Dagerskog and Sorenfors, 1978 [7] observed almost half the time necessary to reach the same center temperature in beef patties compared to convection and contact heating. Shibukawa et al., 1989 [32] found out that the surface temperature was 10 % higher for radiation than convection processes in cookie baking. The exception is for the evaporation rate that showed to be 5% less (Sato,H. et al., 1987 [31]) for the infrared heated food, due to the earlier crust formation.

The innovation of using an infrared heating element in the same cavity as of

the microwave heating generator dates back from 1970 [18] and have been developed since then. The main purpose of using infrared heating back there was to assist microwave heating in terms of reaching a more homogeneous temperature distribution on the target food and drying up the accumulated moisture due to the pressure driven moisture flow, hence, developing the desired color at the food surface [24]. Recently, though, new halogen lamps have being introduced in the appliances market as a heat source comparable to microwave due to its penetrability properties, with the advantage of having a very homogeneous distribution. Some combination ovens, having the microwave as well the infrared heating elements are already available in the national market as well in Europe [30][11] [17]. Due to the lack of knowledge on near-infrared heating of foods, the most part of this research is going to focus in understanding this phenomenon. Afterwards, the application of these findings on a combination heating mode with microwave heating is going to be addressed.

Other science fields as computer graphics, microelectronics and the paper and wood industries have tried modeling infrared radiation. Although infrared heating is a well established science based on the radiation equation, general solutions are hardly obtainable due to the complexity of its equations. Therefore, most of the publications on the infrared heating of foods are still empirical and experimental [28]. The enclosure solution has been developed in channels by Franca et al.[12], 3-D furnaces [1], and often in its 2-D and 1-D mode [28], [27]. The radiant thermal model is not common in the context of heating foods inside an oven. Infrared heating in terms of total flux at food surface is not found in the literature. The

approach of gray surfaces is usual on the engineering field because it can give us rough information on the actual heating that is going on the objects of study. But the availability of optical properties varying with wavelength compelled us to study the radiation equation in a non-gray analysis for the food, which seams rightly appropriate since the emissions from infrared sources varies in a large spectrum from 700 nm to 2500 nm, comprehending the near, medium and far infrared.

For the modeling of the surface heat flux of a food placed inside an oven, the use of the radiation equation [21] [33] is essential and some adjustment was performed in order to yield a more suitable equation for the numerical analysis. For the equations, see Section 3.3.2. Because of its non-linear nature and the fourth power dependence with temperature we can expect an unusual magnitude of the heat flux emitted by the infrared sources, requiring a deep study for its quantification and prediction.

The optical properties of the food being heated, on the other hand, are essential for the quantification of the right amount of infrared energy being absorbed at the food surface and transmitted therefore inwards, in the food medium. Of significant importance is the emissivity property as it is directly input in the radiation flux equation. Its dependence with wavelength will assure us the best infrared source to be used for the heating of various foods. The goal is to be able to get the radiation flux variation that reaches the food surface with different sources of infrared. To date, analysis of radiative heat transfer in foods has not included non-gray food surfaces.

The radiation modeling will enable us to handle oven modifications regarding source and food placement, and cycling time, as well as other oven configurations.

Using the numerical method, the influence of these changes in the amount of heat the food surface is receiving may be predicted and should lead to a more efficient and controllable heating equipment.

The last chapter of this dissertation, "Combined Microwave and Infrared Heating of Foods in an Oven", chapter 5, was done in collaboration with Srikanth S. Reddy Geedipalli.

1.3 Thesis Objectives

1. To measure optical properties in potato tissue in the near-infrared range of 0.7 - 2.5 μm (chapter 2).

2. To develop a comprehensive study of infrared heating of foods for the non-gray situation. The goal is to obtain better quantitative understanding of the infrared heating process that should improve the heating performance (chapters 3 and 4) .

3. To predict the temperature distribution in the food for combined infrared - microwave heating by coupling electromagnetic model with infrared. The electromagnetic model itself was developed by a fellow graduate student (chapter 5).

4. To validate the numerical simulation results through an experimental set up, using fiber optical probes for the temperature measurement (chapters 3, 4 and 5).

Chapter 2

MEASUREMENT OF OPTICAL PROPERTIES OF FOODS IN NEAR AND MID-INFRARED RADIATION

2.1 Introduction

As new appliances are being developed constantly to satisfy the need for easier food preparation with improved quality and increased energy efficiency, new heating modes have been investigated. The use of infrared heating in domestic ovens is old and comes back and forth according to the availability and pricing of the electrical energy compared with gas in different countries.

The quality of prepared foods depends on different modes of heat exchange because of the different surface properties of foods. The crust formation and color development as function of convective or radiative heating was experimentally investigated by [7] and [32]. The change of evaporation rate with these two heating modes was also investigated experimentally by [22] and [31]. The food surface texture in baking under convective heating and infrared heating was investigated by [34]. All of these studies report the same trend of more intense and rapid changing in food characteristics with infrared heating.

The innovation of using an infrared heating element in the same cavity as of the microwave heating dates back from 1970 [18] and has been developed since them. The main purpose of using infrared heating back there was to aid the microwave heating in terms of a better homogeneous heating and the development of color at the food surface, hence, drying up the accumulated moisture due to the pressure driven moisture flow [24]. Recently, though, the halogen lamp has being introduced in appliances as a heat source comparable to microwave due to its increased penetration into the food. Some combination ovens, having the microwave as well the infrared heating elements are already available [30] [11] [17].

Due to the lack of knowledge on near-infrared heating of foods, most part of this research is going to focus in understand this phenomenon of volumetric heating. Afterwards, the application of these findings on a combination heating mode with microwave heating is going to be addressed.

Study of radiative heat transfer properties in food dates back to 1969 [13] and it is one of the most comprehensive works in application of infra-red radiation in

food processing. In his work,[13] there are some citation of spectral transmittance and reflectance data. It assumes a variation of properties with thickness but there is no consideration of moisture content of the samples taken.

Experimental data by Il'yasov and Krasinov [16] illustrates the influence of product nature and thickness on the spectral properties of a series of foodstuffs, determined at 1.1 μm wavelength. Their data, unfortunately, show a deviation from the energy balance, i.e, the well-known relation:

$$1 = \rho + \alpha + \tau \tag{2.1}$$

where ρ stands for reflectance, α stands for absorptance and τ, for transmittance.

This deviation is attributed to the technical difficulties encountered in measuring radiative properties in foodstuffs [5].

In the study of Dagerskog and Osterstrom [6], a good attempt was made to understand the nature of the attenuation of the infrared radiation in different food media. They used pork, potato and bread. No mention was made to moisture content of the samples, though. They suggested some scattering effects as in Ginzburg [13], for the explanation of reflectance dependence with thickness.

A more comprehensive work was done in the field of paper and pulp industry, by Ojala and Lampinen [27]. They used a FT-IR spectrometer (Fourier Transform - Infrared Spectrometer) and only performed measurements on samples taken out of the drying process. It is clear in their work the dependence of optical properties with wavelength and moisture content in the case of paper. Paper reflectance would decrease with adding water to increase moisture content in the paper samples. They

also presented the dependence of the properties on the basis weight (g/m^2) of paper. The scattering of the radiation in paper was more discussed in the work of Pettersson et al. [29]. They presented a theoretical model based on a layer-structured system to explain the infrared attenuation, assuming paper as a homogeneous material.

Aside from the food and paper industry, the interest is big in the area of material sciences for new ceramic materials, used mainly in energy applications (automobile, space vehicles and jet engines). The use of reticulated porous ceramics (RPC)- a membrane constructed in a manner to form a network - in those systems has draw attention to the need of known attenuation and scattering coefficients when exposed to radiation. There is an interesting illustration of the dependence of radiative properties and material porosity in the work of Hendricks and Howell [15]. In their work, they found out that transmittance in RPC decreases with increased porosity (pore sizes decreased).

In none of these works though we can find a comprehensive study of radiative properties spectral dependence when reducing moisture content (as in drying or baking processes).

The highly porous and open structure of foods, mostly filled with water, creates complex electromagnetic scattering and interference patterns within the structure, which tremendously complicates radiative modeling in these materials.

The work done by Hendricks and Howell [15] suggests a novel radiative modeling technique that effectively treats this complex radiative interaction by quantifying the direct transmittance fraction and incorporating it into a discrete ordinates formulation to predict experimental reflectance and transmittance behavior, in small

reticulated porous ceramics test samples.

This is the approach that is used in this research, since potato tissue - the food chosen in this investigation (more about the reason for this choice under the Methodolgy section, page 14)- can be simplified by a matrix of starch granules spherical in shape (averaging size 80 μm diameter)- although in reality they are ellipsoidal [36]- immersed in water.

Radiative properties are going to be taken with variation on water content inside the potato matrix. This is an issue never addressed in the literature. A recent work of Junqueira and Lage [19] addressed the influence of different fluids inside a matrix of RPCs. Because their primordial interest was the attenuation of laser into different matrix, they did not vary water content in the matrix. But from their work it is very clear that the attenuation of a matrix filled with water does not compare with the dried matrix, i.e., it is not an additive phenomenon since we can expect some physical-chemical interaction of the water with the solid matrix resulting in unexpected attenuation results.

2.2 Definition of Terms

Hemispherical Absorptance (α) It is the fraction of incident radiation upon a surface that is converted to some other forms of energy (kinetics, thermal, etc.). It is calculated as:

$$\alpha_\lambda = (1 - T_{0,\lambda})(1 - \rho) = 1 - \rho + T_{0,\lambda}(\rho - 1) \tag{2.2}$$

where $T_{0,\lambda}$ is defined following the definition of direct transmittance (see Equation 2.3).

Hemispherical Reflectance (ρ) It is the fraction of incident radiation upon a surface that reflects back from its original path. Can include scattered back reflection.

Hemispherical Transmittance It is the fraction of incident radiation that crosses the material at distance s from surface, after absorption and scattering phenomena took place inside the material.

Scattering It is a mechanism that redirects the radiant energy from its original direction of propagation due to a combination effect of reflection, refraction and diffraction.

Direct Transmittance It is the fraction of incident radiation that directly crosses the porous material without absorption or scattering effects (attenuation). Defined in the case of reticulated (constructed in such a manner as to form a material network) porous ceramics [15]. The direct transmittance factor is a two-dimensional property of any given porous material, and is a different property than the material porosity (a 3-D property). It is the 2-D alignment of the porous structure which determines T(s), and materials of similar porosities can have many different 2-D alignments.

As can be seen in Figure 2.1, the quantity *1-(R+T)* is then the fraction of radiative intensity that interacts with the starch structure through normal

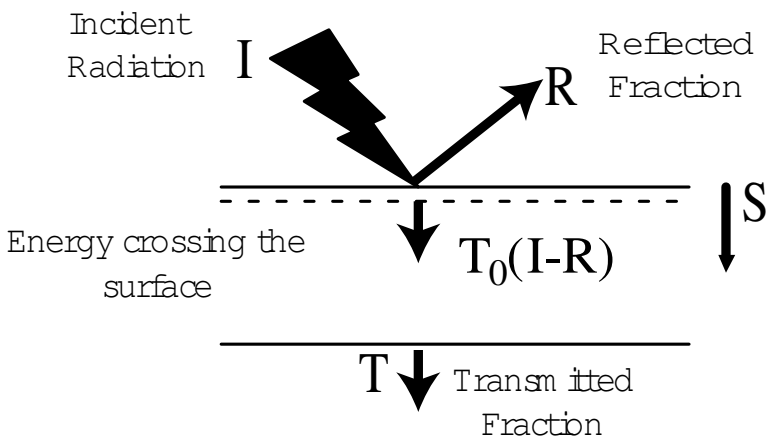

Figure 2.1: Direct transmitted fraction concept

absorption and scattering processes. Through the experimental measurements mentioned previously, it was found that this fraction obeys an exponential relationship:

$$\frac{T(s)}{T_{0,\lambda}(I-R)} = \exp(s * -\delta_\lambda) \tag{2.3}$$

where $T_{0,\lambda}$ and δ_λ are experimentally derived direct transmittance coefficients for the particular food in study (potato, in this case). Worth noticing is that Equation 2.3 is based on the same exponential decay as proved by Beer-Lambert's law for absorption of light in an aqueous medium.

Penetration Depth It is the distance from surface into a material that propagates electromagnetic energy, where the incident radiation decays approximately 37% (i.e., $1/e$ of its surface value). The penetration depth parameter is taken

as $1/\delta_\lambda$ (Equation 2.3) and it is preferred in this study for means of comparison with microwave penetration depth. Penetration depth parameter has units of distance.

2.3 Objectives

The specific objectives of this study are to:

1. Measure reflectance and transmittance of electromagnetic radiation in potato tissue in the near-infrared range of 0.7 - 2.5 μm.

2. Measure the dependence of reflectance and transmittance on the moisture content and thickness of potato tissue.

3. Determine the penetration depth of near infrared radiation in potato tissue.

2.4 Methodology

Spectral hemispherical reflectance and transmittance measurements were obtained using a computer - automated Model 740 dual-source spectroradiometer system from Optronic Laboratories, Inc., Orlando, Fl. This system created unidirectional, monochromatic incident radiation (1.2 mm beam diameter) impinging on flat, 2.5 cm diameter disk samples of varying thickness. Incident radiation was centered on the disk axis and directed approximately along the disk axis (10^0 off-normal angle

per system design specifications). Test samples external boundaries were kept non-reflective. All measurements were taken at room temperature as this research and experimental set-up were not designated to study temperature dependent effects.

Measurement uncertainties in reflectance and transmittance were $\pm$ 10 %. This was determined by measuring repeatability on a variety of samples and using different spectroradiometer configurations in overlapping wavelength bands.

Potato was the chosen food material in this research due to its easy availability and sample preparation. Potato is also common food item throughout the world. However, we had to deal with the enzymatic darkening that occurs in potato tissues when exposed to oxygen.

Raw potato being a material with very high moisture content ($>$ 85%), and because the radiative properties for water are well understood [37], we limited our investigation to the 0.7 to 2.5 μm range, beyond which, water shows almost a constant and high value absorptivity.

Before any study on spectral properties and moisture content dependence could be carried out, we had to eliminate the other variables that could affect the results somehow. The sample thickness and heat treatment had to be set out so that we could see properties variation with moisture content alone. The heat treatment was also used in samples undergoing drying, so to avoid any enzymatic darkening of the potato tissue.

2.4.1 Spectroradiometer

The spectroradiometer used in this research - OL 740 Optronic Laboratories, Inc. system (Figure 2.2) - comprises of a Visible-IR Dual Source Attachment - Model 740-20 D/IR; a monochromator - model 750 -M-S ; integrating sphere model 740-70 (Figure 2.3) and, detectors with head and module: DH-300- Silicon Detector Head with Detector Support Module AC current mode - DSM-1A and PbS Detector Head - DH - 340 with Detector Support Module - Voltage mode - DSM-2. This equipment resides in the Light Measurement Laboratory at the Computer Graphics Department, Cornell University. The two detectors vary in their utility range with the Silicon detector being used in the near-infrared range and the PbS detector used in the medium-infrared range (refer to Figure 2.4, for detector's range definition).

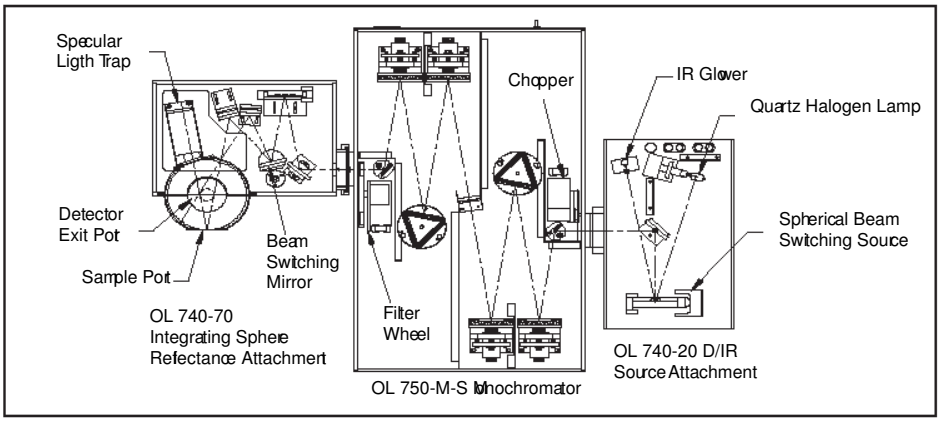

Figure 2.2: Diffuse reflectance and transmittance measurement system layout (Top view) [20].

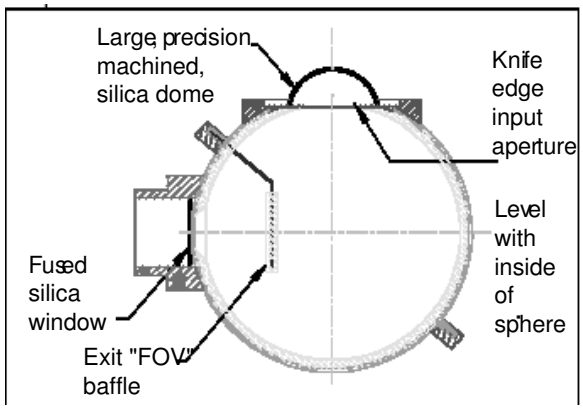

Figure 2.3: An schematic view of the integrating sphere attachment to the spectro-radiometer [20].

Thermal Infrared Sources

The ceramic rod was the most used infrared heating element until 1984 when the halogen lamp gained attention by the appliance industry. The difference between these two types of heating elements is mainly in the emitted infrared radiation. Ceramic rods have their maximum emissive power of the order of 10^{10}W/(m.m^2), around the wavelength of 2.34 μm (2340 nm), at 1293 K . Halogen lamps, on the order hand, have their maximum emissive power of the order of 10^{11}W/(m.m^2), in the wavelength of 1.3 μm (1300 nm), at 2212 K. This maximum emissive power being one order of magnitude higher than that for the ceramic rods.

Some part of halogen lamps emissive power is still in the visible light range; that is why the near-infrared (halogen) heating mode is sometimes referred by appliance

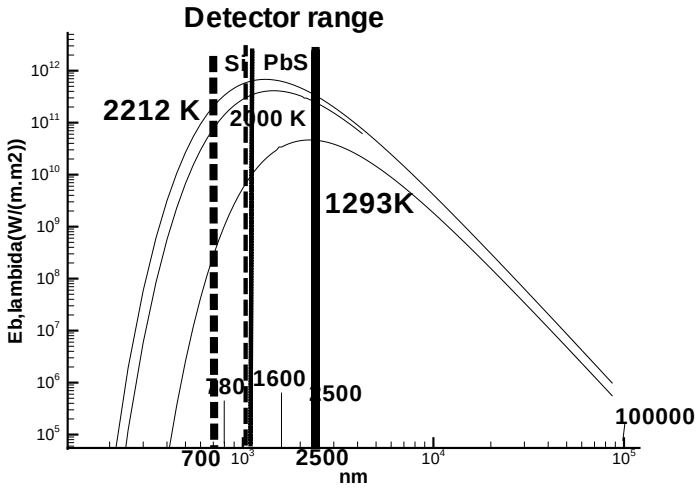

Figure 2.4: Spectral emissive power (W/(m.m^2)).

manufactures as "light" heat.

Ceramic rods vary in their ceramic composition but usually are a metal rod with a ceramic cover. They don't require any special building assembly and in this sense are easier to manufacture than the halogen lamps.

Halogen lamps (also called tungsten lamps, quartz lamps or incandescent lamps) are a complex system comprised by the tungsten filament - the one that is usually incandescent - involved by one kind of halogen gas - usually the iodine - all in a fused quartz enclosure.

The halogen compound included inside the quartz envelope combines with the tungsten evaporated from the hot filament. This forms a compound that is electrically attracted back to the tungsten filament. The return of the tungsten to the filament means that the incandescent lamp can be run with a long life at a higher

filament temperature and, more importantly, remain at precisely the same color temperature. But this also requires an intricate refrigeration system on the back of the lamp so to avoid higher temperatures that could damage the filament.

The OL 740-20 Source Attachment is designed specifically for use with OL spectroradiometer as the stable irradiance source required for detector spectral response, reflectance and transmittance measurements. It consists of a source module with all-mirror imaging optics and mounts to the entrance port of the OL Series Monochromator. The OL 740 - 20D/IR is a dual source unit, which incorporates both a 150 W quartz-halogen lamp and an infrared ceramic glower. A precision manual beam switching mirror selects which source is to be utilized for a particular wavelength region. The 150-watt quartz halogen lamp is a compact DZE type lamp that is utilized in the 0.25 to 3.5 μm range while the ceramic rod glower is more suitable for the 2.5 to 10 μm range, following manufacturer recommendations.

2.4.2 Measurement Process

Reflectance measurements were done through a comparison method using a calibrated sample of known reflectance in a different port; to complete one measurement the equipment first scans the comparison port and then scans the sample port. It took twice as much time to complete a reflectance measurement compared to a transmittance measurement. The latter, in its turn, required one calibration scan with an empty transmittance port - 100 % calibration - and then the samples would be scanned and given a percentage of transmittance compared to the calibration one. The actual value for transmittance reported in this research corresponds to

T(s) as described earlier (Figure 2.1).

To verify the isotropic assumption for the potato media, measurements were made with potato samples of 1 cm thickness . This was accomplished rotating the sample in the sample holder for three different positions with respect to the initial position: a quart position - obtained rotating the sample clockwise in a 90^0 angle and a half position - obtained rotating the sample clockwise in a 180^0 angle. No significant difference in the measurements was noticed.

2.4.3 Sample Preparation

Sample Thickness and Heat Treatments

Preliminary measurements were made with samples at two different thicknesses of 1 and 3 cm and diameter of 2.5 $\pm$ 0.2 cm. The purpose of those measurements were to verify if reflectance would vary with thickness. Reflectance had very good agreement and little variation between the two thicknesses (Figure 2.5). The increased variation, specially at the very low wavelengths, is due to the lower limit of the detector.

To obtain the effect of moisture content, samples were dried after being boiled in water to avoid the enzymatic darkening that can occur from exposure to oxygen. To make sure that properties were not affected by the two different boiling processes of 5 and 10 minutes under microwave heat, these results were compared with those of raw potato (Figure 2.6). The measurement was done under the halogen source irradiation. When not stated, sample thickness of 1 cm was used.

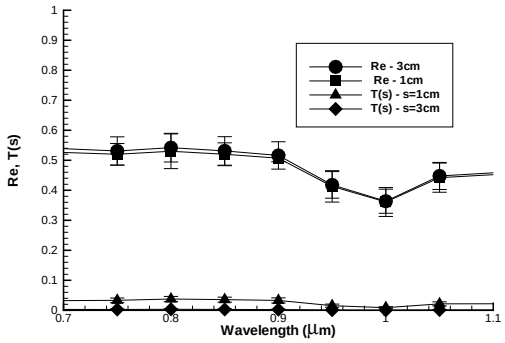

Figure 2.5: Spectral reflectance (Re) and spectral transmittance (T(s)) with $s = 1$ cm or $s = 3$ cm, with near-infrared source.

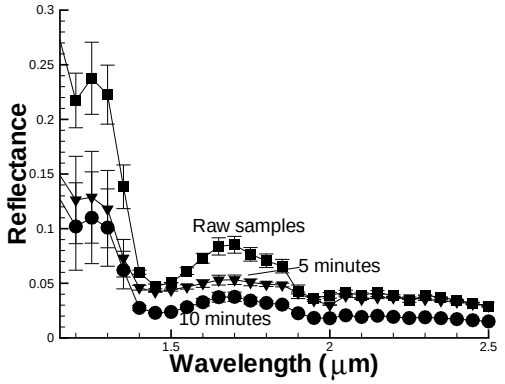

Figure 2.6: Variation of spectral reflectance with potato samples of different heat treatments and raw samples.

The biggest variation in profile occurred comparing raw sample measurements with the cooked samples measurement. In between the two different heat time exposures there was no significant variation in profile. The results in Figure 2.6 can be explained because of different starch gelatinization stages in the potato tissue, as can be seen in Figures 2.7 a-c.

Slicing

Potato disk samples were cut from raw potatoes, 2.5 ± 0.2 cm in diameter and 1.0 ± 0.2 cm thickness (s). For the purpose of penetration depth measurements, thin slices were taken out of the thicker samples with the use of a micrometer blade. Due to the difficulty in getting thin samples - 0.2mm thick - samples were cut within an expected range and then had their thickness measured using a digital caliper (Fowler Ultra Cal Mark III, Fred. V, Fowler Co, Inc.). The reported thickness, *s*, for those samples was averaged between three different angles along the sample diameter.

Drying and Bleaching

Whenever samples had to be dried using high velocity air, heat treatment was given to the samples placed in water - 10 minutes, 100^0C under microwave heating. Samples that had to undergo this kind of heat treatment would be referred as cooked samples from now on in this text. For high moisture content samples, they were left to equilibrate at room temperature of 21^0C. Reduced moisture samples were prepared from previous cooked samples and dried using high velocity air at

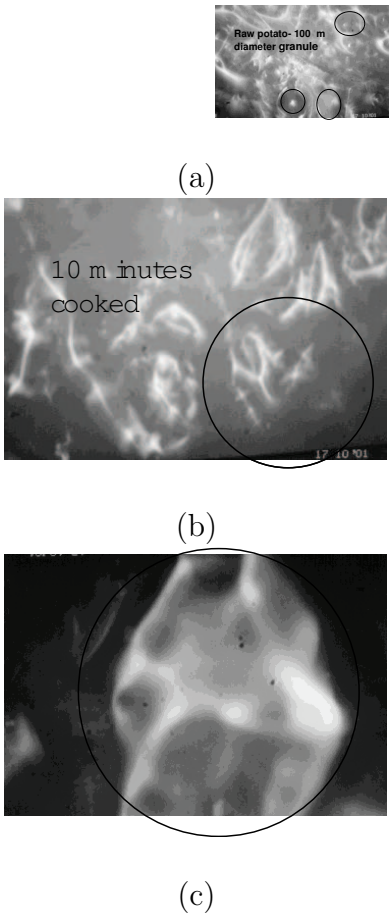

Figure 2.7: Pictures of (a) raw potato sample, (b) same potato sample after 10 minutes of cooking in boiling water and (c) an enlargement (three times) of detail in (b). Pictures taken with Metallurgical microscope, Model ML-MET (Meiji Labax Co. Ltd, Tokyo, Japan).

approximately 75^0C at different times. The thinner samples were held between two metal screens during this process.

Moisture Content Measurement

Samples were left to equilibrate at room temperature in a container with silica gel and then their weight was measured before and after each optical property determination. Gravimetric method was used to determine moisture content by keeping the samples for 24 hours at 60^0C in an oven (Blue Line, Blue M Electric Co. - model OV 18 SA).

2.4.4 Calculation of Penetration Depth

As stated before (Section 2.2), penetration depth coefficients were calculated from the exponential fitting (Equation 2.3) of transmittance data at different sample thickness for each wavelength band in the range. The exponential curves and subsequent R^2 values for moisture contents of 82, 77, 72, 70 and 67 % can be found in the Appendix A. See more about this calculation on Section 2.5.4, "Spectral Variation of Penetration Depth with Moisture Content".

2.5 Results and Discussion

2.5.1 Detector Sensitivity: Signal to Noise Ratio in the 0.85-1.15 μm Range

To validate the results using both detectors Silicon and PbS, in the 0.85-1.15 μm range, measurements of the 100% signal - i.e, no material in the transmittance port of the integrating sphere - and 100% noise - i.e, no sources on - were taken in the equipment.

Integrating devices generally fall into two categories: transmissive diffusers and reflective diffusers. Transmissive devices, commonly referred to as "cosine diffusers", rely on scattering materials and shape to give their cosine response. However, scattering is strongly dependent on the wavelength of light so the bluer wavelengths are scattered more strongly than redder wavelengths. This leads to the generally observed strong wavelength dependence of cosine response for such devices [20]. By manufacturer recommendation, the range between 0.25 to 2.5 μm was chosen to match both the integrating sphere and the detector attachment to the spectroradiometer.

Nevertheless, we investigated signal/noise ratio for both detectors in this wavelength range. For the PbS detector, signal/noise ratio is of the order of 1, in this wavelength range. Therefore, the PbS detector was not used in this range. A signal/noise ratio of more than 5 orders of magnitude was seen for the Si detector which was used instead.

2.5.2 Effect of the Source of Radiation (Ceramic Rod and Halogen Lamp)

To observe any effect of the source of radiation within the same wavelength range (1.1 - 2.5 μm), reflectance measurements were taken on potato discs of 2.5 cm diameter, 1 cm thickness and, high moisture content ($83 \pm 2\%$). This is shown in Figure 2.8. Variation due to source, as seen in this figure, is a small fraction ($< 10\%$) of the measured reflectance in potato tissue (as shown in Figure 2.9 later) and, can be considered acceptable.

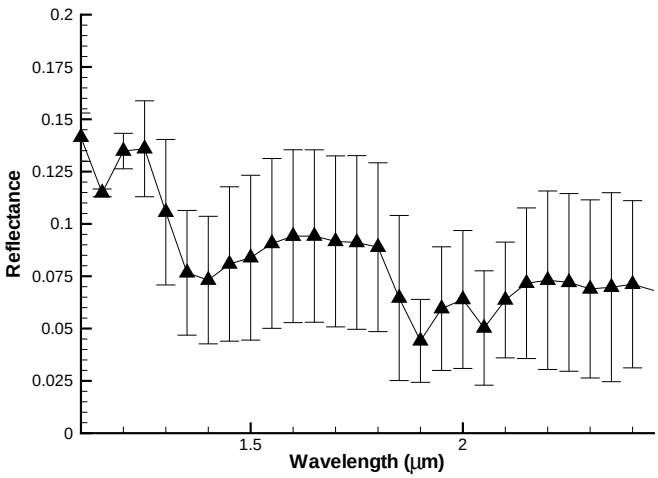

Figure 2.8: Variation in the reflectance measurement due to the two sources (ceramic rod and halogen lamp) for potato of high moisture content ($83 \pm 2\%$). The error bars show the range from one source to the other and the mean values are denoted by the triangle.

2.5.3 Variation of Spectral Reflectance with Moisture Content

Hemispherical reflectance in potato tissue at three levels of moisture content was obtained using the drying method described earlier (see Section 2.4.3). This is shown in Figure 2.9.

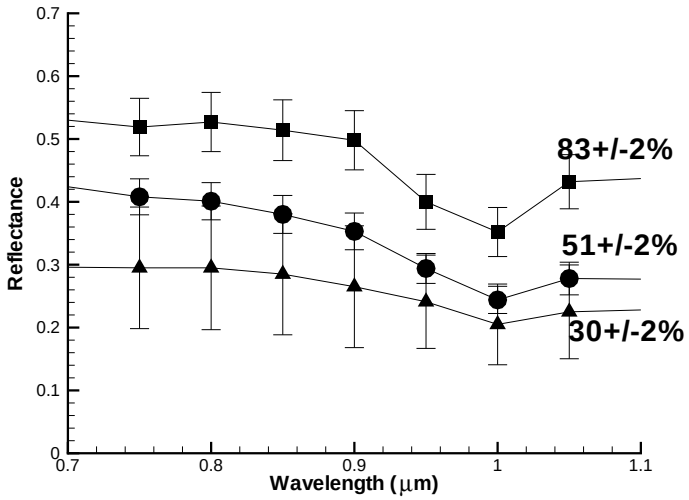

Figure 2.9: Variation of spectral reflectance in potato tissue of 1 cm thickness at moisture content levels of $83 \pm 2\%, 52 \pm 2\%$ and $31 \pm 2\%$.

These results can be explained by considering the change in the porous matrix of the potato tissue. The cellular pore that contain the starch are mainly sustained by a complex matrix of cellulose and water. With water being removed from this

matrix, a collapse is expected resulting in both smaller cellulose pore and starch granules, which results in less scattered energy at the surface. The change in color intensity of the dried samples is a good example of this phenomenon - from light yellow to deep yellow.

Dependence of spectral hemispherical transmittance on moisture content, on the other hand, can not be explained in the same way. Although we would expect more transmittance occurring with less water in the energy path, the collapse of pore right at the surface would change the matrix setting allowing for absorption to change at surface. This phenomenon is discussed in the results for penetration depth when the T_0 coefficient is determined (Figure 2.12).

2.5.4 Spectral Variation of Penetration Depth with Moisture Content

Figures A.1 through A.5 in Appendix A show energy transmitted, T, as a function of sample thickness, s, at different moisture content of the samples in the wavelength range of 0.7 - 1.1 μm, following Equation 1.3. This wavelength range was chosen due to the intense spectral dependence of transmittance at the 0.7 - 2.5 μm range (two orders of magnitudes at 1.4 μm), as can be seen from Figure 2.10.

By fitting exponentially the transmittance data for each moisture content, penetration depth is calculated (see Equation 2.3). The graphs with the least square approximations for moisture contents of 82, 77, 72, 70 and 67 % can be seen in Appendix A. Better results (R^2 above 0.85) came from higher moisture contents.

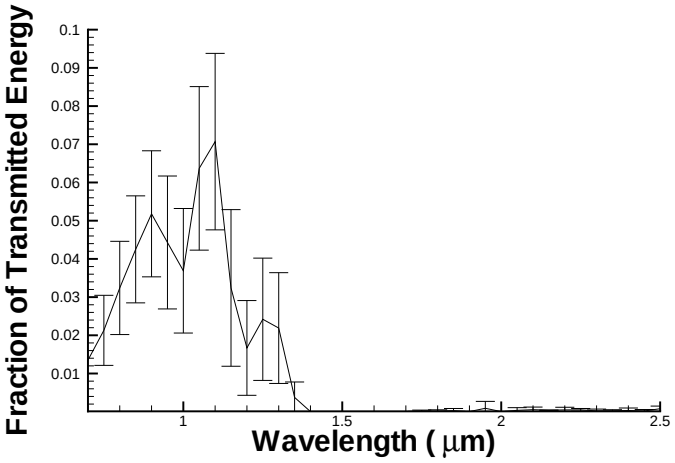

Figure 2.10: Transmitted energy, *T(s)*, at $s = 1$ cm in the 0.7 - 2.5 μm range.

Difficulty arises (R^2 around 0.80) with the lower moisture content samples, for longer wavelengths. Figure 2.11 shows the spectral variation of the penetration depth, $1/\delta$, with moisture content.

The coefficient T_0, in Equation 2.3 (Section 2.2), corresponds to the actual energy passing the interaction region at surface; penetration depth by itself can not tell us all about the amount of energy penetrating the medium. The variation of the spectral coefficient T_0 (Figure 2.12) with moisture content is a reflection of the two dimensionality aspect of this property. It reflects the change in the 2-D alignment of the starch matrix during drying. It is the radiation that passed through the structure at $s = 0$ (Figure 2.1).

Absorptance, in turn, is calculated as Equation 2.2. For effect of calculations in the radiative model (Chapter 3), Equation 2.2 will be used for values of absorptance

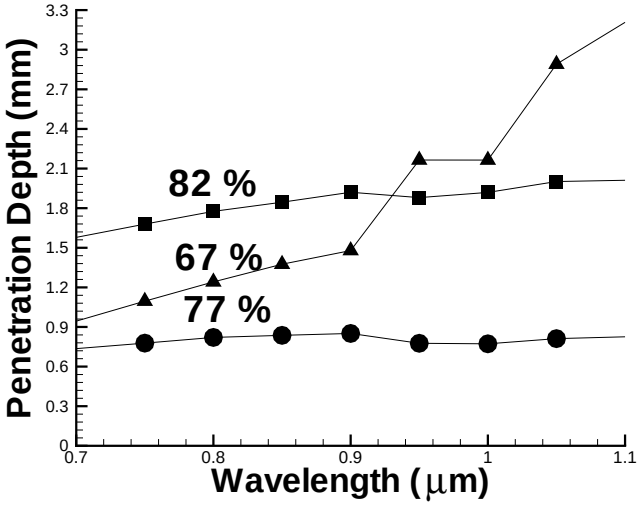

Figure 2.11: Spectral variation of penetration depth of potato tissue at various moisture contents in near-infrared heating.

in the 0.7 - 1.1 μm range. Besides that range, absorptance will be taken as $1 - \mathrm{Re}$, since transmittance values are very low at this range (Figure 2.10). Figure 3.3 shows absorptance values for the 0.7 - 2.5 μm range.

2.5.5 Penetration Depth for Near-Infrared Heating and Microwave Heating Compared

One of our goals in studying the infrared behavior at food surfaces is to be able to combine infrared with microwave in a judicious manner. Thus, it is useful to compare the penetration depth of microwave energy (defined in a similar way as Equation 2.3) with that of infrared energy observed in this study.

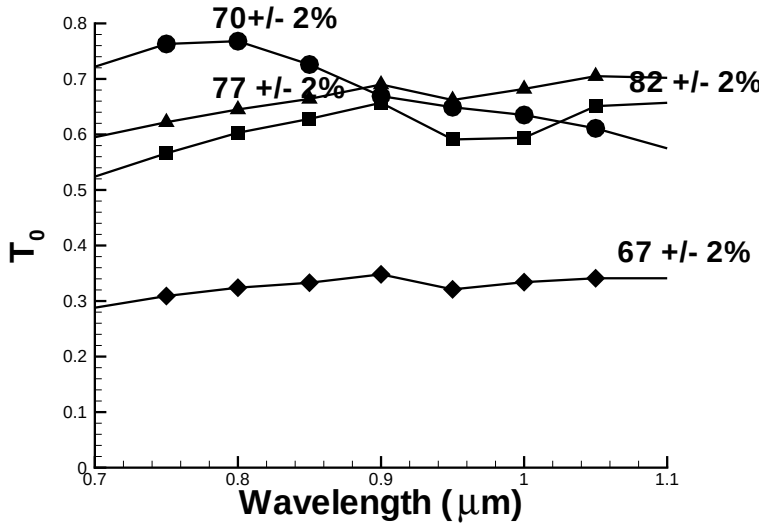

Figure 2.12: Spectral variation of coefficient T_0 with moisture content, in near-infrared heating.

We can find that penetration depths for raw potato are of the same order of magnitude, being 2 mm in the near-infrared heating (this work), 4.8 mm in [6] and 8.7 mm for the microwave heating at 2.45 GHz [23]. For potato with 67 % moisture content, penetration depth was of the order of 3.5 mm in this study. For ham, penetration depths reported are of 2.4 mm in near-infared heating [6] and 4.8 mm for microwave heating at 2.45GHz [39].

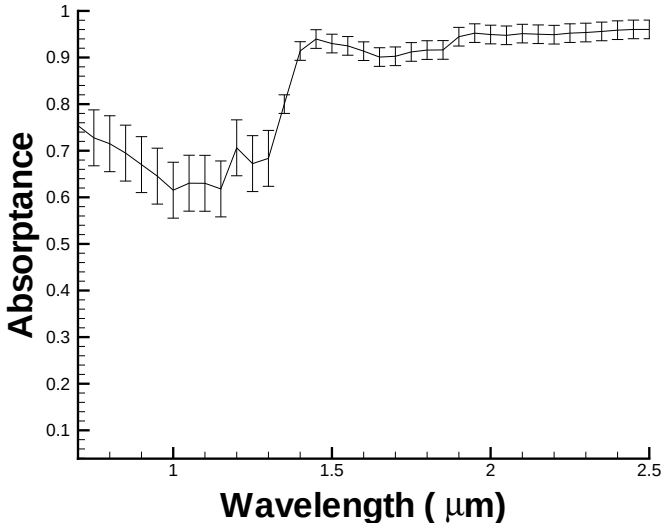

Figure 2.13: Spectral absorptance in near-infared heating, calculated using Equation 2.2.

2.6 Conclusions

1. Energy from halogen lamps, emitted in the near and mid-infrared range, has higher penetration depth and therefore heats more volumetrically, compared with energy from ceramic rods, that emit mostly in the far infrared range .

2. Reflectance in the near infrared range increases with moisture content, thus decreasing the energy coupled in the food.

3. Penetration depth of energy from halogen lamps is of the same order of magnitude as in microwave heating, although somewhat smaller. Penetration depth is also a strong function of moisture content and wavelength.

4. Surface structure of the food material has a significant effect on the radiation balance at the surface and this effect varies with moisture content.

Chapter 3

RADIATIVE HEAT TRANSPORT MODELING INSIDE AN OVEN: PROBLEM FORMULATION AND EXPERIMENTAL SETUP

List of Symbols

A_i	Area of surface i, m^2
c	Speed of light, 2.998 $\times 10^8$ m/s
$c_{i,k}$	Average shape function for element i

c_p	Specific heat, J/kg $\cdot$ K
c_2	14388 μm $\cdot$ K
dA	Differential of area
$dF_{dA_i - dA_j}$	Differential view factor
$E(\mathbf{r})$	Black body emissive power at point $\mathbf{r}$, W/m^2
$F_{A_i - A_j}$	View factor
F^*_λ	Band energy ratio
g	Acceleration of gravity , m/s^2
$G(\mathbf{r})$	Irradiation onto a surface, in terms of the position vector $\mathbf{r}$, W/m^2
Gr	Grashof number
h	Planck's constant, 6.626 $\times 10^{-34}$ Js
h_c	Convective heat transfer coefficient, W/m$^2 \cdot$ K
H	Height measurement, m
$J(\mathbf{r})$	Radiosity in terms of the position vector $\mathbf{r}$, W/m^2
k	Bolzmanns constant, 1.3806 $\times 10^{-23}$J/K
k_c	Thermal conductivity, W/m $\cdot$ K
Nu	Nusselt number
P_{ave}	Average perimeter of the thermal load, m
Pr	Prandtl number
q_c	Convective heat flux, W/m^2
q_r	Radiative heat flux, W/m^2
$\mathbf{r}$	Position vector
Ra	Raleigh number

S	Surface area, m^2
t	Time, s
T	Temperature, K or C
Z	Height measurement, m

Greek Letters

$\alpha(\mathbf{r})$	Absorptance of surface at point $\mathbf{r}$
β	Compressibility factor, K^{-1}
δ_{ij}	Kronecker delta
$\epsilon(\mathbf{r}\ )$	Emissivity in terms of the position vector $\mathbf{r}$
θ	Shape function
λ	Wavelength, m
λ^{th}	Referred to the "th" wavelength, m
ν	Kinematic viscosity, m^2/s
ξ	Square root of the surface area , m
ρ	Reflectance
ρ_0	Density, kg/m^3
σ	Stefan-Bolzmann's constant, $5.67 \times 10^{-8} W/m^2 \cdot K^4$
ϕ	Any given quantity
Φ	Numerical effective value

Subscripts

λ	At given wavelength, or per unit wavelength
∞	Ambience
s	Macro-surface
n	Number of elements
N	Number of element faces
k	Node of an element face
$nbands$	Number of wavelength bands
$load$	Related to a load
air	Surrounding air properties

3.1 Introduction

The enhancement of new appliances for food preparation with efficiency and better food quality with less time has demanded that the scientific society put a focus to study in a fundamental level the new heating methods that the appliance industry invented or developed. The overall quality of prepared foods depends on the different modes of heat exchange because of the dissimilar internal and surface properties of foods, resulting in different rates of crust formation and color development, among others. These properties vary as a function of convective or radiative heating. This was experimentally investigated by [7] and [32].

The change of evaporation rate with these two heating modes - convective and radiative heating - was also investigated experimentally by [22] and [31]. The food surface texture in baking under convective heating and infrared heating was inves-

tigated by [34]. Almost all of these studies report the same trend of more intense and rapid changing in food characteristics with infrared heating. Dagerskog and Sorenfors, 1978 [7] observed almost half the time necessary to reach the same center temperature in beef patties compared to convection and contact heating. Shibukawa et al., 1989 [32] found out that the surface temperature was 10 % higher for radiation than convection processes in cookie baking. The exception is for the evaporation rate that showed to be 5% less (Sato,H. et al., 1987 [31]) for the infrared heated food, due to the earlier crust formation.

The use of infrared heating in domestic ovens is old and comes back and forth according to the availability and pricing of the electrical energy compared with gas in different countries. The innovation of using an infrared heating element in the same cavity as of the microwave heating generator dates back from 1970 [18] and have been developed since then. The main purpose of using infrared heating back there was to assist microwave heating in terms of reaching a more homogeneous temperature distribution on the target food and drying up the accumulated moisture due to the pressure driven moisture flow, hence, developing the desired color at the food surface [24]. Recently, though, new halogen lamps have being introduced in the appliances market as a heat source comparable to microwave due to its penetrability properties, with the advantage of having a very homogeneous distribution. Some combination ovens, having the microwave as well the infrared heating elements are already available in the national market as well in Europe [30][11] [17].

Due to the lack of knowledge on near-infrared heating of foods, the most part of this research is going to focus in understanding this phenomenon. Afterwards,

the application of these findings on a combination heating mode with microwave heating is going to be addressed.

Other science fields as computer graphics, microelectronics and the paper and wood industries have tried modeling infrared radiation. Although infrared heating is a well established science based on the radiation equation, general solutions are hardly obtainable due to the complexity of its equations. Therefore, most of the publications on the infrared heating of foods are still empirical and experimental [28]. The enclosure solution has been developed in channels by Franca et al.[12], 3-D furnaces [1], and often in its 2-D and 1-D mode [28], [27].

The radiant thermal model is not common in the context of heating foods inside an oven. Infrared heating in terms of total flux at food surface is not found in the literature. The approach of gray surfaces is usual on the engineering field because it can give us rough information on the actual heating that is going on the objects of study. But the availability of optical properties varying with wavelength compelled us to study the radiation equation in a non-gray analysis for the food, which seams rightly appropriate since the emissions from infrared sources varies in a large spectrum from 700 nm to 2500 nm, comprehending the near, medium and far infrared.

For the modeling of the surface heat flux of a food placed inside an oven, the use of the radiation equation [21] [33] is essential and some adjustment was performed in order to yield a more suitable equation for the numerical analysis. For the equations, see Section 3.3.2. Because of its non-linear nature and the fourth power dependence with temperature we can expect an unusual magnitude of the heat flux emitted by

the infrared sources, requiring a deep study for its quantification and prediction.

The optical properties of the food being heated, on the other hand, are essential for the quantification of the right amount of infrared energy being absorbed at the food surface and transmitted therefore inwards, in the food medium. Of significant importance is the emissivity property as it is directly input in the radiation flux equation. Its dependence with wavelength will assure us the best infrared source to be used for the heating of various foods. The goal is to be able to get the radiation flux variation that reaches the food surface with different sources of infrared. To date, analysis of radiative heat transfer in foods has not included non-gray food surfaces.

The radiation modeling will enable us to handle oven modifications regarding source and food placement, and cycling time, as well as other oven configurations. Using the numerical method, the influence of these changes in the amount of heat the food surface is receiving may be predicted and should lead to a more efficient and controllable heating equipment.

3.2 Objectives

The present research develops a comprehensive study of infrared heating of foods for the non-gray situation. The goal is to obtain better quantitative understanding of the infrared heating process that should improve the heating performance. The specific objectives are:

1. The application of the radiative model to a 3-D cavity, with non-gray optical

properties of food and to predict the heat flux in a food surface for infrared heating. Use thermal heat flux sensors (HFS-3, Omega) and fiber optic probes to validate the numerical predictions;

2. To perform sensitivity analysis on the model for different food positions and different source locations and predict performance of different foods and oven internal wall emissivities.

3.3 Problem Formulation

The physical problem that will be considered is the radiative heat transfer inside an oven (a 3D enclosure) that has a halogen lamp at one or more of the inside surfaces and a food material placed somewhere inside the enclosure for the purpose of being heated (see Figure 3.1). The halogen lamp emits radiation in the near infrared range of wavelength and the food surface radiative properties can vary with wavelength. The lamp is cycled on-off. Heat flux over food and other surfaces is computed from numerically solving the radiative heat exchange equation. The surface heat flux from the lamp is used as a boundary condition. Temperatures are, then, computed in the food using the heat conduction equation. The effects of various heating parameters are then achieved through sensitivity analysis of the numerical model.

3.3.1 Assumptions for the Enclosure Model

The following are some of the major assumptions in developing the mathematical formulation:

1. All surfaces are diffuse , with no directional dependence: the small distance between surfaces and proportionality of oven surfaces and food validate this assumption;

2. Radiation dominant problem: the natural convection in the system is handled as surface convection;

3. Food is a solid conductive body inside the oven, but non transparent, i.e., opaque to thermal radiation.

3.3.2 Radiative Heat Transfer Equation

The radiative heat transfer equation is obtained by combining the radiative surface energy balance and Kirchoff's law, i.e, absorptance equals emssivity for zero transmittance. Writing it in terms of the position vector, $\mathbf{r}$, the total radiation incident on the surface, *irradiation* $\mathbf{G}$ and *radiosity* $\mathbf{J}$, becomes:

$$J(\mathbf{r}) = \epsilon(\mathbf{r})E(\mathbf{r}) + \rho(\mathbf{r})G(\mathbf{r}) \tag{3.1}$$

In Equation 3.1, $E(\mathbf{r})$ is the total blackbody emission at the point $\mathbf{r}$ provided the temperature is known. It is given by the Stefan-Boltzman law.

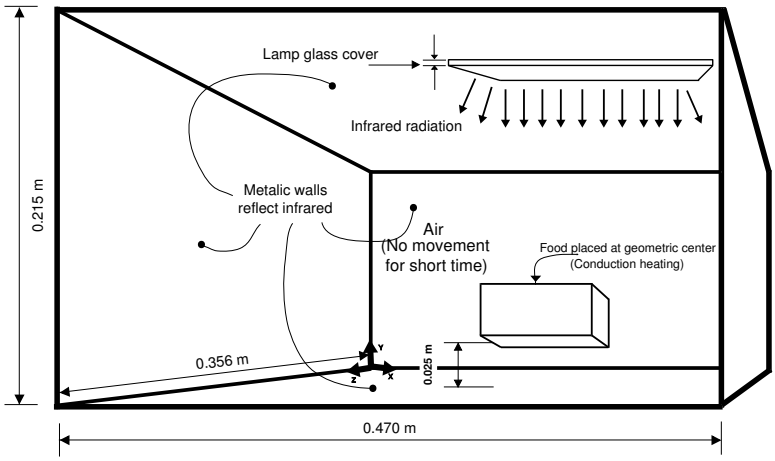

Figure 3.1: Schematic of the radiation dominant problem. The geometry of the oven is rectangular, of size 0.470 m $\times$ 0.356 m $\times$ 0.215 m. The food inside the oven is a potato slab of geometry 0.0470 m $\times$ 0.0356 m $\times$ 0.0215 m that has a volume of 3.6 $\times 10^{-5}$ m^3. Food is placed at 2.5 cm above the geometric center of the oven's bottom surface, resting on a quartz glass tray, parallel to the 0.470 m $\times$ 0.356 m oven surface.

$$E_T = \int_0^\infty \frac{2\pi hc^2}{\lambda^5(e^{\frac{hc}{\lambda kT}} - 1)} \, \mathrm{d}\lambda = \sigma T^4 \tag{3.2}$$

From the schematic of the enclosure, Figure 3.2, for an opaque surface, i.e., no energy passing through the object surface, the energy balance can be written as:

$$q_r(\mathbf{r}) = J(\mathbf{r}) - G(\mathbf{r}) = \epsilon(\mathbf{r})E(\mathbf{r}) - \alpha(\mathbf{r})G(\mathbf{r}) \tag{3.3}$$

Writing now the *irradiation* in terms of the total *radiosity* over the surface A, from the definition of the view factor, $F_{\mathrm{d}A'-\mathrm{dA}}$:

$$G(\mathbf{r})dA = \int_A J(\mathbf{r}')dF_{dA'-dA}dA' \tag{3.4}$$

Inserting Kirchhoff's law in Equation 3.3, solving for *radiosity*, J, and substituing in Equation 3.4 results in the following integral equation that relates temperature and heat flux at each location, $\mathbf{r}$, in the enclosure:

$$\frac{q_r(\mathbf{r})}{\epsilon(\mathbf{r})} - \int_A \left(\frac{1}{\epsilon(\mathbf{r}')} - 1\right) q_r(\mathbf{r}')dF_{dA-dA'} = E(\mathbf{r}) - \int_A E(\mathbf{r}')dF_{dA-dA'} \tag{3.5}$$

An assumption used to come to Equation 3.5 is that the radiosity is constant for a determined surface A. This assumption is relaxed later with the definition of macro-surfaces in the numerical implementation of the problem (see Section 3.4.2). Kirchhoff's Law, where food emissivity, ϵ, equals its absorptance, is considered valid although temperatures of the source and food are somewhat different [3]. The non-gray model has the emissivity in Equation 3.5 varying with wavelength. The two

band approximation for absorptance shown in Figure 3.3 is used for food surface emissivity when it is considered non-gray.

Equation 3.5 provides the radiative heat flux, q_r, on a surface element at constant temperature (see Section 3.4.2) and it is used as a boundary condition over a surface for calculating heat conduction.

3.3.3 Governing Equations and Boundary Conditions for Heat Conduction

The energy equation (Equation 3.6) is solved for the entire cavity (food and air), iteratively, calculating the radiative flux in a segment of the boundary of the air in the cavity, at each iteration that the temperature field is solved.

$$\rho_0 c_p \frac{\partial T}{\partial t} = k_c \nabla^2 T \tag{3.6}$$

Initial temperature is constant in the entire domain. Adiabatic walls formed the perfect diffuse enclosure. Radiant fluxes are assumed diffuse from halogen lamp, which is modelled from the bottom glass cover (see Figure 3.4). Radiant fluxes occur only between solid surfaces (source, walls and food). The air is non-absorbing (non-participating). Boundary conditions on all surfaces for the energy equation are as follows:

$$\underbrace{-k_c \left.\frac{\partial T}{\partial n}\right|_c}_{\substack{\text{conduction from} \\ \text{solid to surface}}} - \underbrace{\left(-k_{\text{air}} \left.\frac{\partial T}{\partial n}\right|_{\text{air}}\right)}_{\substack{\text{conduction from} \\ \text{surface to air}}} = -q_r + h_c(T_s - T_{\text{air}}) \tag{3.7}$$

where k_c is the thermal conductivity of solid (food), k_{air} is the thermal conductivity

of the air, n is the outward normal direction to the food surface, T is temperature, T_s is the food surface temperature, T_{air} is the air temperature inside the oven, q_r is the net radiative flux absorbed by the food surface as calculated using the enclosure equation (Equation 3.5) and h_c is the convective heat transfer coefficient over the food surface.

The two terms on the left side of equation 3.7 respectively represent conduction from within the food to the food surface, and from the food surface to the surrounding air. In general, these fluxes would fully account for the conduction heat transfer from the food to the surface, and the heat flux from the surface to the air (even if moving). However, since in this study we treat the air as quiescent (i.e., not moving), we do two things, both arbitrarily, to partially account for the effect of air movement or convection: first, to enhance conduction, we increase the value of thermal conductivity of air, k_{air}, in equation 3.7 by 70% and, second, we add a small additional heat transfer to the air via the heat transfer coefficient h_c on the right side of equation 3.7 (see Section 3.4.7 for further discussions).

The foregoing is further justified because the convective air flow is a short transient process. It is induced with the start of heating and then relaxes almost to zero when the radiant source is shut off. Thus, the induced convective air flow is expected to be very weak, and we essentially neglect it.

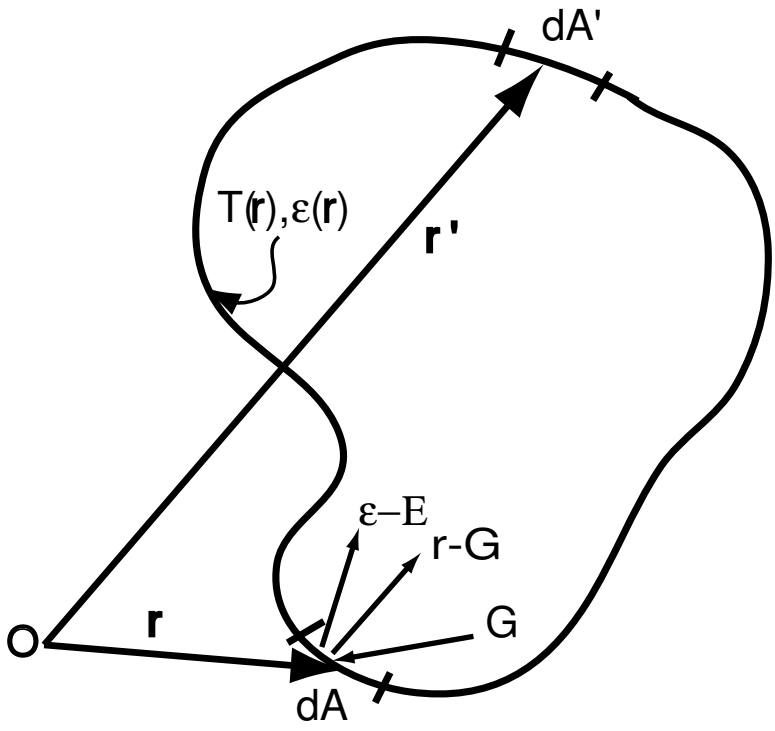

Figure 3.2: Radiative exchange in a gray diffuse enclosure and the principle of a surface energy balance.

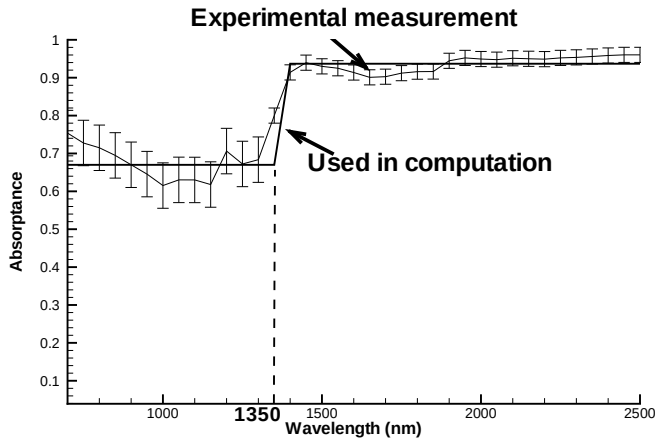

Figure 3.3: Spectral absorptance of potatoes in the near and mid-infrared range. See Section 2.5.4.

3.4 Methodology

3.4.1 Numerical Solution

The integral equation (Equation 3.5) is solved numerically. One of the assumptions in this equation is that surface temperature is constant. This is implemented by considering each element of the boundary surface as a radiating surface. If temperature does not vary significantly over a part of the boundary, an alternative approach is to "lump" together elements on the boundary and consider this group of element sides as a macro-surface for purposes of radiation exchange computation.

3.4.2 The Macro-surface Concept for Radiation Calculations

As described above, a macro-surface is a collection of adjacent element faces. Each element face has various quantities such as area, temperature and emissivity, associated with it. In order to use the macro-surface approach, each macro-surface must have an effective temperature and emissivity associated with it. Given a quantity ϕ_k, associated with node k of an element face i, the effective value of this quantity, Φ, for the macro-surface comprised of N element faces is computed by:

$$\Phi = \frac{1}{A_s} \sum_{i=1}^{N} (A_i (\sum_{k=1}^{n} c_{ik} \phi_k)) \tag{3.8}$$

where A_i is the area of element i, A_s is the area of the macro-surface, i.e, $A_s = \sum A_i$; n is the number of elements in the macro-surface; $c_{ik} = (\int (\theta_{ik} \mathrm{d}A))/A_i$ is an average

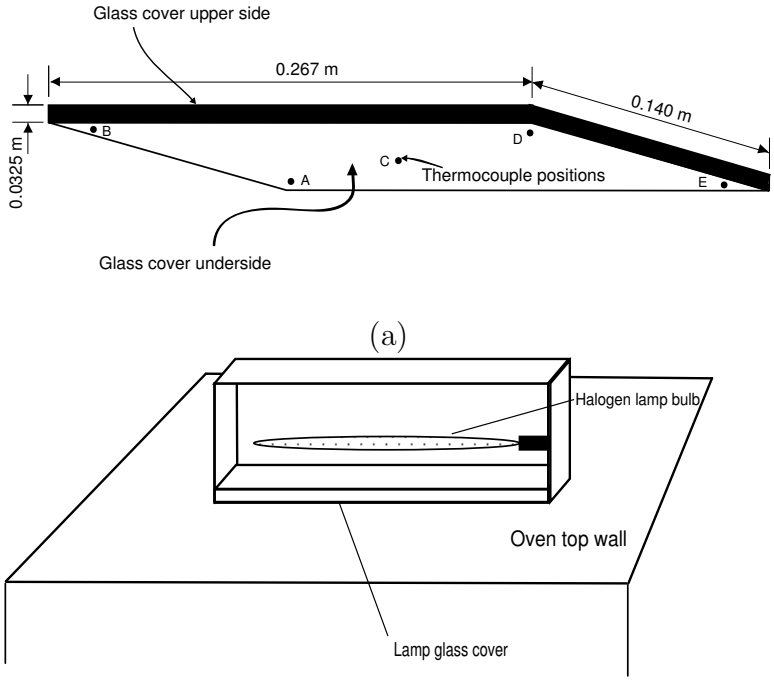

Figure 3.4: Schematic showing a) the bottom face of the lamp glass cover and thermocouple positions, A-E, and b) lamp case, showing the halogen bulb and the lamp glass cover.

shape function for element i; and θ_{ik} is the shape function at node k of element i.

Thus, Equation 3.8 can be used to "lump" the elemental quantities of temperature or emissivities into surface quantities. These values are then used to calculate the macro-surface heat flux. Normally, the assumption of constant radiosity becomes less limiting in this way, since the number of subsurfaces can be increased substantially to obtain sufficient resolution of the variations. The macro-surface values for heat flux due to radiation can then be used as boundary conditions for the energy equation.

3.4.3 Numerical Implementation of the Radiative Exchange in an Enclosure

Equation 3.5 is an integral equation which solution is difficult since the unknown dependent variable appears in the integral. One way to solve this problem is to numerically subdivide the surfaces participating in the radiative exchange.

Dividing a gray diffuse enclosure into N isothermal subsurfaces over which the properties (i.e., the temperature, the radiative properties and the heat flux) are assumed to be constant. Writing for the subsurface A_i, with summation over all other subsurfaces A_j, Equation 3.5 becomes:

$$\sum_{j=1}^{N} \left(\frac{\delta_{ij}}{\epsilon_j} - \left(\frac{1}{\epsilon_j} - 1 \right) F_{i-j} \right) q_{rj} = \sum_{j=1}^{N} (\delta_{ij} - F_{i-j}) E_j \tag{3.9}$$

Thus, the problem has been transformed into a form suitable for numeric calculations. For an enclosure of N subsurfaces, N equations need to be solved and the

problem can be cast into matrix form.

Numerical Implementation: Gray vs. Non-gray Formulation

Equation 3.9 gives the net radiation heat flux due to a wall-to-wall exchange. One major assumption in this equation is that the surface must be gray. If one assumes that emissivity can be written as a band function of wavelength and each band exhibits a "gray-diffuse" behavior, then Equation 3.9 can be written for each wavelength band.

$$\sum_{j=1}^{N}\left(\frac{\delta_{ij}}{\epsilon_{\lambda,j}}-\left(\frac{1}{\epsilon_{\lambda,j}}-1\right)F_{i-j}\right)q_{\lambda,j}=\sum_{j=1}^{N}(\delta_{ij}-F_{i-j})F_{\lambda}^{*}E_{\lambda,j} \tag{3.10}$$

where, $\epsilon_{\lambda,j}$ is now the emissivity of the j^{th} surface in the λ^{th} band and, F_{λ}^{*} is the band energy ratio given by the Planck's law [33, 10]:

$$F_{\lambda}^{*}=\int_{\Lambda_{\lambda}}^{\Lambda_{\lambda+1}}\frac{15c_2^4\mathrm{d}\eta}{\pi^4\eta^5[\exp(c_2/\eta)-1]} \tag{3.11}$$

where $\Lambda_{\lambda}=\lambda_{\lambda}T$, T being absolute temperature and c_2 is a constant equal to 14388 $\mu\mathrm{m}\cdot\mathrm{K}$. Finally, $q_{\lambda,j}$ is the radiative heat flux for the j surface in the λ^{th} band. The boundary condition used in the energy equation is the sum of all heat fluxes over the entire spectrum, i.e., the total number of bands, *nbands*, involved in the non-gray problem and is given by:

$$q_r^j=\sum_{\lambda=1,nbands}q_r^{\lambda j} \tag{3.12}$$

Note that for a gray analysis F^* equals to 1. To solve the energy equation (Equation 3.6) including the non-gray radiative term (Equation 3.12), the code FIDAP (FLUENT Inc.,New Hampshire, US) is used. Fidap uses the hemi-cube formulation for the view factor calculation in the geometry. The hemi-cube formulation is based on Nusselts hemisphere analogy [4]. According to this analogy, any surface which covers the same area on the hemisphere has the same view factor; any intermediate surface geometry can be used without changing the view factor values. The hemisphere is replaced by an hemi-cube geometry. It is mostly used in computer graphics to reduce computation time in image processing [4].

The three major assumptions for the limitations of the hemi-cube method are:

1. Proximity - that the distance between surfaces is great compared to the effective diameter of the surfaces.

2. Visibility - that the visibility between any two surfaces does not change.

3. Aliasing - that the true projection of each visible surface onto the hemi-cube can be accurately accounted for by using a finite resolution hemi-cube.

The hemi-cube assumption has been used in other numerical work [4].

3.4.4 Solution Parameters

A transient analysis was performed for one minute of heating with cycling of the lamp sources. The mesh was developed using hexahedral elements. The density of the mesh varied along the cavity, being denser around food and glass lamp cover

surfaces (Figure 3.5). The time increment was constant throughout the simulation and its value was kept at 0.015 s. A small time increment was necessary.

3.4.5 Input Parameters

Table 3.1 lists input parameters used in this study. All properties were treated as constants and considered isotropic in both air and food. As noted earlier, to partially account for air movement, the thermal conductivity of air was increased from the accepted value of 0.0265 W/mK to the listed value of 0.045 W/mK (a 70% increase) and a convective heat transfer coefficient of 0.47 W/m^2K was added. The food inside the oven is a potato slab, placed at 2.54 cm above the geometric center of the oven's bottom surface.

The GE Advantium^{TM} oven is a combination oven, i.e, it has both microwave heating and halogen heating capabilities. It has two halogen lamps, protected by a quartz glass case, one situated on the top of the oven and the other on the bottom. The lamps can work separately, i.e, the oven user has the choice of using one or the other lamp, or both of them, for each oven intensity. For the purpose of this study, only the top lamp was used. The combined heating study can be seen elsewhere [9].

The oven has the inside dimensions of 0.470 m $\times$ 0.356 m $\times$ 0.215 m (Figure 3.1). All the inside surfaces, besides the lamp covers, are in stainless steel. The power level of both microwave and halogen (infrared) heating is set up through a mechanical dial in the oven control panel. The dial has 10 settings from 1 to 10 for both, microwave and halogen (infrared) heating. There is a separate entry for adjusting the heating time staring from 15 s. The infrared dial settings control the

on-off cycle of the lamps.

Oven capacity is 0.036 m^3 and the food volume is 3.6 $\times 10^{-5} m^3$ (Figure 3.1). The oven surface emissivities are taken as of stainless steel emissivity at 300 K. Lamp emissivities are set equal to values for tungsten filament (Table 3.1).

Potato emissivity is set for two different values in a 2-band approximation for the non-gray problem and then set as 0.88, a weight average value in the $0 - 2.5 \mu m$, for the gray scenario (values are 0.67 for the 1.3 μm range and 0.96 for the range between 1.3and 2.5 μm wavelengths. See Section 2.5.4). Food sample is stationary, i.e, does not move during the experiment.

Table 3.1: Input Parameters

Air density	1.1614 kg/m^3	[3]
Air Specific Heat	1030.0 $J/kg \cdot K$	[3]
Air Thermal Conductivity	0.045 $W/m \cdot K$	[3]
Heat transfer convective coefficient	0.47 $W/m^2 \cdot K$	
Potato density	1000.0 kg/m^3	[36]
Potato Specific Heat	3900.0 $J/kg \cdot K$	[36]
Potato Thermal Conductivity	0.4 $W/m \cdot K$	[36]
Oven surfaces emissivity	0.1	[14]
Lamp surfaces emissivity	0.43	[14]
Potato emissivity(gray)	0.88	[3]
Potato emissivity(non-gray) $\leq$ 1350 nm	0.64	[2]
Potato emissivity(non-gray) $\geq$ 1350 nm	0.96	[2]
Source maximum output energy	75000 W/m^2	

3.4.6 Cycling Boundary Condition for Infrared Source

The transient thermal behavior of the infrared (halogen) lamp that cycles on-off, is approximated using a polynomial growth and an exponential decay function. Maximum output of the halogen lamps in the oven are estimated as follows. The maximum value of the source flux was taken as the maximum output of the halogen lamps, 3 kW for two lamps, comprising the top source. As the area of the glass cover is 0.04 m^2, the approximate maximum value delivered by the lamps is 75000 W/m^2. This value was then multiplied by a time function to represent the transient behavior as described below. The goal was to try different parameters in both the onset phase and the decay phase of the heat source time function, in order to match the behavior of the lamp glass cover during the on-off cycles of the lamp (Figure 3.7), since the model comprises the radiative fluxes delivered from the lamp glass cover (the halogen filament is not modelled).

A polynomial function of the form

$$f(t) = -at^2 + bt \tag{3.13}$$

was fitted for the growth phase of the time function, where a and b are constants obtained through the fitting of the experimental values of the temperature in the glass lamp, during the duty cycle (Figure 3.7). The parameter used as the basis for the matching process in this case was t_{max}, i.e, the maximum value of function $f(t)$ in Equation 3.13.

The temperature drop, after the lamp is turned off, is modeled using an expo-

nential decay, as shown in Equation 3.14.

$$f(t) = e^{-ct} \tag{3.14}$$

To illustrate how parameters t_{max} and c could change the time function profile, refer to Figure 3.8. Figure 3.9 shows the time functions used in the model for the three different settings of the oven. Parameter c had the value of 0.5 for the three settings but parameter t_{max} had values of 0.06981, 0.04761 and 0.03704 respectively for infrared oven settings levels I, V and X.

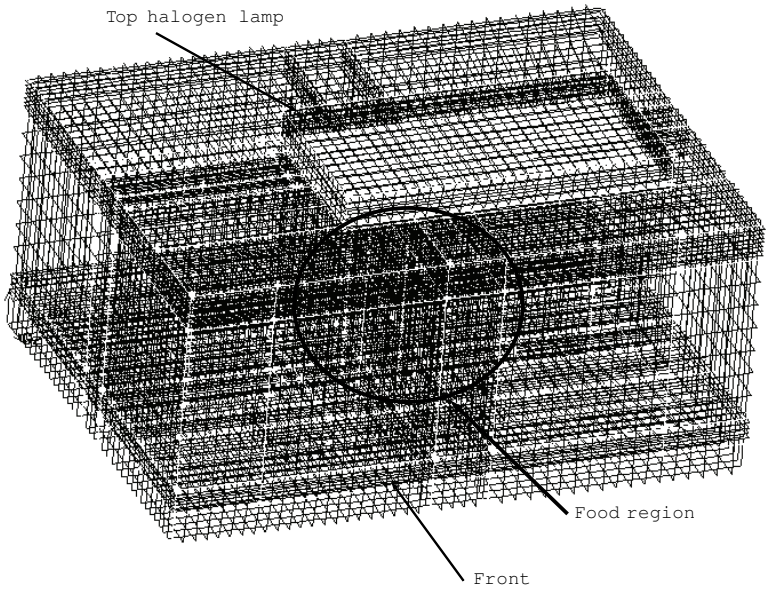

Figure 3.5: Mesh used in the model, with 50000 hexahedral elements for the oven system, including the 360 hexahedral elements for the food volume.

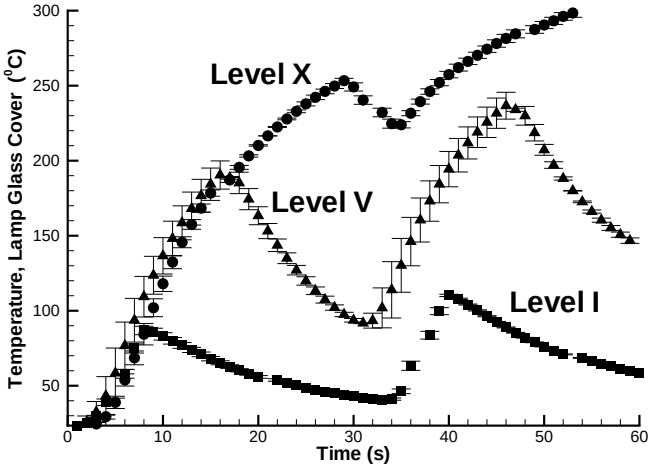

Figure 3.6: Temperature measured at the center position below the top lamp surface (Figure 3.4) during one minute heating for three different infrared setting levels (Levels I, V and X) in the Advantium ^{TM} oven.

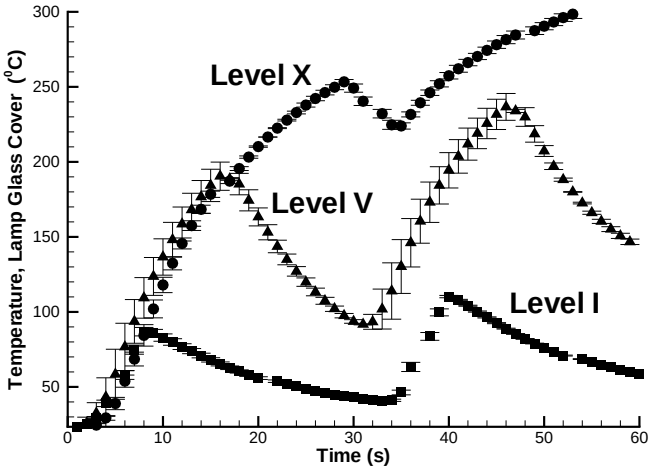

Figure 3.7: Temperature measured at center position below the top lamp surface (Figure 3.4) during one minute heating for three different infrared oven setting levels in the Advantium^{TM} oven - levels I, V and X. Only level I was used to find the right parameters of the heat source time function in the model.

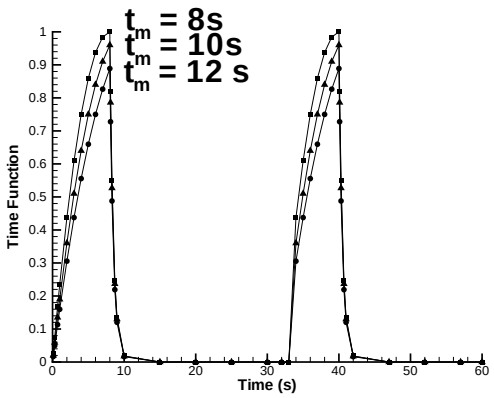

(a)

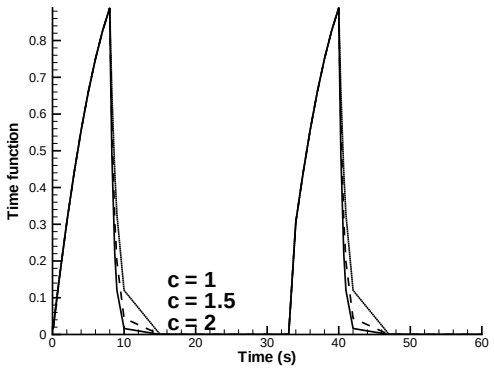

(b)

Figure 3.8: Effect of parameters t_{max}, (a) and c, (b), on the shape of time function for source boundary condition - in the limit of $c \rightarrow \infty$ the function approximates the decay of a step function.

3.4.7 Surface Convection Coefficient

In general, in equation 3.7, the two conductive fluxes on the left side would fully account, respectively, for the heat transfer from inside the food to the food surface and from the food surface to the surrounding air (even if the air is moving). However, since in this study we treat the air as quiescent (i.e., not moving), we arbitrarily increase the thermal conductivity, k_{air} used in equation 3.7 and also add a small additional heat transfer to the air via the heat transfer coefficient h_c on the right side of equation 3.7.

$$q_c = h_c(T_s - T_{\text{air}}) \tag{3.15}$$

Both of the aforementioned changes help account for air movement or convection. The convective air flow is a short transient process. It is induced with the start of heating and then relaxes almost to zero when the radiant heaters are shut off.

When the air is quiescent, the heat transfer from a surface to the air can be accurately calculated with the heat conduction term (second term on the left side) in equation 3.7. At the start of a transient, the rate of *conductive* heat transfer can be expressed in terms of an *effective* heat transfer coefficient, h_c, given approximately by $k_{air}/\Delta z$, where k_{air} is the thermal conductivity of the air, and Δz is the distance to the first finite element node point above the boundary. Based on the mesh spacing used in the present study and an air thermal conductivity of 0.0265 W/mK, the effective h_c is approximately 24 W/m^{2}K.

After sufficient time has passed, the heating processes will set up steady-state free convection flows adjacent to all heated surfaces. For such surfaces, we can esti-

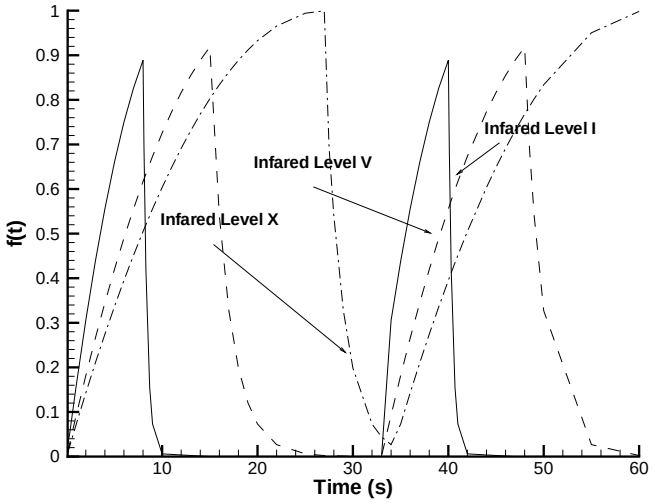

Figure 3.9: Time function used in the model for different level settings in the oven, I, V and X. The value for parameter c was kept as 0.5, but t_{max} had values of 0.06981, 0.04761 and 0.03704 respectively for oven infrared settings levels I, V and X.

mate the *steady*, fully developed heat transfer coefficients from well-known formulas given by [35]

$$Nu_\xi = [(0.545 Ra_H^{0.25})^{1.07} + 3.83]^{0.935} \tag{3.16}$$

where

$$Nu_\xi = \frac{h_c \xi}{k_{air}} \tag{3.17}$$

$$Ra_H = \frac{g\beta(T_s - T_{air})H^3}{\nu^2} Pr \tag{3.18}$$

and

$$\xi = \sqrt{A_{food}} \tag{3.19}$$

$$H = (Z_{max} P_{ave}^2)^{1/3} \tag{3.20}$$

Here A_{food}, Z_{max} and P_{ave} are, respectively, the area of the food surface, the height of the food volume and the averaged perimeter of the food volume. Numerical values in these equations are now calculated and are reported in Table 3.2. Considering a food sample of dimensions 4.7 cm $\times$ 3.56 cm $\times$ 2.15 cm(height), the total surface area is 67 cm^2. The perimeter, P_{ave} is calculated as $2 \times (2.15 + 3.56) = 11.42$ cm and $Z_{max} = 2.15$ cm. The resulting ξ and H values are $\xi = 8.2$ cm and $H = 6.5$ cm. The maximum value of the food top surface temperature, T_s, during the computation period of 60 s is 306 K, assuming level I setting of the oven. Average value of computed temperatures of all nodes in the air above the top food surface at the same instant as T_s is 300 K, which is used as the value for T_{air}. The kinematic viscosity, ν, is 16×10^{-6} m^2/s for air at 303 K. Using these values, Ra_H is calculated

as

$$\begin{aligned} Ra_H &= \frac{g\beta(T_s - T_{air})H^3 Pr}{\upsilon^2} \\ &= \frac{(9.8\text{m/s}^2)(1/300\text{K})(6\text{K})(0.065\text{ m})^3(0.71)}{(16\times 10^{-6}\text{m}^2/\text{s})^2} \\ &= 152421 \end{aligned} \tag{3.21}$$

which leads to

$$Nu_\xi = 13.79 \tag{3.22}$$

$$\begin{aligned} h_c &= \frac{(0.0265\text{W/mK})(13.79)}{0.082\text{m}} \\ &= 4.5\ \frac{\text{W}}{\text{m}^2\text{K}} \end{aligned} \tag{3.23}$$

Table 3.2: Parameter Values Used in Calculating Heat Transfer Coefficient, h_c

A_{food} [cm^2]	Z_{max} [cm]	P_{ave} [cm]	T_{air} [K]	T_s [K]	Pr	Ra	Nu	k_{air} [W/mK]	h_c [W/m^{2}K]
67	2.15	11.42	300	306	0.71	152421	13.79	0.0265	4.5

The cited correlations are for steady, fully developed natural convection flows, not for transients as is the case of this research. The fully developed value of h_c from Table 3.2 is 4.5 W/m^{2}K. This value is much less than the initial effective conduction value of 24 W/m^{2}K. The initial conduction value decays with time, and,

with convection present, would achieve the value of 4.5 W/m^{2}K when convection was fully established. To illustrate the effect of convection on the heat transfer coefficient, Nu and h at other Rayleigh numbers are calculated in Table 3.3. Using

Table 3.3: Nusselt numbers and heat transfer coefficients calculated using Eq. 3.16

	Nu	h [W/m^{2}K]
$Ra = 0$	3.5	1.1
$Ra = 10$	4.3	1.4
$Ra = 10^2$	5.0	1.6
$Ra = 10^3$	6.3	2.0
$Ra = 10^4$	8.6	2.7
$Ra = 10^5$	12.7	4.1
$Ra = 10^6$	20.1	6.5

some of the data from Table 3.3, an approximate sketch of food surface heat flux is shown in Figure 3.10. Rough estimates of the time to set up a diffusion layer and steady state conduction in the air phase gives a value of 5 minutes, as illustrated in this figure. Thus, over a one minute period, heat transfer is expected to be primarily by conduction, and not convection.

In this study, we neglected air movement and assumed that heat transfer in the air was by conduction only. To partially account for the effects of air movement,

we did two things. First, we increased the value of thermal conductivity for air, k_{air}, from the accepted value of 0.0265 W/mK to 0.045 W/mK in the calculations. This increase of 70% would raise the conduction-only curve in Figure 3.10 by a corresponding 70%. Further we added a small amount of convection heat transfer at all surfaces. In equation 3.7, we set h_c equal to 0.47 W/m^{2}K. In Figure 3.10, this value would correspond to an upward shift of the conduction curve by a similar amount. The upward shift is a small fraction of the convective enhancement for a fully developed steady-state flow.

3.4.8 Temperature Measurements

Temperature Measurements in the Food

Temperature history of the top food surface was measured using a fiber optic measurement system made by Fiso Technologies (Quebec, Canada) (Figure 3.11). The system was mounted on the left side of the oven (outside) to allow for the fiber optics probes entering the oven without any door obstruction.

The data system recorded temperatures from the 4 probes every 1.5 s. Temperatures were recorded for two full duty cycles of the oven infrared settings at levels I, V and X, just using the top lamp. The placement of measurement probes over the top food surface is shown in Figure 3.11. Probes were inserted slightly on the potato surface and hold in place using a fiber optic band provided by the manufacturer.

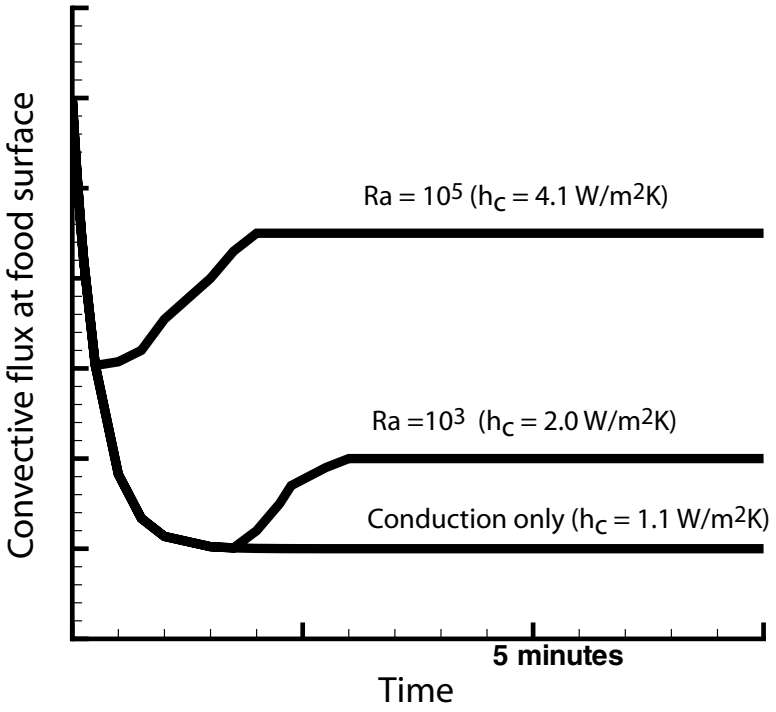

Figure 3.10: Approximate trends in convection transients for various scenarios.

Temperature Measurements over Oven Lamp Surface

For a better understanding of the heat transfer process inside the oven, surface temperature of the lamp glass cover was measured on the underside face, looking inside the oven cavity (Figure 3.4).

Thermocouples type K (Omega Inc., Connecticut, U.S) were used and placed in positions as shown in Figure 3.4. Using a FLUKE Data acquisition Bucket ^{TM} (Fluke Co., Whashington, U.S.), lamp cover glass surface temperature measurements were taken simultaneously with food temperature measurements.

The lamp glass cover temperature profiles for different intensity levels are shown in Figure 3.6. These measurements were used for determination of on-off lamp cycles for the three intensity levels, as described in Section 3.4.6.

3.4.9 Heat Flux Measurements

Omega Thin Film Heat Flux Sensor (HFS-3, Omega Inc., Connecticut, U.S.) was used to measure heat flux. The heart of the HFS Sensor is a differential thermocouple sensor. A thin foil, 40 junction thermopile is bonded to either side of a Kapton^{TM} thermal barrier, which has known thermal characteristics (high absorbance, but very low conductivity). Since the total heat transfer rate is proportional to the temperature difference across the thermal barrier, the rate of heat transfer can be calculated by measuring this difference. The dimensions of the sensor are 15.1 mm $\times$ 8.5 mm, occupying less than 8 % of the total area of the food face ($\sim$ 16 cm^2), with long extension of lead wires for connections. Upper temperature limit is 165 ^{0}C and the

nominal sensitivity is $9 \pm 10\%$ $10^{-9} \mathrm{V/m^2 \cdot s}$. The maximum recommended heat flux is 93961 $\mathrm{W/m^2}$ (30,000 $\mathrm{BTU/ft^2 \cdot h}$).

In order to measure the heat flux through the differential thermocouple, a portable microvolt meter (FLUKE Data acquisition Bucket$^{\mathrm{TM}}$, Fluke Co., Washington, U.S.) was interfaced directly to the sensor with no need of any cold-junction compensation.

The HFS-3 thin films were secured on the top surface of the food using tape as it was heated at different oven infrared settings for one duty cycle of 1 min. The same data acquisition system used for the lamp glass cover temperature measurements was used for the flux measurements (Figure 3.12) with the reading in mV, instead.

The on and off cycles for each infrared level of settings (I, V and X) were measured and they not increase linearly. Results show a 67% increase in the top food heat flux from level I to level V. From level V to level X there was no significant variation in intensity of heat flux with an increase of 2 s of on period time.

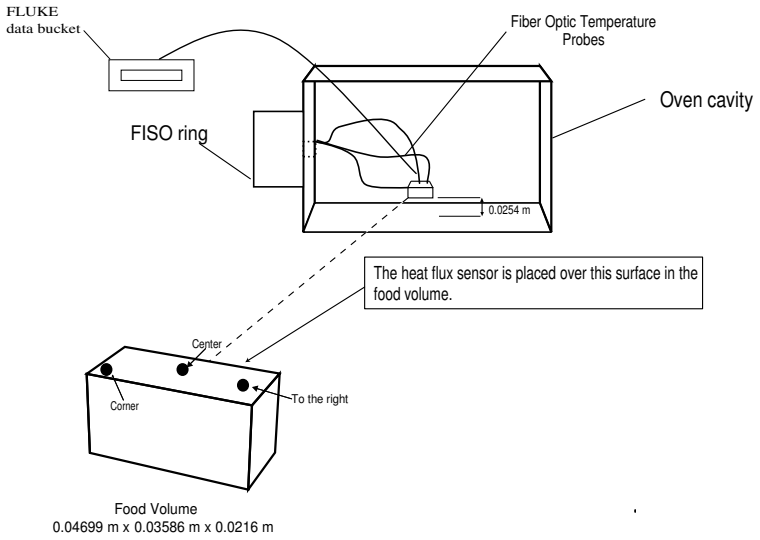

Figure 3.11: Temperature probes location over the top food surface and general experimental set-up.

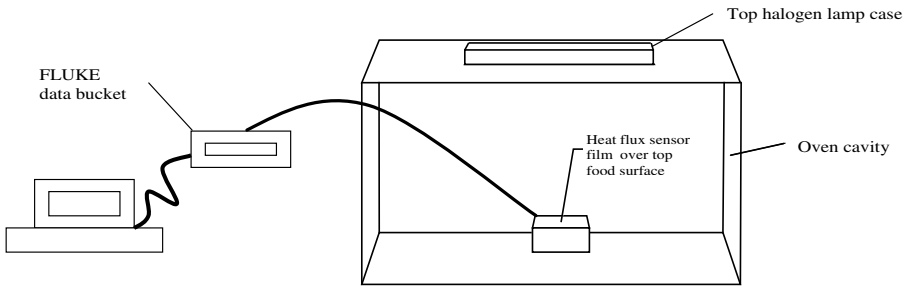

Figure 3.12: Schematic of heat flux data acquisition set up, using FLUKE Data acquisition Bucket^{TM}, Fluke Co., Washington, U.S.

Chapter 4

RADIATIVE HEAT TRANSPORT MODELING INSIDE AN OVEN: Effect of Oven and Food Parameters

4.1 Introduction

In today's life, people became aware of the importance of having healthy meals meaning also the appropriate form of processing to keep its properties, with the least time possible spent in the preparation of meals. That's why appliances' manufacturers keep developing equipment using new approach and technologies. This became a call to the scientific society to study how new heating methods affect

foods under diverse processing methods.

Changes of food during cooking vary as a function of the heating source (convective or radiative, for example) and the dissimilarity of the internal mass and surface properties of that food affecting the crust formation and color development, among others. This was experimentally investigated by [7] and [32].

The change of evaporation rate with these two heating modes (convective and radiative) was also investigated experimentally by [22] and [31]. The food surface texture in baking under convective heating and infrared heating was investigated by [34]. Most of these studies found an intense and rapid changing in food characteristics under infrared heating. Dagerskog and Sorenfors, 1978 [7] observed almost half the time necessary to reach the same center temperature in beef patties compared to convection and contact heating. Shibukawa et al., 1989 [32] found out that the surface temperature was 10 % higher for radiation than convection processes in cookie baking. The exception is for the evaporation rate that showed to be 5% less (Sato et al., 1987 [31]) for the infrared heated food, due to the earlier crust formation.

The infrared heating oven is an old technology and can come back in use according to the availability and pricing of energy.

The combination of an infrared heating element in the same cavity as of the microwave generator dates back from 1970 [18] and have been developed since then. The purpose of such combination is to reach a more homogeneous internal temperature distribution on the target food and to dry up the accumulated water on the surface caused by the internal vapor pressure that drives the moisture out, hence,

developing the desired color at the food surface [24].

Recently the industry developed a new halogen lamp that has the property of generating infrared waves with same penetrability properties as of the microwaves and a very homogeneous distribution. Some combination ovens, having the microwave as well the infrared heating elements are already available in the national market as well in Europe [30][11][17].

The present research is going to focus in understanding the phenomenon of the near-infrared heating of foods and the application on a combination heating mode, with microwaves.

During the process of understanding the behavior of the infrared radiation, many fields as computer graphics, microelectronics, and the paper and wood industries have tried modeling that phenomenon. Nevertheless, general solutions have being hard to obtain due to the complexity of its equations, Therefore, most of the publications on the infrared heating of foods are still empirical and experimental [28]. Some numerical solutions have been developed in recent years as of the enclosure equations developed in channels by Franca et al.[12], and often in its 2-D and 1-D mode [28], [27].

In the literature, we may find few studies of heating foods inside an oven using the radiant thermal model. But the study of infrared heating in terms of total flux at the food surface is not found at all.

The alternative of gray surfaces is usual on the engineering field and it can give us some guidelines on the actual heating that is going on the objects of study, but that simplified approach is not sufficient for the complex analysis of the food mass

behavior. Considering the infrared emissions varies in a large spectra, comprehending the near, medium and far infrared, it looks rightly appropriated to study the radiation equation in a non-gray situation (emmissivities varying with the wavelength).

In the process of modeling the surface heat flux of a food placed inside an oven, the use of the radiation equation [21], [33] was essential and the numerical analysis demanded adjustments to get a more suitable equation. For the equations, see Chapter 3.

The non-linear nature of the radiation equation ([21], [33]) and the fourth power dependence with temperature leads to an unusual magnitude of the heat flux calculation, leading to high intensive heating. As an alternative to understand and solve that problem, we decided to use the optical properties of the food being heated to quantify the right amount of infrared energy that the food surface absolves.

The food emissivity property is a directly input in the radiation equation and its dependence with the infrared wavelength assures the best valuation of the infrared energy that strikes the food. With such properties, we could measure the amount radiative flux that reaches the food surface from variable power.

That kind of radiation modeling gave us the ability to handle oven modifications regarding type and power of infrared source associated with various food positions, in addition to variation of cycling time and other oven configurations. Using the numerical method, we could predict the amount of heat that the food surface receives under any circumstance and consequently we may fine-tune oven settings, saving energy and allowing for better quality in cooking.

4.2 Objectives

The present research develops a comprehensive study of infrared heating of foods for the non-gray situation. The goal is to obtain better quantitative understanding of the infrared heating process that should improve the heating performance. The specific objectives are:

1. The application of the radiative model to a 3-D cavity, with non-gray optical properties of food and oven surfaces to predict the heat flux in a food surface for infrared heating. Use thermal heat flux sensors (HFS-3, Omega) and fiber optic probes to validate the numerical predictions;

2. To perform sensitivity analysis on the model for different food positions and different source locations and predict performance of different food and internal oven walls materials.

4.3 Problem Schematic, Solution and Input Parameters

The physical problem was the analysis of the radiative heat transfer to a food sample within the cavity of an oven that has one or more halogen lamps placed on the inside surfaces as the heating source and emits a near infrared range of wavelength (a 3-D enclosure; see Figure 4.1).

We used in the experiment the GE Advantium^{TM} oven that is a combination oven with one microwave generator and three halogen lamps protected by quartz

glass cases, as the heat sources. Two of these lamps are in a single case placed on the inside top horizontal surface of the oven and the other one on the bottom floor. These incased lamps may be set to work separately, or in conjunction. For the purpose of this study, only the top lamps were used, keeping the bottom lamp and the microwave generator off. The combined heating study can be seen elsewhere [9].

The oven capacity is 0.036 m^3 with a rectangular geometry of 0.470 m x 0.356 m x 0.215 m (Figure 4.1).

All the inside surfaces, besides the lamp covers, are in stainless steel. The oven surface emissivities were taken as of stainless steel emissivity, at 300 K. The lamp emissivities were considered equal to the value for tungsten filament (Table 3.1).

The power level settings for the microwave source and the halogen (infrared) heat sources are adjusted through separate mechanical dials in the front oven control panel. These dials have 10 level settings from 1 to 10, each one respectively, and determine the on-off cycle of the heat sources. For the present experiment, we set the power level on various levels. There is a separate dial to adjust the heat processing time.

The food sample is a potato slab with a volume of 3.6 $\times 10^{-5}$ m^3, also a rectangular geometry of 0.0470 m x 0.0356 m x 0.0215 m, placed at 2.54 cm above the geometric center of the bottom surface of the oven. The food sample is static during the experiment.

Potato emissivity is set for two different values in a 2-band approximation for the non-gray problem and then set as 0.88, a weight average value in the $0-2.5$, for the gray scenario (values are 0.67 for the 1.3 range and 0.96 for the range between 1.3and 2.5 wavelengths. See Section 2.5.4).

All properties were treated as constant and isotropic in both air and food. For other input properties, see Table 3.1.

Heat flux over food and other surfaces is computed from numerically solving the radiative heat exchange equation. Temperatures are then computed in the food using the heat conduction equation. The effects of various parameters are then achieved through sensitivity analysis of the numerical model.

Thermal heat flux sensors (HFS-3, Omega) and fiber optic probes were used to validate the numerical predictions. More details on the problem formulation and numerical solution can be found in Chapter 3.

A transient analysis was performed during one minute of heating with cycling on-off of the lamp sources. The mesh was developed using a finite element hexahedral unit. The density of the mesh varied along the cavity being denser around food and lamp glass cover surfaces (Figure 4.2). The time increment was constant throughout the simulation and its value was kept at 0.015 s. A small time increment was necessary in order to keep error to a minimum.

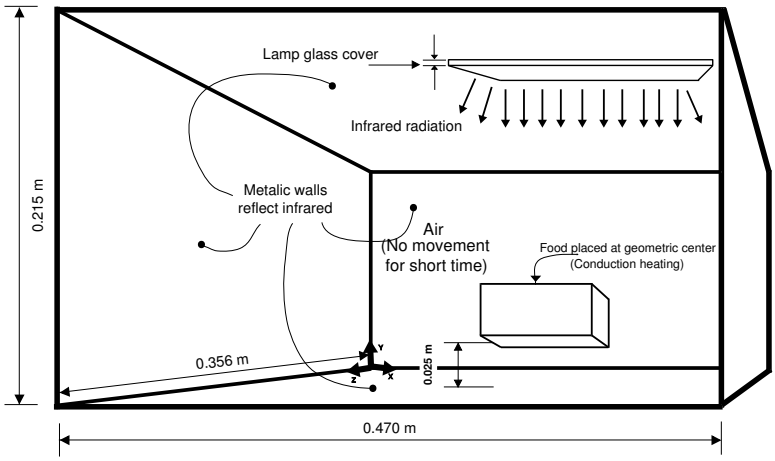

Figure 4.1: Schematic of the radiation dominant problem. The geometry of the oven is rectangular, of size 0.470 m $\times$ 0.356 m $\times$ 0.215 m. The food inside the oven is a potato slab of geometry 0.0470 m $\times$ 0.0356 m $\times$ 0.0215 m that has a volume of 3.6 $\times 10^{-5}\mathrm{m}^3$. Food is placed at 2.54 cm above the geometric center of the bottom surface oven, resting on a quartz tray parallel to the 0.470 m $\times$ 0.356 m oven's surface.

4.4 Results and Discussion

4.4.1 Mesh Convergence

Coupling of irradiation with the energy equation for a 3-D geometry makes the problem computationally intense. In an effort to reduce the computation time, solution convergence was studied as a function of mesh size (h-convergence). Meshes varied in their total number of hexahedral elements. The input parameters were kept constant for all solutions. A heating duration of 60 seconds was simulated.

Increasing element numbers increased computation time almost exponentially (Figure 4.3). As shown in Figure 4.4, temperature values at top food surface center node converged for 50000 elements or higher. Thus, 50000 elements mesh was chosen for most of the simulations (360 elements in the food geometry). Figures 4.2 and 4.5 show the final mesh and the cross-section showing the mesh around food geometry. Temperature contour plots, also showing a good convergence for 50000 elements mesh, can be seen in Figure 4.6.

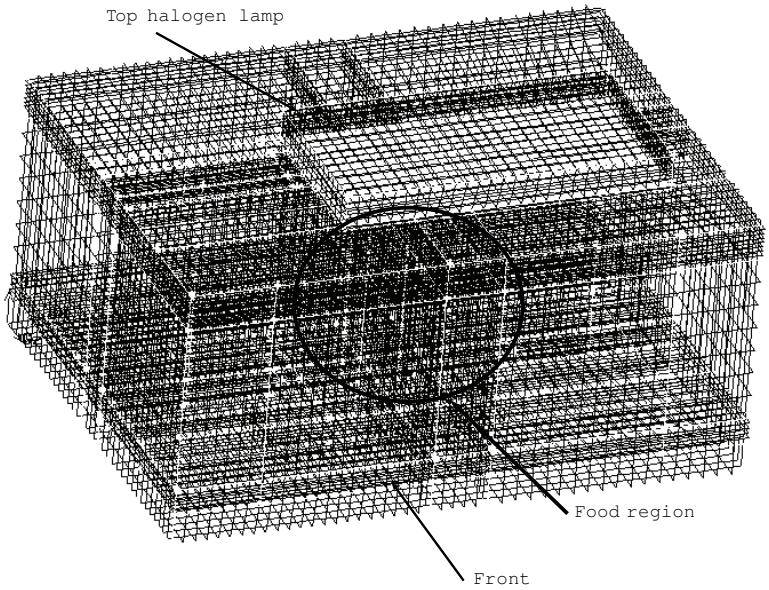

Figure 4.2: Mesh used in the model with 50000 hexahedral elements.

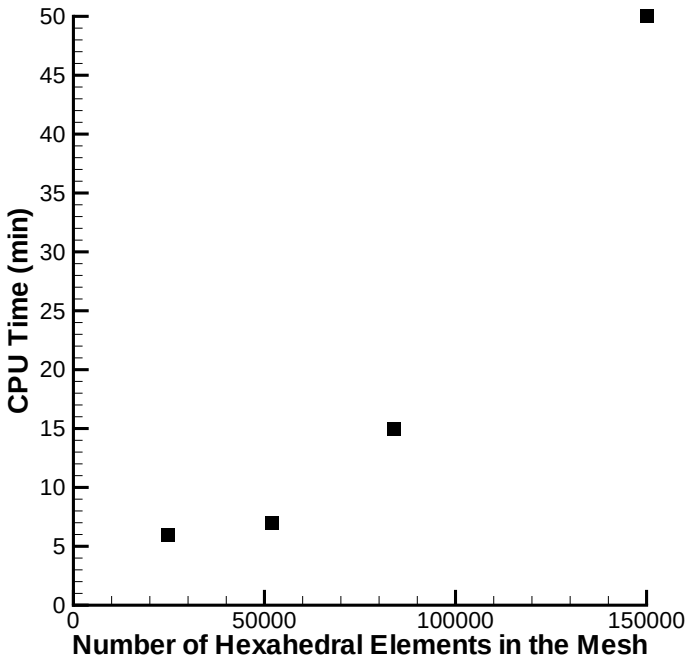

Figure 4.3: Computation time as a function of number of elements in mesh.

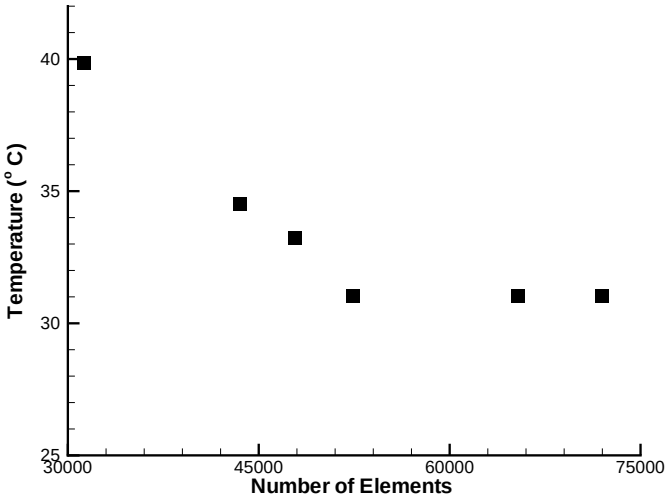

Figure 4.4: Temperatures calculated at the center node of food element (Figure 4.1) for different mesh sizes.

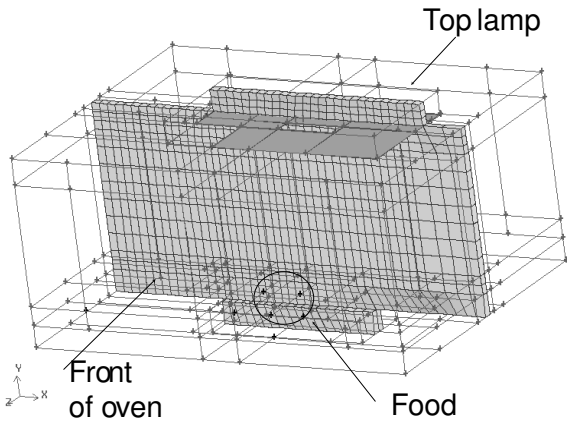

Figure 4.5: Cross-section of mesh showing the region around food geometry. Food volume meshed with 360 hexahedral elements.

4.4.2 Gray versus Non-gray Behavior of Food Surfaces

Gray as well as non-gray food surfaces (emissivities changing with wavelength, as seen in Table 3.1) were considered. The gray emissivity value is a weight average of both non-gray emissivity values shown in the table. Radiative heat transfer inside the oven with food placed in its center at 2.54 cm from bottom oven surface (Figure 4.1) was considered for a 10,000 W/m^2 energy output from the source. The computed results, as seen in Figure 4.7, show higher absorption of energy and consequently higher temperature rise for the gray problem. The non-gray problem had a final temperature of the top food surface that was 3.24^0C lower than when the surface was considered gray. This difference can not be ignored and has to do with the major change in emissivity at food surface around 1.35μm, as noted in Section 2.5.4, "Spectral variation of penetration depth with moisture content". This is the band region of maximum emissive power of the black body curve, as shown in Figure 2.4. If the food emissivity is lower at this wavelength interval (0.64 for wavelengths $< 1.35\mu$m, as in the non-gray model), we should expect less heat being absorbed at the food surface. Consequently, calculated radiative fluxes at the top food surface were also smaller when the food surface was considered non-gray. See more of this discussion, under Section 4.4.6, "Effect of Different Food Emissivities".

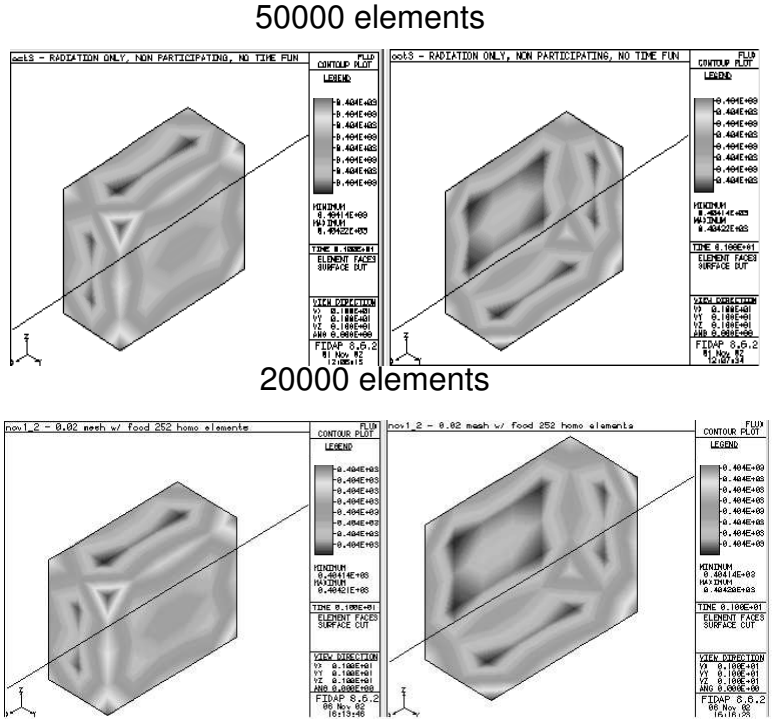

Figure 4.6: Surface temperature contour plots obtained for 10,000 W/m^2 energy output from the source, with input properties as shown in Table 3.1, and different mesh densities.

4.4.3 Comparison with Experiments

To closely match the experiments with simulations, cycling was considered using only the top lamp of the oven. Temperature at the top central position of the food surface was measured for three different dial positions in the front panel of the oven, numbers one, five and ten, corresponding to three different power levels, I, V and X, covering the entire range. The measured temperature values are shown in Figure 4.8.

Temperatures in the food surface follow the transients of the lamp surface temperatures (for a schematic of the experimental set up, see Figure 3.11). These transients provided were obtained through cycling of the intensity level of the heat source. Lamp surface temperature measurements for Level I setting were used to validate the simulation (Figure 3.7).

Temperatures followed the transients given by the time functions of the source term in the energy equation. For level I of the settings, the cycle on-off times were 8 s and 24 s, respectively. For a setting of level V, the cycle on-off times were 18 s and 14 s, respectively, and for level X, the cycle on-off times were 29 s and 7 s, respectively. To minimize the effects of evaporation, etc., that would come with long term heating and are not the emphasis in this research, heating time was restricted to one minute. Even for the highest intensity level, the one minute duration covers more than one cycle of the growth and the decay of the transients. The growth and decay transients depend on the lamp design as it is the transient in the heating element in lamp. The decay in the transient is also contributed by the irradiation from the hot surfaces of the oven. Although the oven wall emissivities are smaller

compared to the food surface emissivities, the total surface area (0.69 m^2) of the oven walls is two orders of magnitude higher compared to the surface area of the food (0.0069 m^2), making the wall contributions to radiation (when infrared source is off) quite significant. In Section 4.4.7, sensitivity analysis varying walls emissivity are explained in details.

Figure 4.9 a shows the radiative flux over the top food surface of potato being heated for 1 minute, at infrared oven setting level I of the Advantium^{TM} oven, top lamp only. Figure 4.9 b shows the temperatures at the top center surface of the food. Temperatures at the glass surface covering the lamp are shown in Figure 4.10.

It is interesting to note how the model well predicted the onset and offset of the heating cycle, as indicated through the boundary condition study performed in Section 3.4.6. It is worth noticing though that the offset was underestimated for the level I case, being not the case for the other oven setting levels, Figures 4.11 and 4.12, as it will be discussed later in this text. One explanation for this behavior is the fact that heat loss effects become more important at lower levels, such as level I, weakening the adiabatic assumption.

Another factor that has to be taken in consideration is that the measured values are also limited by the accuracy (+/- 1 ^{0}C) and reaction time ($< 1.5s$) of the fiber optic probes. Nevertheless, the trends were well captured in the model.

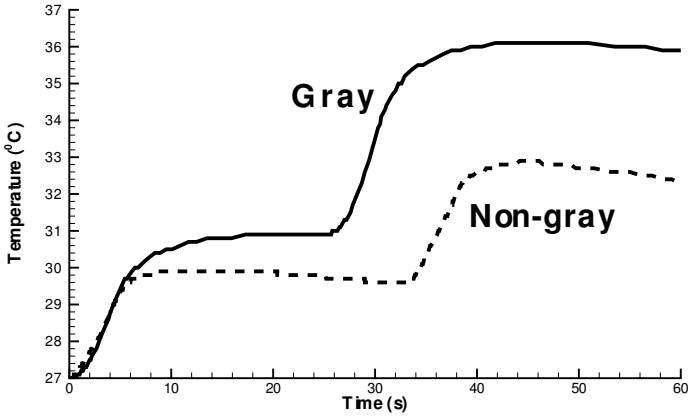

Figure 4.7: Computed temperature at the center node on the top food surface (Figure 3.11) during one minute heating for gray ($\epsilon = 0.67$ up to 1.3 and 0.96 above 1.3) and non-gray assumptions ($\epsilon = 0.88$) of food surface.

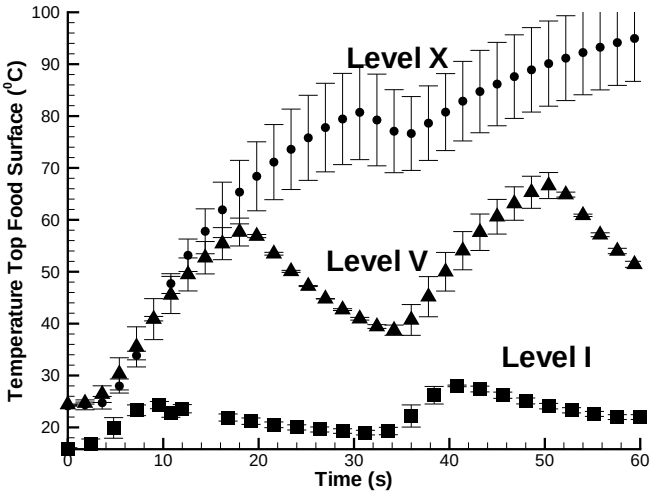

Figure 4.8: Experimental temperatures at the center of top food surface (see Section 3.4.8) for heating at three different intensity levels (I, V and X) of the Advantium^{TM} oven.

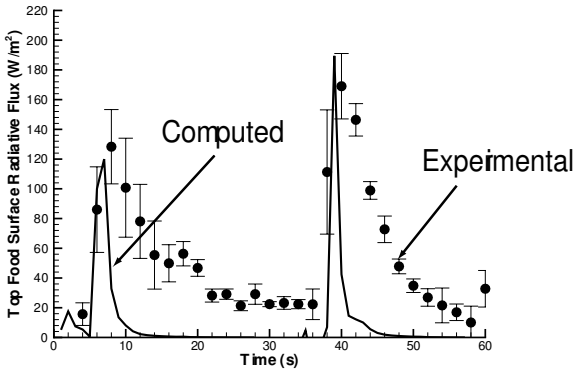

(a)

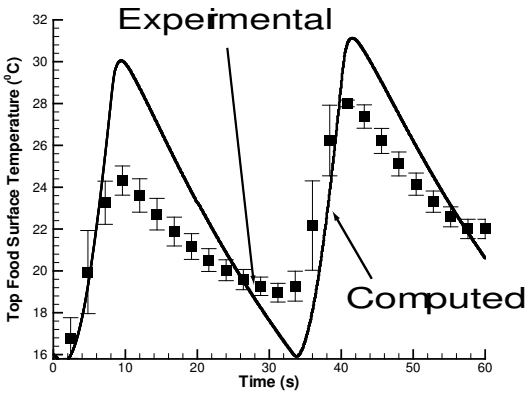

(b)

Figure 4.9: Computed and experimental results for level I intensity of the halogen lamp, at the center of top food surface (Figure 4.1), using top lamp only: a) radiative flux and b) temperature profiles.

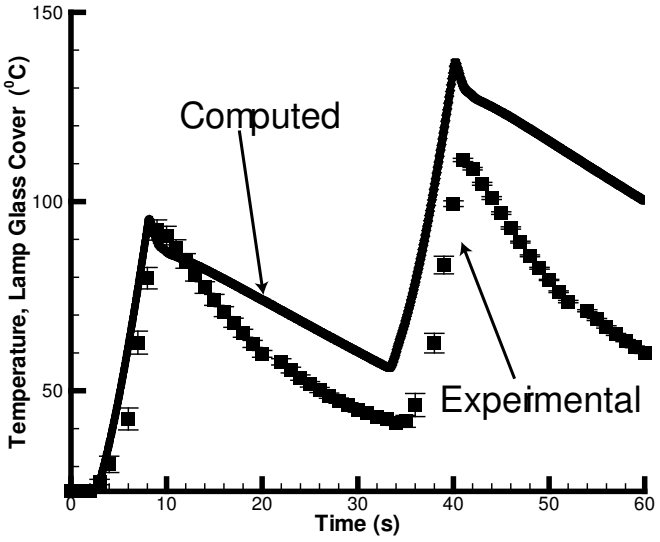

Figure 4.10: Temperature at the center of glass lamp cover (Figure 3.4) for level I, using top lamp only.

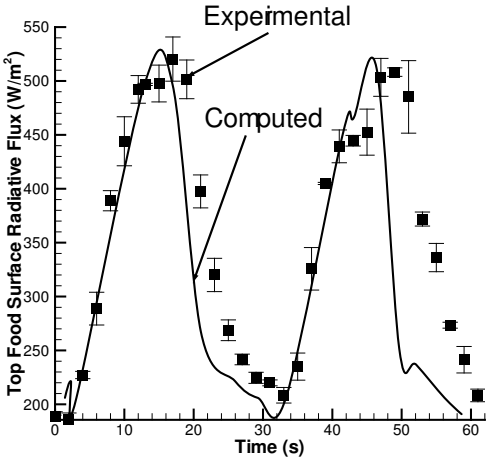

(a)

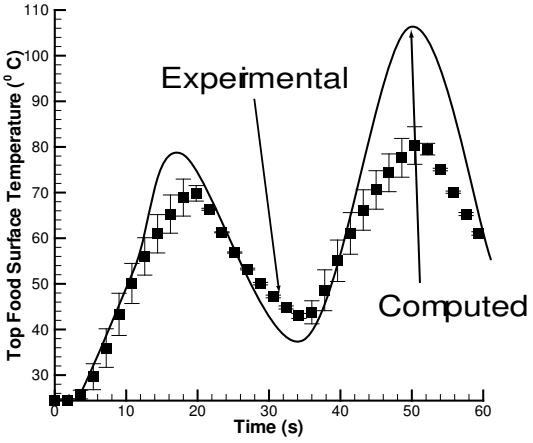

(b)

Figure 4.11: Computed and experimental results for level V intensity of the halogen lamp, at the center of top food surface (Figure 4.1), using top lamp only: a) radiative flux and b) temperature profiles.

4.4.4 Global Energy Balance in the Oven

For effect of checking overall results and order of magnitudes, a global energy balance was performed, considering no losses (adiabatic walls) and the top lamp as the source of heat to the system (interior of oven). The maximum power of the lamps is 3 kW (1.5 kW, each top lamp). The surface area of the glass lamp cover is approximately 0.04m^2, which will give a flux of 75kW/m^2, nominal maximum. For all settings, the radiative flux from lamp has a transient reaching maximum after 7.5 s, 17.5 s and 28 s for oven settings I, V and X respectively, determined experimentally (Figure 4.10).

Considering the lowest level, setting I, it is noticed experimentally an average increase in 3 ^{0}C in 5 s of heating, assuming a homogeneous heating of the whole food volume. For this specific case, for a food mass of 0.035 kg, with specific heat of $3900\text{J/kg} \cdot \text{K}$, the total energy absorbed is 409.5 J, in 5 s of heating, or 81.9 W. Dividing this value for the whole area of the food, assuming uniform properties, results in an average of 122.2W/m^2 heat flux received at the food surface, during the first 5 s of heating.

The maximum values measured and calculated in this model, as shown in Figure 4.9 b, are 122 and 119 W/m^2, respectively, for experimental and computed values. Certainly, differences can be attributed to real energy losses in the system.

Now, calculating back that the food received 81.9 W in the first 5 s of heating for setting level I, assuming an average of 22500 W/m^2 for the energy delivered in 5 s from the lamps (half of the value of 60 % of 75kW/m^2, on the onset of Level I infrared heating), the energy received by the food surface is almost 55.5 % of the

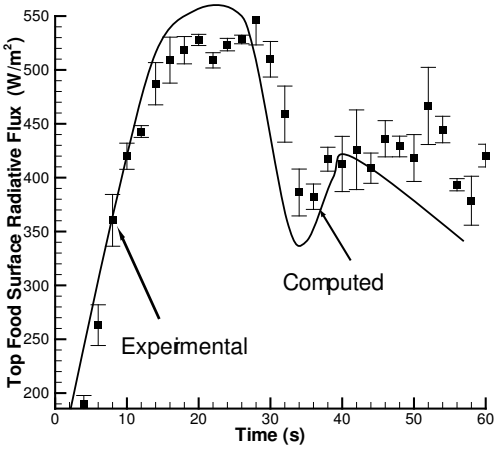

(a)

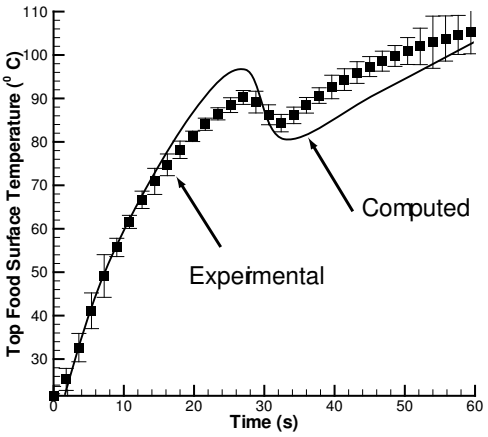

(b)

Figure 4.12: Computed and experimental results for level X intensity of the halogen lamp, at the center of top food surface (Figure 4.1), using top lamp only: a) radiative flux and b) temperature profiles.

energy delivered by the lamps. The US Department of Energy [26] reported that only 6 % of the energy output of a typical household oven is actually absorbed by the food being heated, considering real losses. In this case, the GE Advantium^{TM} oven has shown a considerable improvement in terms of energy delivered to the food material being heated. This has to be confirmed with further investigation of the global energy losses in the oven, which was not the scope of this research.

4.4.5 Effect of Different Infrared Power Levels

Effects of varying the power levels of the infrared lamp on the radiative flux profiles at the food surface can be seen in Figures 4.9a, 4.11a, and 4.12a for the oven settings (power levels) of I, V and X, respectively. Corresponding temperatures for the three oven settings can be seen in Figures 4.9 b, 4.11 b, and 4.12 b, respectively.

Interesting to note is the maximum value for radiative flux for the three different infrared oven settings, levels (I, V and X). While for level I maximum radiative flux was in the order of 200 W/m^2, for levels V and X the maximum values were in the order of 500 W/m^2 and 600 W/m^2, respectively. For all intensity levels, infrared heating can be considered instant heating, since the lag time to reach maximum radiative flux and temperature was not more than 20 seconds even for the highest level of heating. As discussed earlier, computation for levels V and X show a more smooth computed curve if compared to level I. This can be attributed to heating losses being more significant at lower power levels of infrared.

The method to simulate the increasing power levels was determined using the rationale of delivering fractions of the lamp maximum power as discussed in Section

3.4.6.

4.4.6 Effect of Different Food Emissivities

In order to evaluate the effect of different food emissivities, the radiative heat flux at the food surface was calculated for maximum and minimum values of possible food emissivities, as shown in Figure 4.13 a. For foods al lower moisture contents, emissivities are well below 0.5 [3], reducing the radiative absorption at the food surface.

These calculations were made using the gray model in order to validate the need for a non-gray model, due to the differences found in the radiative flux at the food surface. If no major differences were found, there wouldn't be a need for the non-gray model in this problem. Figures 4.13 a and b show variation of radiative fluxes and temperature profiles for different food emissivities, in a gray model. The emissivity value of 0.88 is an weight average of the emissivities for the two bands, 0.64 and 0.96, as shown in table 3.1. The non-gray simulation is also shown in Figure 4.13 so that to check the overestimation of the gray model once more. Top surface food temperatures in the gray model were at least 14 % greater than the temperatures in the non-gray model, confirming the need to use the non-gray model in these calculations.

As can be seen in Figures 4.13 a and b, the reduction of 20% in the food emissivity value resulted in a decrease of 20 % in the highest top food surface temperature, as well in the radiative flux at the top food surface (a decrease of $\sim$ 20%), for infrared oven setting level X.

4.4.7 Effect of Different Wall Surface Emissivities

An example of changing the oven wall emissivities over the range of 0.05 - 0.1, on the food surface radiative flux can be seen in Figure 4.14 a. This emissivity range was chosen in function of the different stainless steel emissivities encountered in [14]. While the radiative fluxes at the food surface changed slightly ($\sim$ 2% variation), the temperatures at the food surface changed almost 10% (Figure 4.14 b). This shows that the radiative effect in this case is not predominant, which lead us to conclude that the diffusion effects had a higher impact on resulting food surface temperatures.

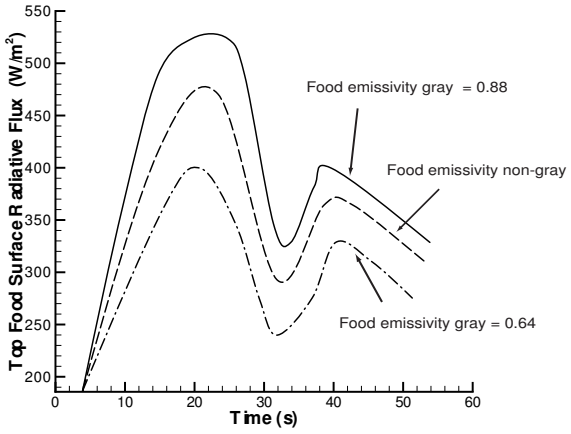

(a)

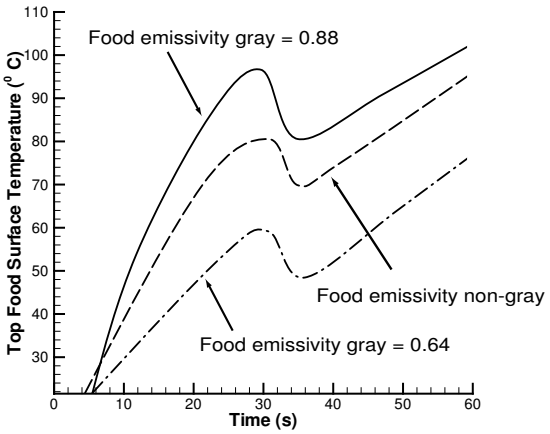

(b)

Figure 4.13: Computed radiative flux, (a), and temperature, (b), at the center of top food surface (Figure 4.1) for level X, using top lamp only - changing food emissivities.

4.4.8 Effect of Different Food Positions

The effect of having the food 2 inches higher in the oven increases the flux incident on the top food surface by 8.3%, as shown in Figure 4.15 a. The 6 and 8 cm positions from the bottom surface were chosen because these are rack positions available in most domestic ovens. The maximum temperature in the top food surface was calculated to be over 120^0C (Figure 4.15 b). At this temperature, some burning at the food surface could occur. As proposed in the hypotheses, the infrared heating is intensive, with possibilities of browning reactions occurring at the food surface due to temperatures over 100^0C in less than 1 minute of heating. This study could help oven manufacturers predict the best position for the racks inside the oven. Cooking time for different foods could be predicted, reducing the costs of try-and-error experimentation.

4.4.9 Effect of Changing Lamp Positions

The effect of having the top lamps located in a position away from the center on the radiative flux at the food surface was investigated by placing the top lamps skewed to the right, as shown in Figure 4.1. Food surface temperatures for a heat source of 10000 W/m^2 and after 5 s of heating are shown in Figure 4.16. Food lateral surface is seem to be cooler for the central location of the oven lamp (upper figure) as compared to when the lamp is located skewed to the right (lower figure). These results imply that a non-symmetric position of the lamp could have a significant detriment in the heating uniformity of the food inside the oven.

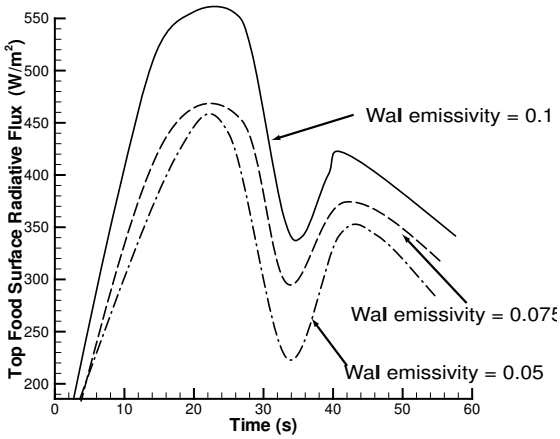

(a)

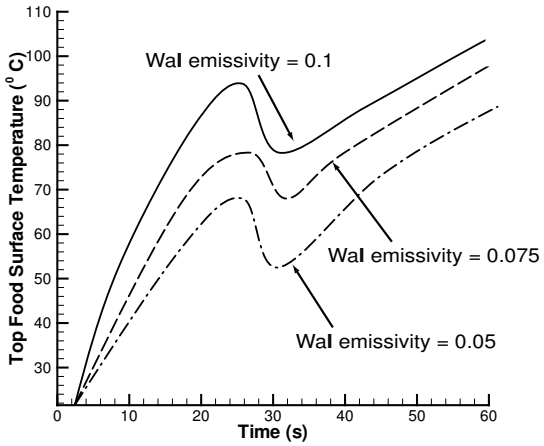

(b)

Figure 4.14: Computed radiative flux, (a), and temperature, (b), at the center of top food surface (Figure 4.1) for level X, using top lamp only - changing wall emissivities.

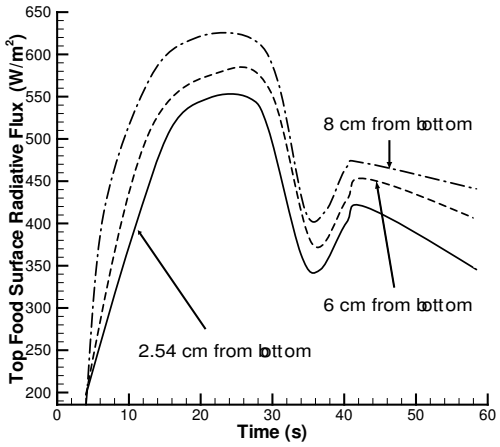

(a)

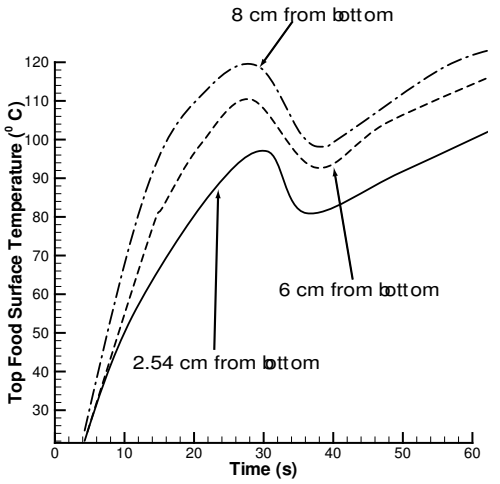

(b)

Figure 4.15: Computed radiative flux, (a), and temperature, (b), at the center of top food surface (Figure 4.1) for level X, using top lamp only - changing food position.

4.5 Conclusions

1. The enclosure radiative model is able to evaluate the radiative fluxes over a food surface inside an oven cavity.

2. The non-gray model of food emissivities is found to be more appropriate for the prediction of radiative heat fluxes than the gray model, which overestimated the radiative heat exchange in the system.

3. Lowering food emissivities (gray case) reduced the radiative flux delivered to the food surface and reduced the food surface temperatures.

4. Variation in oven wall emissivity in the range 0.05 - 1 has a small effect on the radiative fluxes delivered to the food, but a larger effect on food surface temperatures.

5. The geometric and spatial dependence of the radiative heat flux in an enclosure was confirmed by sensitivity analysis, changing both the oven lamp position and the food position inside the oven. Higher fluxes and temperatures were observed for more symmetric placement of the lamp.

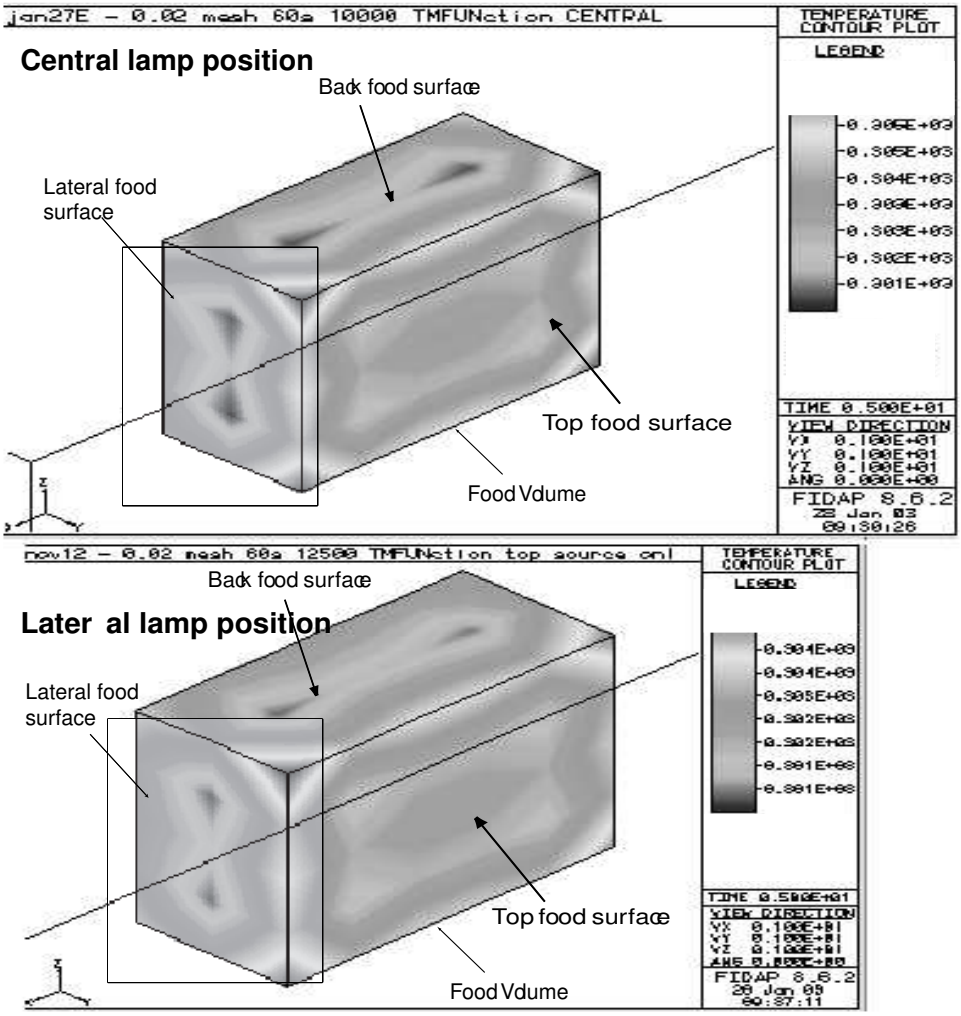

Figure 4.16: Temperature contour plots for the food, heated by central and skewed top lamp positions, showing the variation on heating pattern for the lateral food surface.

Chapter 5

COMBINED MICROWAVE AND INFRARED HEATING OF FOODS IN AN OVEN

Marialuci Frangipani Almeida and Srikanth S. Reddy Geedipalli.

List of Symbols

a	Length, m
$\mathbf{A}$	Vector potential , telsa meters
A_i	Area of surface i, m^2
$\mathbf{B}$	Magnetic flux density, V/m
c	Speed of light, 2.998 $\times 10^8$ m/s
c_p	Specific heat, $J/kg \cdot K$
dA	Differential of surface area, for the infrared model

$dF_{dA_i - dA_j}$	Differential view factor
ds	Differential of surface area
dV	Differential of volume
$\mathbf{D}$	Electric flux density , Coulombs/m^2
$\mathbf{E_m}$	Electric field intensity, V/m
$\mathbf{E}(\mathbf{r})$	Black body emissive power at the point $\mathbf{r}$, W/m^2
$F_{A_i - A_j}$	View factor
$\mathbf{G}(\mathbf{r})$	Irradiation onto a surface, in terms of the position vector $\mathbf{r}$, W/m^2
h	Planck's constant, 6.626 $\times 10^{-34}$ Js
h_c	Convective heat transfer coefficient, W/m$^2 \cdot$ K
h_m	m$^{1/2}$
$\mathbf{H}$	Magnetic field intensity , A/m
H	Height measurement, m
H_o	45 A/m
$\mathbf{J_m}$	Current density , A/m^3
$\mathbf{J}(\mathbf{r})$	Radiosity in terms of the position vector $\mathbf{r}$, W/m^2
k	Bolzmanns constant, 1.3806 $\times 10^{-23}$J/K
k_c	Thermal conductivity of solid (food), W/m $\cdot$ K
k_{air}	Thermal conductivity of the air, W/m $\cdot$ K
P	Power loss, W/m^3
P_{in}	Power input in any volume V_o, W/m^3
q_c	Convective heat flux, W/m^2
q_{gen}	Heat source for the energy equation W/m^3

q_r	Radiative heat flux, W/m^2
$\mathbf{r}$	Position vector
S	Surface area, m^2
t	Time, s
T	Temperature, K or C
V_o	Volume in the electromagnetic model, m^3
V	Scalar potential, Volts
x	x-direction of coordinates system
y	y-direction of coordinates system
z	z-direction of coordinates system

Greek Letters

$\alpha(\mathbf{r})$	Absorptance of surface at point $\mathbf{r}$
β_m	$1/m$
ϵ_m	Dielectric constant, $\epsilon_m = \epsilon_o(\epsilon^{'} - j\epsilon^{"})$,F/m
ϵ_o	Free space permittivity , 8.854×10^{-12} F/m
$\epsilon(\mathbf{r}\ )$	Emissivity in terms of the position vector $\mathbf{r}$
$\epsilon^{'}$	Dielectric constant , 50.5
$\epsilon^{"}$	Dielectric loss , 15.5
λ	Wavelength, m
λ^{th}	Referred to the "th" wavelength, m
μ	Permeability, $4\pi \times 10^{-7}$ H/m

ρ Reflectance

ρ_e Electric charge density, Coulombs/m^3

ρ_0 Density, kg/m^3

σ Stefan-Bolzmann's constant, 5.67 $\times 10^{-8} W/m^2 \cdot K^4$

σ_c Electric conductivity , S/m

ω Angular frequency , $2\pi \times 2.45$ GHz

5.1 Introduction

The enhancement of new appliances for food preparation with efficiency and better food quality with less time has demanded that the scientific society put a focus to study in a fundamental level the new heating methods that the appliance industry invented or developed. The overall quality of prepared foods depends on the different modes of heat exchange because of the dissimilar internal and surface properties of foods, resulting in different rates of crust formation and color development, among others. These properties vary as a function of convective or radiative heating. This was experimentally investigated by [7] and [32]. The innovation of using an infrared heating element in the same cavity as of the microwave heating generator dates back from 1970 [18] and have been developed since then. The main purpose of using infrared heating back there was to assist microwave heating in terms of reaching a more homogeneous temperature distribution on the target food and drying up the accumulated moisture due to the pressure driven moisture flow, hence, developing the desired color at the food surface [24]. Recently, though, new halogen lamps have being introduced in the appliances market as a heating source comparable to

microwave due to its penetrability properties, with the advantage of having a very homogeneous distribution. Some combination ovens, having the microwave as well the infrared heating elements are already available in the national market as well in Europe [30][11] [17].

5.2 Literature Studies Modeling of Combination Microwave and Infrared Heating

The modeling of combination heating has evolved from the modeling of the heating models alone, i.e, microwave heating and infrared (halogen) heating. Most of the references indicated the modeling for a different application then food. Zohm et al. [42], per example, studied the thermal processing of silicon wafers with microwave co-heating. Turner et al. [38], on the other hand, related a comprehensive numerical investigation of combined microwave and convective drying on pine wood. They used a self-developed code that included development of drying equations for porous media. For the microwave modeling, though, they used semi-analytic solution method. Microwave modeling of heating of liquids was investigated by Zhang et al. [41]. They used a Finite-Difference-Time-Domain for the simulation in a 3-D model.

For infrared modeling, numerical solutions have been developed in different fields of study, as in [12] [1]. The radiant thermal model is not common in the context of heating foods inside an oven. Infrared heating in terms of total flux at food surface is not found in the literature.

In Datta and Ni [8], a 1-D model was studied for infrared and hot air assisted microwave heating. Microwave power flux in this case was assumed as an exponential decay with varying penetration depth.

Nicolai et al. [25] studied the optimal control of microwave combination ovens for food heating, as part of a major project. They used an electromagnetic model uncoupled from the food heat model. They were able to obtain a qualitatively agreement between simulation and experiment in the case of a food gel placed inside the oven cavity, but no quantitative accomplishments were reported.

5.3 Objectives

1. The application of the electromagnetic model coupled with energy transfer in a food inside a 3-D cavity to predict the temperature distribution in the food

2. To validate the numerical simulation results through an experimental set up, using fiber optical probes for the temperature measurement.

5.4 Problem Formulation

The physical problem that will be considered is the combination of the infrared and microwave heat transfer inside an oven (a 3D enclosure) that has a halogen lamp at one or more of the inside surfaces , as well, a microwave generator with a wave guide finishing at one of the inside wall surfaces of the oven. A food material is placed inside the enclosure for the purpose of being heated (see Figure 5.1). The halogen

lamp emits radiation in the near infrared range of wavelength and the food surface radiative properties can vary with wavelength. The lamp is cycled on-off, according with the intensity level, set in a dial, with levels from 1 to 10. In the same way, microwave power can be chosen but independently. Heat flux over food and other surfaces will be computed from numerically solving the radiative exchange equation in the air and food (see Chapter 3). Separately, the electromagnetic field distribution inside the same cavity, governed by Maxwell's equations, is solved so that the power absorbed by the dielectric food placed inside the cavity can be calculated. Using the surface heat flux, calculated through the radiative heat transfer model, temperatures will then be computed in the food using the heat conduction equation with a source energy term, from the electromagnetic calculations.

5.4.1 Governing Equations, Boundary Conditions and Input Parameters for Microwave Heating

Maxwell's equations are solved for the entire cavity and can be seem from Equations 5.1 to 5.4.

$$\nabla \times \mathbf{E_m} = -\frac{\partial \mathbf{B}}{\partial t} \tag{5.1}$$

$$\nabla \times \mathbf{H} = \mathbf{J}_m + \frac{\partial \mathbf{D}}{\partial t} \tag{5.2}$$

$$\nabla \bullet \mathbf{D} = \rho_e \tag{5.3}$$

$$\nabla \bullet \mathbf{B} = 0 \tag{5.4}$$

where D is the electric flux density, ρ is the free charge density, E_m is the electric field intensity, B is the magnetic flux density, J_m is the current density and H is the magnetic field intensity.

The following three constitutive equations (equations 5.5 to 5.7) complete the set of required equations to solve for electric and magnetic fields.

$$\mathbf{D} = \epsilon_m \mathbf{E_m} \tag{5.5}$$

$$\mathbf{B} = \mu \mathbf{H} \tag{5.6}$$

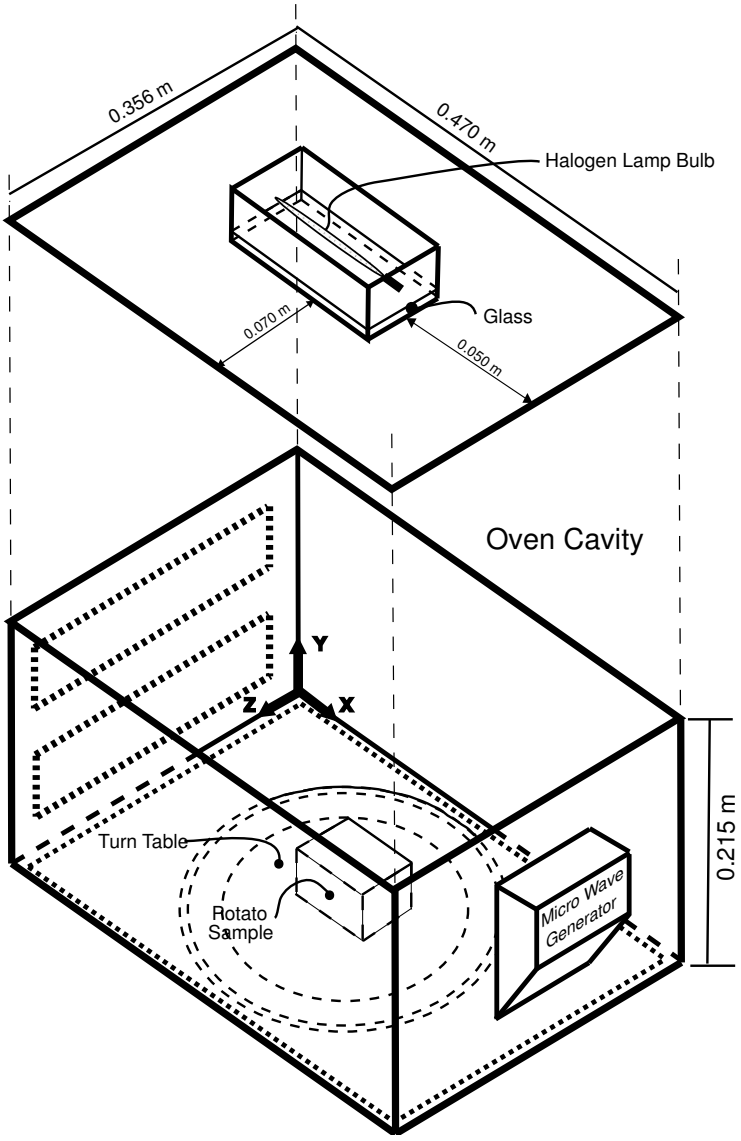

Figure 5.1: Schematic of the combination heating oven that includes microwave plus infrared (halogen) heating. The geometry of the oven is rectangular, of size 0.470 m $\times$ 0.356 m $\times$ 0.215 m. The food inside the oven is a potato slab of geometry 0.0470 m $\times$ 0.0356 m $\times$ 0.0215 m, with a total volume of 0.00003 m^3. Food is placed at 2.5 cm above the geometric center of the bottom surface in the oven.

$$\mathbf{J}_m = \sigma_c \mathbf{E_m} \tag{5.7}$$

Potential Functions

Equations 5.1 to 5.7 represent a complex system of equations and solving them in their original form is possible only for simple cases. Using a vector potential approach to reduce these equations makes it easier to solve them numerically, though.

If we define $\mathbf{A}$ to be the vector potential and V to be the scalar potential, Equations 5.6 and 5.7 can be written as following:

$$\mathbf{B} = \nabla \times \mathbf{A} \tag{5.8}$$

$$\mathbf{E_m} = -\nabla V - \frac{\partial \mathbf{A}}{\partial t} \tag{5.9}$$

Then, using a few basic vector identities, the governing equation for vector potential is written as Equation 5.10.

$$\nabla^2 \mathbf{A} - \mu \epsilon_m \frac{\partial^2 \mathbf{A}}{\partial t^2} = -\mu \mathbf{J}_m \tag{5.10}$$

The corresponding non-homogeneous wave equation for scalar potential is given as Equation 5.11.

$$\nabla^2 V - \mu \epsilon_m \frac{\partial^2 V}{\partial t^2} = -\frac{\rho_e}{\epsilon_m} \tag{5.11}$$

Equations 5.10 and 5.11 are solved using the commercial code ANSYS v.8 (Canonsburg, PA, U.S.A) and $\mathbf{B}$ and $\mathbf{E}_m$ are calculated from Equations 5.8 and 5.9.

Boundary Conditions

Boundary conditions at an interface of two media can be derived by applying the integral form of Maxwell's equations to a small region at the interface. For the case of a microwave cavity, boundary conditions need to be specified on the walls of the cavity which are considered to be perfect electrical conductors. Inside a perfect conductor, electric field is zero. Using this condition, together with the Maxwell's equation leads to boundary conditions on the air-wall interface, Equations 5.12 and 5.13.

$$E_{m,tangential} = 0 \tag{5.12}$$

$$B_{normal} = 0 \tag{5.13}$$

Equations 5.12 and 5.13 translated in terms of potential become Equations 5.14 and 5.15.

$$A_{tangential} = 0 \tag{5.14}$$

$$V = 0 \tag{5.15}$$

Excitation

The excitation for the microwave oven is through a horn waveguide. The shape of the waveguide is designed to transmit maximum possible power from the magnetron to the cavity.

From the shape of the antenna projected into the waveguide, it can be safely assumed that the electromagnetic field distribution can be approximated by TE10 mode. The transverse component of the electric field in TE10 mode can be given by 5.16.

$$\mathbf{E}_{m,y}(x,y,z;t) = \frac{\omega\mu}{h_m^2}\ (\frac{\pi}{a})\ H_o\ \sin(\frac{\pi x}{a})sin(\omega t - \beta_m z) \tag{5.16}$$

But due to the reflection of waves back from the cavity, Equation 5.16 may not represent the exact electric field distribution inside the waveguide.

Power Loss Calculation

Electromagnetic waves carry energy within themselves and this gets absorbed in the dielectric material. Power input in any volume V enclosed by surface S can be given by Equation 5.17.

$$P_{in} = \oint (\mathbf{E}_m \times \mathbf{H}) \cdot \text{ds} = -\frac{\partial}{\partial t}\int_V (1/2\,\epsilon_m \mathbf{E}_m^2 + 1/2\ \mu H^2)\,\text{dV} \tag{5.17}$$

Power absorbed by the dielectric food, then, can be written down in a simple form as in Equation 5.18.

$$P(x,t) = 1/2\,\omega\,\epsilon_o\,\epsilon^{"}_{eff}\,\mathbf{E}^2_m \tag{5.18}$$

Input Parameters

For electromagnetic modeling, input excitation was obtained by doing an experiment with water as a load as explained in [40]. The dielectric properties of potato are well documented and were taken from [40], as well. Since dielectric properties of potato do not vary a lot with temperature, constant properties were used. Test runs with changing dielectric properties validate the use of constant values. Same thermal properties of potato, as shown in Table 5.1, are used in the microwave simulation. The reader should look into [9] for the input data used for the electromagnetic simulation.

5.4.2 Governing Equations, Boundary Conditions and Input Parameters for Infrared Heat Exchange

The infrared (halogen) heating model can be seen in its entirety in Chapter 3. In here, only the main aspects of the simulation are going to be described in order to couple with the microwave model.

Assumptions for the Infrared Enclosure Model

The following are some of the major assumptions in developing the mathematical formulation:

1. All diffuse surfaces, no directional dependence: the small distance between surfaces and proportionality of oven surfaces and food validate this assumption;

2. Radiation dominant problem: the natural convection in the system is handled as surface convection;

3. Food is a solid conductive body inside the oven, but non transparent, i.e., opaque to thermal radiation.

Radiative Heat Transfer Equation

The radiative heat transfer equation is obtained by combining the radiative surface energy balance and Kirchoff's law. Writing it in terms of the position vector, $\mathbf{r}$, the total radiation impinging in the surface, *irradiation* $\mathbf{G}$ and *radiosity* $\mathbf{J}$, becomes:

$$J(\mathbf{r}) = \epsilon(\mathbf{r})E(\mathbf{r}) + \rho(\mathbf{r})G(\mathbf{r}) \tag{5.19}$$

In Equation 5.19, $E(\mathbf{r})$ is the total blackbody emission at the point $\mathbf{r}$ provided the temperature is known. It is given by the Stefan-Boltzman law.

$$E_T = \int_0^\infty \frac{2\pi hc^2}{\lambda^5(e^{\frac{hc}{\lambda kT}} - 1)}\,\mathrm{d}\lambda = \sigma T^4 \tag{5.20}$$

From the schematic of the enclosure, Figure 5.2,for an opaque surface, i.e., no energy passing through the object surface, the energy balance can be written as:

$$q_r(\mathbf{r}) = J(\mathbf{r}) - G(\mathbf{r}) = \epsilon(\mathbf{r})E(\mathbf{r}) - \alpha(\mathbf{r})G(\mathbf{r}) \tag{5.21}$$

Writing now the *irradiation* in terms of the total *radiosity* over the surface S, from the definition of the view factor, $F_{\mathrm{d}A'-\mathrm{dA}}$:

$$G(\mathbf{r})dA = \int_S J(\mathbf{r}')dF_{dA'-dA}dA' \tag{5.22}$$

Inserting Kirchhoff's law in Equation 5.21, solving for *radiosity*(J) and back in Equation 5.22 results in the following integral equation that relates temperature and heat flux at each location, $\mathbf{r}$, in the enclosure:

$$\frac{q_r(\mathbf{r})}{\epsilon(\mathbf{r})} - \int_S \left(\frac{1}{\epsilon(\mathbf{r}')} - 1\right) q_r(\mathbf{r}')dF_{dA-dA'} = E(\mathbf{r}) - \int_S E(\mathbf{r}')dF_{dA-dA'} \tag{5.23}$$

An assumption used to come to Equation 5.23 is that the radiosity is constant for a determined surface S. This assumption is relaxed later with the definition of macro-surfaces in the numerical implementation of the problem (see Section 3.4.2). Kirchhoff's Law, where food emissivity, ϵ, equals its absorptance, is considered valid although temperatures of the source and food are somewhat different [3]. The non-gray model has the emissivity in Equation 5.23 varying with wavelength. The two band approximation for absorptance shown in Figure 5.3 is used for food surface emissivity when it is considered non-gray.

Equation 5.23 provides the radiative heat flux, q_r, on a surface element at constant temperature (see Section 3.4.2) and it is used as a boundary condition over a surface for calculating heat conduction.

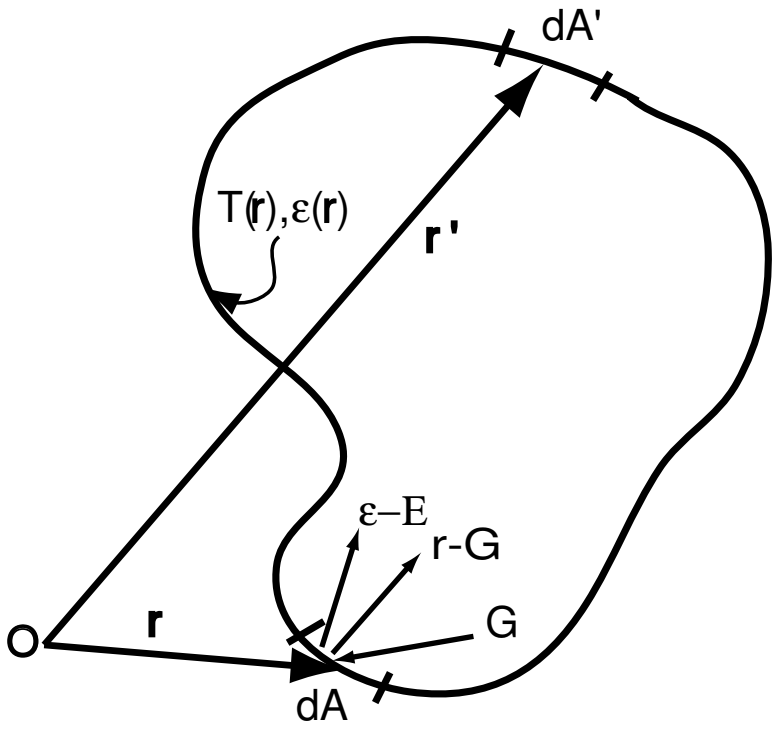

Figure 5.2: Radiative exchange in a gray diffuse enclosure and the principle of a surface energy balance, used in the infrared model.

Solution and Input Parameters

A transient analysis was performed for one minute of heating with cycling of the lamp sources. The mesh was developed using a finite element hexahedral unit. The density of the mesh varied along the cavity being denser around food and glass lamp cover surfaces (Figure 5.4 a). The time increment was constant throughout the simulation and its value was kept at 0.015 s. A small time increment was necessary.

See Table 5.1 for input properties for the infrared model. All properties were treated as constant and isotropic in both air and food. The oven has the inside dimensions of 0.470 m x 0.356 m x 0.215 m (Figure 5.1). All the inside surfaces, besides the lamp covers, are in stainless steel. The power level of both microwave and halogen (infrared) heating is set up through a mechanical dial in the oven control panel. The dial has a range form 1 to 10 both for microwave as well as for halogen (infrared) heating. There is a separate entry for adjusting the heating time staring from 15 s.

Oven capacity is 0.036 m^3 and the food volume is 0.0036 m^3 (Figure 5.1). The oven surface emissivities are taken as of stainless steel emissivity at 300 K. Lamp emissivities are set equal to values for tungsten filament.

Potato emissivity is set for two different values in a 2-band approximation for the non-gray problem and then set as 0.88, a weighted average value in the $0 - 2.5$, for the gray scenario (values are 0.67 for the 1.3 range and 0.96 for the range between 1.3and 2.5 wavelengths. See Section 2.5.4). Food sample is stationary, i.e, does not move during the experiment.

Table 5.1: Input Parameters

Air density	1.1614 kg/m^3	[3]
Air Specific Heat	1030.0 $J/kg \cdot K$	[3]
Air Thermal Conductivity	0.045 $W/m \cdot K$	[3]
Heat transfer convective coefficient	0.47 $W/m^2 \cdot K$	
Potato density	1000.0 kg/m^3	[36]
Potato Specific Heat	3900.0 $J/kg \cdot K$	[36]
Potato Thermal Conductivity	0.4 $W/m \cdot K$	[36]
Oven surfaces emissivity	0.1	[14]
Lamp surfaces emissivity	0.43	[14]
Potato emissivity(gray)	0.88	[3]
Potato emissivity(non-gray) $\leq$ 1350 nm	0.64	[2]
Potato emissivity(non-gray) $\geq$ 1350 nm	0.96	[2]
Source maximum output energy	75000 W/m^2	

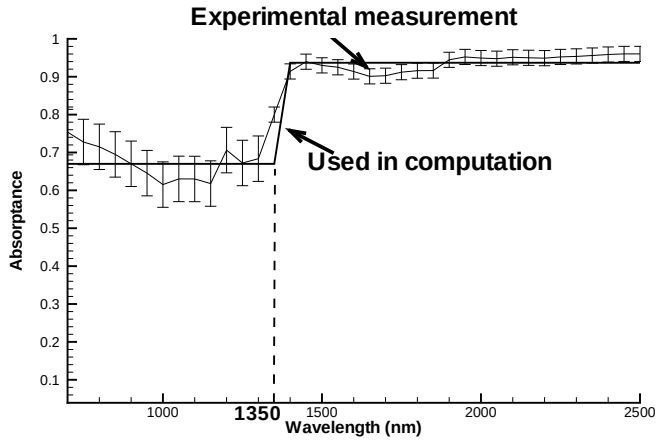

Figure 5.3: Spectral absorptance of potato used in the computation of infrared heating (see Section 2.5.4).

5.4.3 Governing Equations, Boundary Conditions and Input Parameters for Conduction Heating in the Food

The energy equation (Equation 5.24) is solved for the entire cavity (food and air), iteratively, calculating the radiative flux in a segment of the boundary of the air in the cavity, at each iteration that the temperature field is solved.

$$\rho_0 c_p \frac{\partial T}{\partial t} = k_c \nabla^2 T + q_{gen} \tag{5.24}$$

where q_{gen} is the power density, with units as J/m^3, calculated in Equation 5.18. Initial temperature is constant in the entire domain. Adiabatic walls formed the perfect diffuse enclosure. Radiant fluxes are assumed diffuse from halogen lamp, which is modelled from the bottom glass cover (see Figure 3.4). Radiant fluxes occur only between solid surfaces (source, walls and food). The air is non-absorbing (non-participating). Boundary conditions on all surfaces for the energy equation are as follows:

$$\underbrace{-k_c \left.\frac{\partial T}{\partial n}\right|_c}_{\substack{\text{conduction from} \\ \text{solid to surface}}} - \underbrace{\left(-k_{\text{air}} \left.\frac{\partial T}{\partial n}\right|_{\text{air}}\right)}_{\substack{\text{conduction from} \\ \text{surface to air}}} = -q_r + h_c(T_s - T_{\text{air}}) \tag{5.25}$$

where k_c is the thermal conductivity of solid (food), k_{air} is the thermal conductivity of the air, n is the outward normal direction to the food surface, T is temperature, T_s is the food surface temperature, T_{air} is the air temperature inside the oven, q_r is the net radiative flux absorbed by the food surface as calculated using the enclosure equation (Equation 3.5) and h_c is the convective heat transfer coefficient over the food surface.

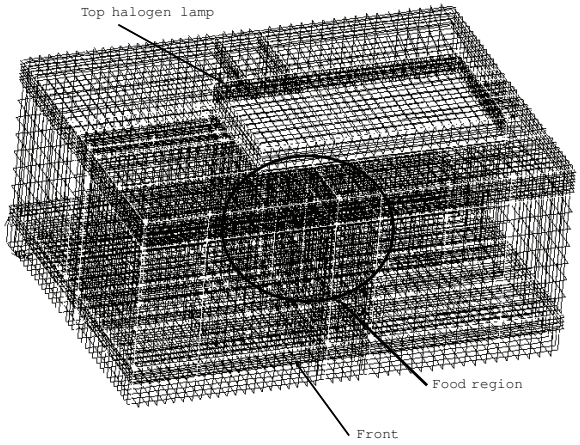

(a)

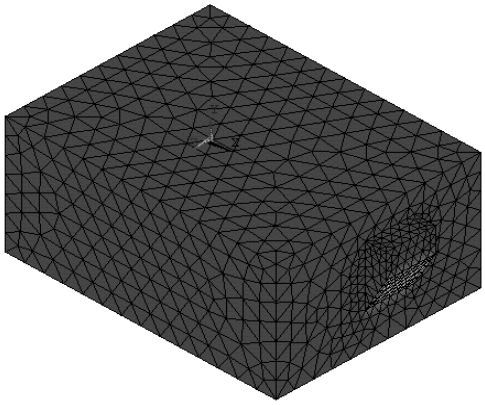

(b)

Figure 5.4: Finite element mesh used in the computation of infrared heating, with 50000 hexahedral elements for the oven system, (a); Finite element mesh used in the computation of electromagnetic field in the entire oven tetrahedral elements with 110000 nodes (b).

The two terms on the left side of equation 5.25 respectively represent conduction from within the food to the food surface, and from the food surface to the surrounding air. In general, these fluxes would fully account for the conduction heat transfer from the food to the surface, and the heat flux from the surface to the air (even if moving). However, since in this study we treat the air as quiescent (i.e., not moving), we do two things, both arbitrarily, to partially account for the effect of air movement or convection: first, to enhance conduction, we increase the value of thermal conductivity of air, k_{air}, in equation 5.25 by 70% and, second, we add a small additional heat transfer to the air via the heat transfer coefficient h_c on the right side of equation 5.25 (see Section 3.4.7 for further discussions).

The foregoing is further justified because the convective air flow is a short transient process. It is induced with the start of heating and then relaxes almost to zero when the radiant source is shut off. Thus, the induced convective air flow is expected to be very weak, and we essentially neglect it.

5.5 Methodology

5.5.1 Numerical Solution of the Electromagnetics and Heat Transfer Equations

The equations of electromagnetics (Equations 5.10 to 5.15) as well as the equation for infrared heat transfer (Equation 5.23) were solved numerically. For the electromagnetic equations, ANSYS v.8 (Canonsburg, PA, USA) finite element package was

used. Detailed convergence study led to the use of 110000 tetrahedral nodes for the entire cavity (Figure 5.4 b, with 386 tetrahedral elements in the food mesh, 30000 nodes) . For the radiative heating calculations FIDAP v.8 (Fluent Inc., Lebanon, NH, USA) finite element package was used, with 50000 hexahedral elements for the entire cavity and 360 elements for the food. Further details of the radiative calculations are provided in 3. Further details for the electromagnetics calculations can be found in [9].

5.5.2 Coupling of Electromagnetics and Heat Transfer Simulations

Coupling of microwave and infrared simulations were performed through linking the outputs of the two finite element packages mentioned above (Figure 5.5). Using constant dielectric property for the first cycle, the electromagnetic simulation is carried out. Heat generated values (J/m^3) are found for the food volume, using Equation 5.17, which are input in the thermal simulation using FIDAP, as heat sources in each gaussian point for the FIDAP elements (8 gaussian points in the case of hexahedral elements) (Section 5.4.3). A subroutine is used to load the heating source in the FIDAP model.

The infrared and microwave power cycling is as shown in Figure 5.6. Every 1 s the temperature field is entered in ANSYS to update the electromagnetic field, the output from which (heat generation values) is input to the FIDAP model.

5.5.3 Experimental Set-up

Temperature history of the top food surface was taken using a fiber optic system (Fiso Technologies - Quebec, Canada) (Figure 5.7) that recorded temperatures from the 4 probes every 1.5 s interval. Temperatures were recorded for two full infrared duty cycles of the oven in Level I settings, for the case of 1) infrared only, and 2) infrared coupled with microwave heating.

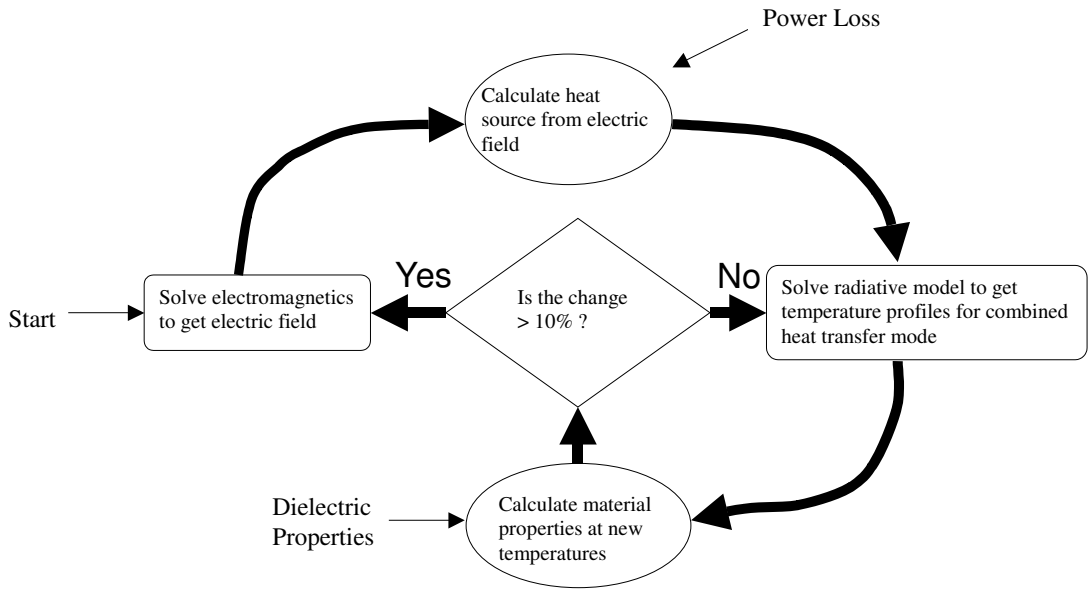

Figure 5.5: Flow chart showing the coupling of the electromagnetic and the heat transfer (including the infrared radiation) model.

5.6 Results

5.6.1 Experimental Results

Figures 5.8 a-c show experimentally measured transient temperatures at several locations during one minute of heating, infrared setting Level I and microwave power level 1.

As expected, combination of heating modes increases temperatures in the top food surface in general (maximum temperature of 31^0C for the combined mode compared to 28^0C for the infrared only heating). Surface temperature profiles for microwave only heating are quite different from infrared only heating. However, the combined heating shows profiles that appear quite similar to infrared only heating, thus leading to conclude that infrared heating will predominate the trend in surface temperature developments, at least for the power level combinations in these figures.

5.6.2 Experimental Validation of Model

Figure 5.9 a shows computed and experimental temperature values for the infrared only heating, for oven setting Level I. Figure 5.9 b compares the simulation and the experimental results for microwave only heating. Power level one of microwave is used which has the microwave power on from 3 to 6 seconds and 33 to 36 seconds for a "one minute cycle" (Figure 5.6). An exact match for such a complicated model is difficult to achieve. The measured values are also limited by the accuracy (+/- 1 ^{0}C) and reaction time (< 1.5s) of the fiber optic probes. Considering the limitations of the measurement and the model, the match between the experiment and the model

is very good.

Figure 5.9 c compares the computed and the experimental results for combination heating. Note that the plot is for a surface node, and hence there is a surge in the temperature because of infrared heating. Also note, the heating cycles of infrared and microwave overlap, with the infrared heating dominating the microwave heating. Therefore, the microwave cycling is not very obvious, though a closer look can confirm the presence of microwave heating. The effect of microwave heating is more obvious during the times when the infrared lamps are off. A significant reduction in the slope of the graph during the infrared off cycle can be observed when we compare the temperature history of combination heating to infrared only heating.

5.6.3 Uniformity of Infrared, Microwave and Combination Heating, Described Using Contour Plots

Figures 5.10 a-c show computed temperature contours at the food surface, for infrared oven setting level I and microwave power level 1. Food is placed horizontally in a plane one inch over the bottom plane in the center of the cavity (see Figure 5.1).

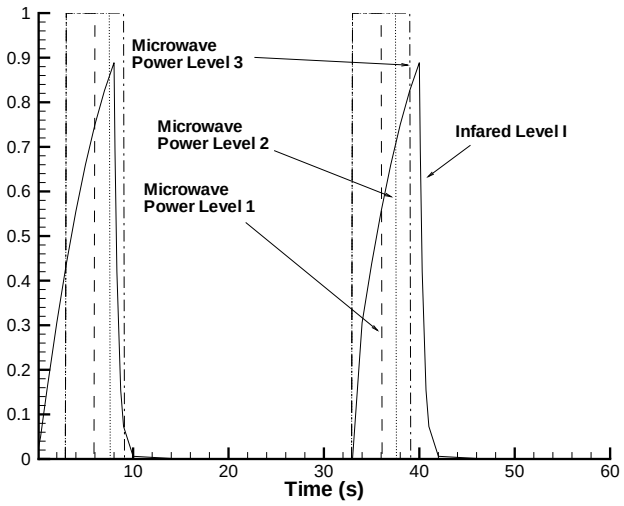

Figure 5.6: Cycling of infrared and different microwave power levels as used in this model.

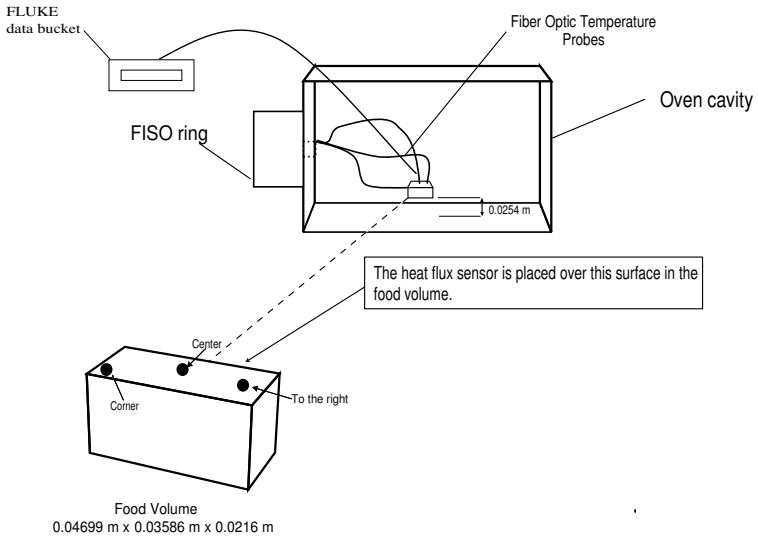

Figure 5.7: Schematic of data acquisition set up (temperature and flux) and probes location over the top food surface.

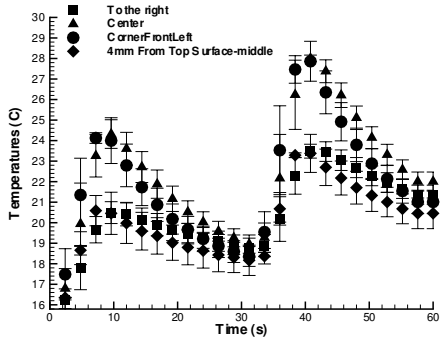

(a)

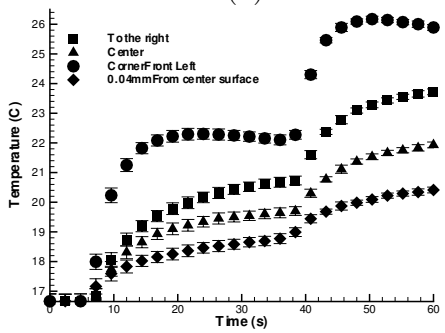

(b)

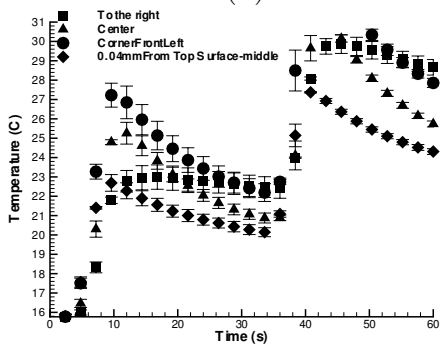

(c)

Figure 5.8: Experimentally measured temperatures at the top food surface for a) infrared only heating, b) microwave only heating , and c) combined infrared-microwave heating. Level I, intensity and power level, was used for both infrared and microwave.

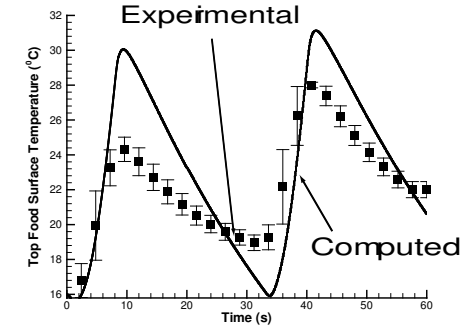

(a)

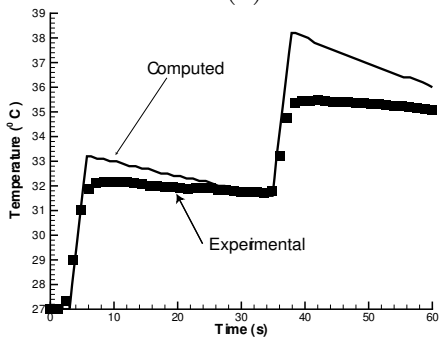

(b)

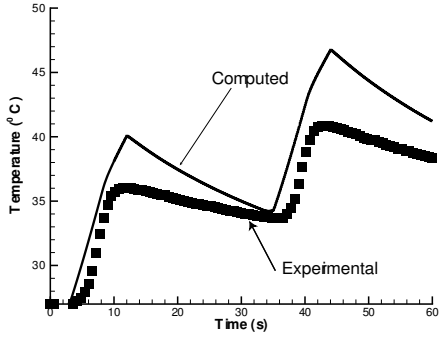

(c)

Figure 5.9: Temperature profile at the top central food surface (Figure 5.7) for a) infrared only, oven setting Level I heating, b) microwave only, power level 1 heating and c) combined microwave-infrared heating.

In the infrared (halogen) only heating (Figure 5.10 a), the result is a more homogeneous surface heating, if compared with the microwave only heating. Figure 5.10 b shows edge heating with more intense internal heating characteristics of microwave heating, with inside temperatures of the order of 35^0C (internal hot spots). Combined microwave and infrared heating (Figure 5.10 c) shows again more homogenous surface heating, moving the hot spot to the surface.

5.6.4 Statistical Analysis of the Uniformity of the Three Modes of Heating

Figures 5.11 a-f show temperature contours for combined heating at 7, 16.5, 33, 40, 47.5 and 60s, respectively.

As seen in these contour plots (Figures 5.11 a-f), infrared heating is limited by its lack of reasonable penetration and microwave heating is limited by the presence of hot and cold spots. The combination heating visually appears to be significantly better. A more scientific method to quantify this uniformity of heating is required to make any concrete conclusions.

The simplest measure of non-uniformity, the standard deviation, is a very good statistic to quantify the non-uniformity in temperature [40]. But standard deviation can sometimes get biased due to the presence of a few extreme data points, which can be expected in microwave heating. For cases where safety and quality are of primary importance, a better statistic for non-uniformity would be the range of temperature in the food material - the range being given by the difference of

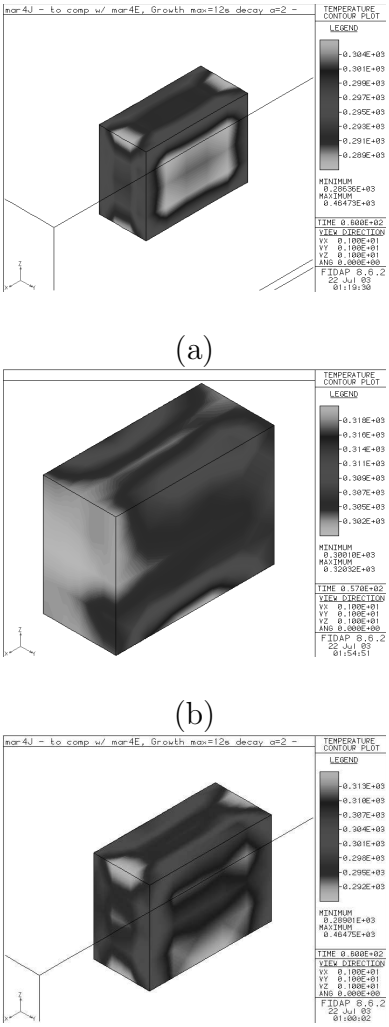

Figure 5.10: Computed temperature profiles showing the food surface for a) infrared oven setting Level I only, b) microwave power level 1 only and c) combined microwave power level 1 and infrared level I heating.

maximum and the minimum temperature in the food. Due to the presence of a few extreme temperatures from the simulation results, a smaller, but equally representative range not involving the extreme points should be considered. In this study, the difference between the 90-percentile value and the 10-percentile value is considered to give a good measure of non-uniformity.

Table 5.2 quantifies the non-uniformity in heating based on standard deviation. The first column has the mean temperature rise of the food volume in 60 seconds of heating. It can be seen that the mean temperature rise in combination heating is approximately the sum of infrared and microwave heating. This is expected based on the fact the both are independent modes of heating, and are additive, changing only the final temperature distribution. Comparing the standard deviation directly would make sense only if the mean temperature rise were the same for all the three cases. Combination heating is considerably faster, leading to higher variation in temperatures and hence the higher standard deviation. The standard deviation per unit rise in mean temperature (called the Coefficient of Variation, COV) gives us the true picture of non-uniformity. Table 5.2 shows that the COV value of combination heating is substantially lower for either infrared or microwave heating.

Table 5.2 shows also the non-uniformity quantified based on the range of temperature values. The difference between temperatures for the 90^{th} and 10^{th} percentiles is assumed to safely represent most of the food volume temperatures. This difference divided by the mean temperature rise accurately depicts the non-uniformity. Table 5.2 clearly shows the significant improvement obtained by using combination heating over either of the individual modes of heating. Figure 5.12 shows how the

mean and percentile values changes with time for microwave only and combination infrared-microwave heating. Clearly, combined heating has a lower range temperature differences between the 90^{th} and 10^{th} percentile, while showing a more intense heating with temperature values in the food almost 50 % higher than the stand alone heating modes.

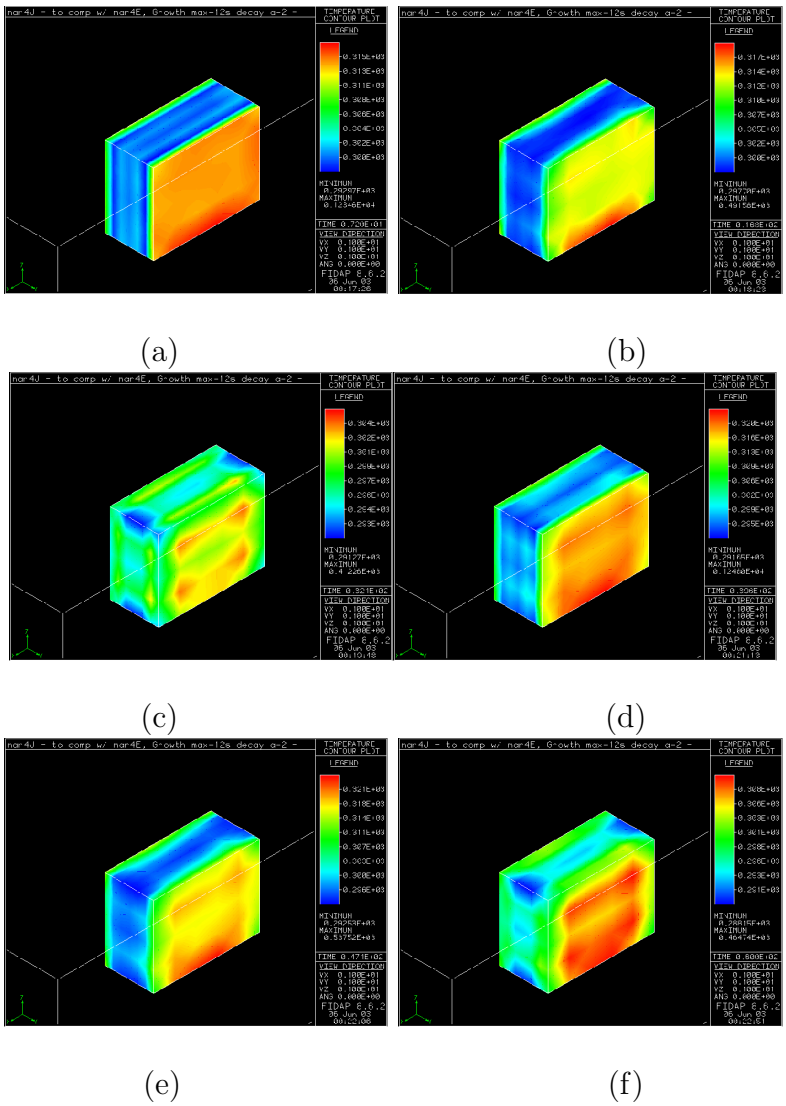

(a) (b)

(c) (d)

(e) (f)

Figure 5.11: Computed surface temperature contours, a-f, for combined microwave and infrared heating for level I at 7, 16.5, 33, 40, 47.5 and 60 seconds of heating, respectively.

Table 5.2: Non-uniformity in Temperature Distribution

COV, 90^{th} and 10^{th} percentiles - Infrared and Microwave Setting Level I

Heating Mode/Variable	IR Heating	MW Heating	Comb. Mode
Mean Temperature Rise	6.78	8.8	15.46
Standard Deviation	4.26	4.94	5.21
COV	0.6283	0.5614	0.337
10 Percentile	3.20	4.64	11.08
90 Percentile	10.36	12.96	19.84
Difference	7.16	8.32	8.76
Difference/Rise	1.0560	0.9454	0.5666

5.6.5 Effect of Different Microwave Power Levels on the Uniformity of Combination Heating

The objective of this research is to optimize the heating ability of the oven based on temperature uniformity and speed of cooking. The ultimate goal would be to optimize the heating ability of the oven based on factors like uniformity and speed of cooking. Tables 5.2 to 5.4 provide temperature data for infrared oven setting level I and microwave power levels 1, 2 and 3, for which cyclings are shown in Figure 5.6.

The data clearly shows that as the microwave power levels are increased, the heating is dominated by microwave power and the advantages of using combination-heating decrease. It should however be noted that the combination heating is still better than the individual modes.

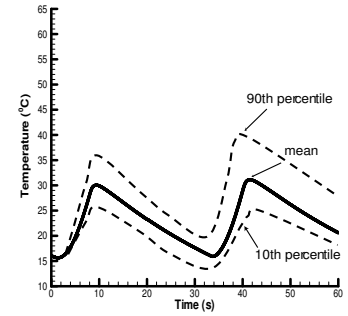

(a)

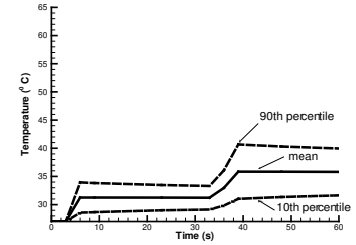

(b)

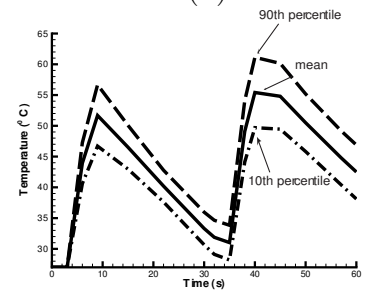

(c)

Figure 5.12: Computed temperature profiles, showing the 90^{th} and 10^{th} percentiles, for a) infrared only intensity level I, b) microwave only, power level 1 and c) combined microwave-infrared heating.

Table 5.3: Non-uniformity in Temperature Distribution

COV, 90^{th} and 10^{th} percentiles - Microwave Level 2

and Infrared setting Level I

Heating Mode/Variable	IR Heating	MW Heating	Comb. Mode
Mean Temperature Rise	6.78	19.46	26.10
Standard Deviation	4.26	11.09	12.59
COV	0.6283	0.5699	0.4824
10 Percentile	3.20	10.13	15.51
90 Percentile	10.36	28.76	36.69
Difference	7.16	18.66	21.18
Difference/Rise	1.0560	0.9589	0.8115

Table 5.4: Non-uniformity in Temperature Distribution

COV, 90^{th} and 10^{th} percentiles - Microwave Level 3

and Infrared setting Level I

Heating Mode/Variable	IR Heating	MW Heating	Comb. Mode
Mean Temperature Rise	6.78	29.30	35.22
Standard Deviation	4.26	16.50	18.92
COV	0.6283	0.5631	0.5372
10 Percentile	3.20	15.42	19.30
90 Percentile	10.36	43.18	51.14
Difference	7.16	27.76	31.84
Difference/Rise	1.0560	0.9474	0.9040

5.6.6 Manipulation of Surface Heating Using Combination Heating

A well-known drawback of microwave heating is its lack of providing surface browning on food materials. Higher temperatures are needed on the surface to achieve any amount of browning or crispness.

The surface heating capacity of infrared can be used with microwave heating to cause better surface texture for food items. Table 5.5 shows the mean temperature rise and the non-uniformity over the top surface of the potato sample. The surface

mean temperature is higher than the overall food temperature and the temperature distribution is considerably more uniform. By intelligently using higher infrared power levels and optimizing the power cycling of both the modes, a much better food product can be obtained in a substantially shorter time.

5.7 Conclusions

1. Combined microwave and radiative heating of food in an oven was modeled using coupled solution of the equations of electromagnetics, radiative exchange and conduction heating inside the food.

2. Using quantitative measures such as mean temperature rise and standard deviation, it was demonstrated that combination heating leads to more uniform heating, without compromising the speed of heating. These conclusions were validated using several combinations of microwave and infrared power levels.

3. Addition of infrared heating to microwaves was shown to improve the uniformity in surface temperatures besides increasing the temperature values.

Table 5.5: Non-uniformity in Temperature Distribution

COV and 90^{th} and 10^{th} percentile - Surface, Microwave power 1

and Infrared setting Level I

Heating Mode/Variable	IR Heating	MW Heating	Comb. Mode
Mean Temperature Rise	9.12	8.95	18.06
Standard Deviation	2.49	3.64	5.44
COV	0.273026	0.406704	0.301218
10 Percentile	7.02	5.89	13.48
90 Percentile	11.22	12.01	22.64
Difference	4.2	6.12	9.16
Difference/Rise	0.460526	0.683799	0.507198

Chapter 6

CONCLUSIONS

This thesis addressed the general problem of cooking food by electromagnetic waves in an oven. The heating was either by thermal radiation from radiant heaters in the roof of the oven, or by microwaves generated by a microwave generator in the oven. The two modes of heating can be separate or simultaneous.

The thesis was organized into three separate, but related, studies. Each study was written as an individual research paper, with its own introduction, problem description, results section, and discussion.

In the first study, entitled "Measurement of Optical Properties of Foods in Near and Mid-infrared Radiation", included as chapter 2, optical properties of reflectance, absorptance and transmittance in a potato tissue were measured as a function of wavelength, using a spectroradiometer.

Second study, "Radiative Heat Transport Modeling Inside an Oven: Problem Formulation and Experimental Set-up", included as chapter 3, developed a 3-D

radiative heat exchange model of an oven-food system, using a commercial finite-element package. The air in the oven was assumed transparent to the radiation. Heat conduction was assumed in the entire oven (food and air) for the short duration.

It was directly followed by the third study, "Radiative Heat Transport Modeling Inside an Oven: Effect of Oven and Food Parameters", included as chapter 4, where results for the model are shown. Wavelength dependence of emissivity (non-gray surface), food surface and oven wall emissivities effects are described.

Last study, "Combined Microwave and Infrared Heating of Foods in an Oven", included as chapter 5, was a joint effort with Srikanth S. Reddy Geedipalli. I was able to provide the experimental work and radiative model (using FIDAP software) for the chapter while Mr. Geedipalli worked on the electromagnetic model using ANSYS commercial software. We both worked on coupling both software for the results. This study is also part of Mr. Geedipalli's M.S. thesis. In this study, Maxwell's equations of electromagnetics were solved for the same cavity using separate finite element software and the volumetric heat generation in the food, obtained from this model, was input to the radiative heat transfer model, thus coupling them.

The final conclusions for the thesis are listed below, by chapters.

Conclusions for the study "Measurement of Optical Properties of Foods in Near and Mid-infrared Radiation", included as chapter 2, are:

1. Energy from halogen lamps, emitted in the near and mid-infrared range, has higher penetration depth and therefore heats more volumetrically, compared with energy from ceramic rods, that emit mostly in the far infrared range .

2. Reflectance in the near infrared range increases with moisture content, thus decreasing the energy coupled in the food.

3. Penetration depth of energy from halogen lamps is of the same order of magnitude as in microwave heating, although somewhat smaller. Penetration depth is also a strong function of moisture content and wavelength.

4. Surface structure of the food material has a significant effect on the radiation balance at the surface and this effect varies with moisture content.

Conclusions for both studies, "Radiative Heat Transport Modeling Inside an Oven: Problem Formulation and Experimental Set-up", included as chapter 3, and "Radiative Heat Transport Modeling Inside an Oven: Effect of Oven and Food Parameters", included as chapter 4, are:

1. The enclosure radiative model is able to evaluate the radiative fluxes over a food surface inside an oven cavity.

2. The non-gray model of food emissivities is found to be more appropriate for the prediction of radiative heat fluxes than the gray model, which overestimated the radiative heat exchange in the system.

3. Lowering food emissivities (gray case) reduced the radiative flux delivered to the food surface and reduced the food surface temperatures.

4. Variation in oven wall emissivity in the range 0.05 - 0.1 has a small effect on the radiative fluxes delivered to the food, but a larger effect on food surface temperatures.

5. The geometric and spatial dependence of the radiative heat flux in an enclosure was confirmed by sensitivity analysis, changing both the oven lamp position and the food position inside the oven. Higher fluxes and temperatures were observed for more symmetric placement of the lamp.

Conclusions for the study "Combined Microwave and Infrared Heating of Foods in an Oven", included as chapter 5, are:

1. Combined microwave and radiative heating of food in an oven was modeled using coupled solution of the equations of electromagnetics, radiative exchange and conduction heating inside the food.

2. Using quantitative measures such as mean temperature rise and standard deviation, it was demonstrated that combination heating leads to more uniform heating, without compromising the speed of heating. These conclusions were validated using several combinations of microwave and infrared power levels.

3. Addition of infrared heating to microwaves was shown to improve the uniformity in surface temperatures besides increasing the temperature values.

Appendix A

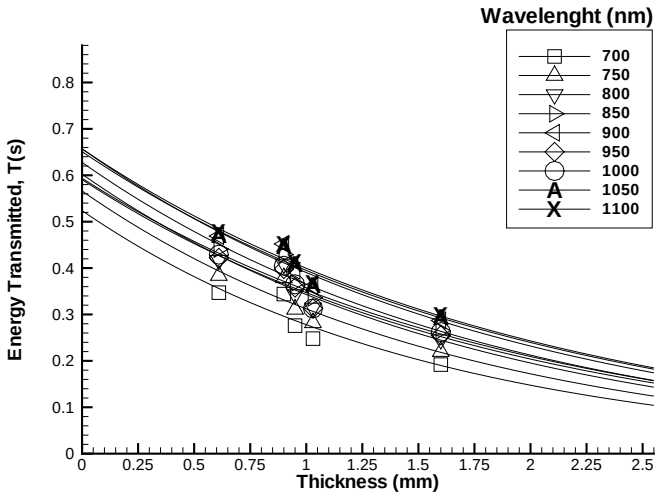

Figure A.1: Energy transmitted for various sample thicknesses of potato at 82 +/- 2% moisture content. Lines are fitted through data points.

Table A.1: Results from least square approximations: Penetration Depth (mm), T_0 and R^2 - 82 and 77% moisture content samples

Moisture Content	Wavelength(nm)	Delta (mm)	T_0	R^2
82	700	1.578532	0.5238	0.8618
82	750	1.678979	0.5662	0.8735
82	800	1.775884	0.6025	0.8885
82	850	1.845018	0.6278	0.9008
82	900	1.920492	0.6571	0.913
82	950	1.880053	0.5908	0.9085
82	1000	1.919017	0.5937	0.8846
82	1050	2.001601	0.6509	0.9222
82	1100	2.011263	0.657	0.9283
77	700	0.777847	0.5949	0.9962
77	750	0.777847	0.6224	0.9836
77	800	0.820743	0.6453	0.954
77	850	0.83682	0.6641	0.93
77	900	0.850991	0.6901	0.9032
77	950	0.776639	0.662	0.9402
77	1000	0.0772499	0.682	0.9423
77	1050	0.811754	0.7045	0.9218
77	1100	0.82559	0.7025	0.9112

Table A.2: Results from least square approximations: Penetration Depth (mm), T_0 and R^2- 72 and 70% moisture content samples

Moisture Content	Wavelength(nm)	Delta (mm)	T_0	R^2
72	700	0.401429	0.5864	0.8949
72	750	0.450268	0.5896	0.8851
72	800	0.488424	0.5977	0.8839
72	850	0.533675	0.5878	0.8693
72	900	0.583328	0.5848	0.8512
72	950	0.581226	0.5939	0.8574
72	1000	0.593648	0.6055	0.8469
72	1050	0.652018	0.61	0.8281
72	1100	0.674536	0.6038	0.8209
70	700	1.55159	0.7221	0.8551
70	750	1.093733	0.7221	0.8551
70	800	1.308044	0.768	0.9597
70	850	1.132375	0.726	0.9824
70	900	1.48368	0.6688	0.9781
70	950	1.36612	0.6493	0.9777
70	1000	1.251721	0.6353	0.9751
70	1050	1.129305	0.6111	0.9731
70	1100	1.02976	0.5751	0.9752

Table A.3: Results from least square approximations: Penetration Depth (mm), T_0 and R^2- 67% moisture content samples

Moisture Content	Wavelength(nm)	Delta (mm)	T_0	R^2
67	700	0.944109	0.2882	0.9345
67	750	1.09553	0.309	0.9239
67	800	1.241619	0.3239	0.9118
67	850	1.375327	0.332	0.8963
67	900	1.478852	0.348	0.8808
67	950	2.164502	0.321	0.861
67	1000	2.164034	0.3337	0.8413
67	1050	2.890173	0.341	0.7663
67	1100	3.207184	0.3407	0.7363

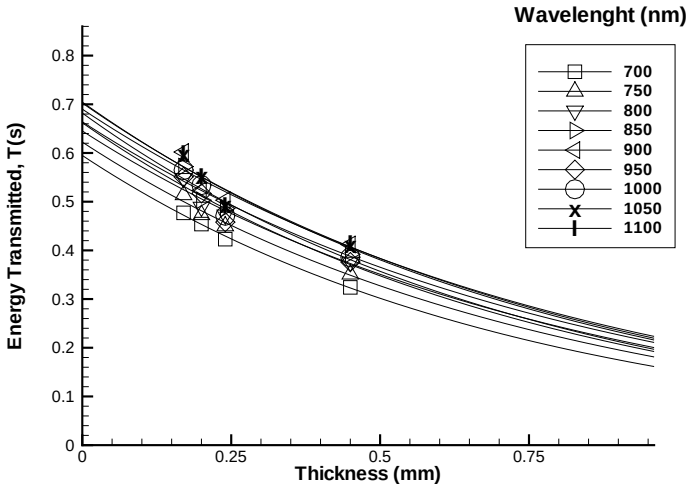

Figure A.2: Energy transmitted for various sample thicknesses of potato at 77 +/- 2% moisture content. Lines are fitted through data points.

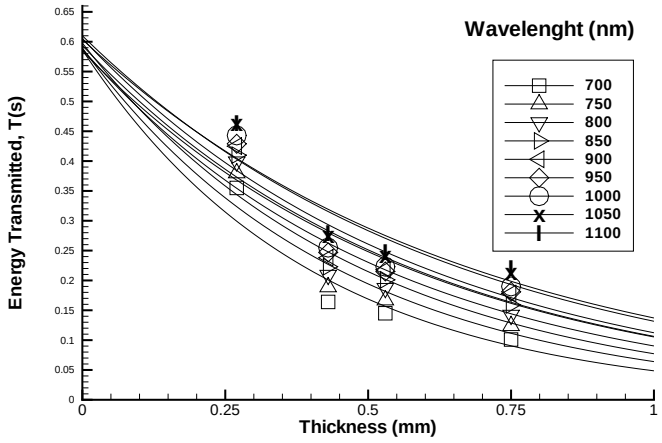

Figure A.3: Energy transmitted for various sample thicknesses of potato at 72 +/- 2% moisture content. Lines are fitted through data points.

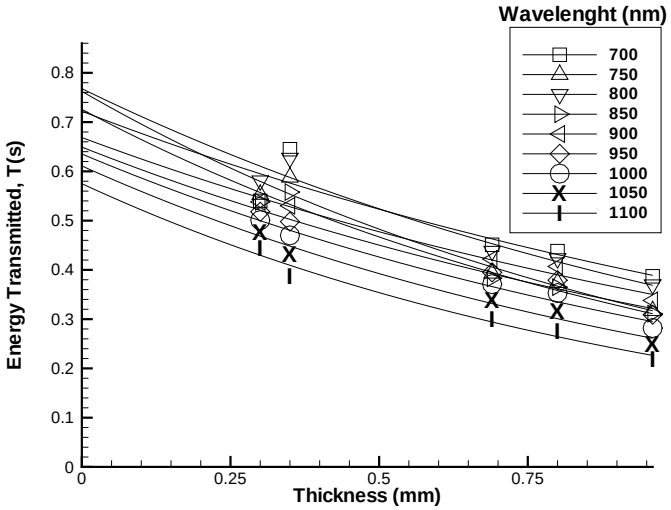

Figure A.4: Energy transmitted for various sample thicknesses of potato at 70 +/- 2% moisture content. Lines are fitted through data points.

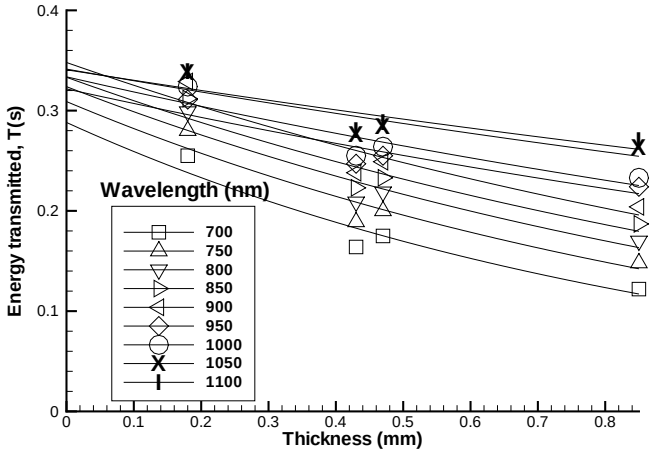

Figure A.5: Energy transmitted for various sample thicknesses of potato at 67 +/- 2% moisture content. Lines are fitted through data points.

Bibliography

[1] B.R. Adams and P.J. Smith. Three dimensionally discrete ordinates modeling of radiative transfer in a geometrically complex furnace. *Combustion science and Technology*, 88(5-6):293–308, 1993.

[2] M.F. Almeida. *Modeling Infrared and Combination Infrared-Microwave Heating of Foods in an Oven*. PhD thesis, Cornell University, 2004.

[3] A. Bejan. *Heat Transfer*. Number in . John Wiley Sons, Inc., , edition, 1993. .

[4] M.F. Cohen and D.P. Greenberg. The hemi-cube: A radiosity solution for complex environments. *Computer Graphics*, 19(3):31–40, 1985.

[5] S. Constantine. Infrared radiative drying in food engineering: a process analysis. *Biotechnology progress*, 2(3):109–119, 1986.

[6] M. Dagerskog and L. Osterstrom. Infra-red radiation for food processing i. a study of the fundamental properties of infra-red radiation. *Lebensmittel-Wissenschaft u. Technologie*, 12:237–242, 1979.

[7] M. Dagerskog and P. Sorenfors. A comparison between four different methods of frying meat patties. i. heat transfer, yield and crust formation. *Lebensmittel-Wissenschaft u. Technologie*, 11:306–311, 1978.

[8] A.K. Datta and H. Ni. Infrared and hot air assisted microwave heating of foods for control of surface moisture. *Journal of Food Engineering*, 51:355–364, 2002.

[9] Srikanth G. Marialuci A. Datta, AK. Novel combination heating ovens: numerical modeling and experimental validation. *ICEF 9*, 2004.

[10] Nicodeme P. Rickmans Y. Wouters P. Dupret, F. and M. Crochet. Global modeling of heat transfer in crystal growth furnaces. *Int. J. Heat Mass Transfer*, 33(9):1849 – 1871, 1990. .

[11] General Electric. Us6068146 radiant oven, January 2000. Inventors: Uzgiris, E.E.; Ackerman, J.F. and Lillquist, R.D.

[12] F.H.R. Franca, O.A. Ezekoye, and J.R. Howell. Inverse boundary design combining radiation and convection heat transfer. *Journal of Heat Transfer-Transactions of the ASME 2001*, 75:14–18, 2001.

[13] A.S. Ginzburg. *Application of Infra-red Radiation in Food Processing*. Leonard Hill Books, London, 1969.

[14] G.G. Gubareff, J.E. Janssen, and R.H. Torborg. *Thermal Radiation Properties Survey - a review of the literature*. Honeywell Research Center, 1960.

[15] T.J Hendricks and J.R. Howell. New radiative analysis approach for reticulated porous ceramics using discrete ordinates method. *Journal of Heat Transfer*, 118:911+, Nov 1996.

[16] S.G. Il'yasov and V.V. Krasnikov. *Physical Principles of Infrared Irradiation of Foods*. Hemisphere Pub. Corp., New York, 1 edition, 1991. edited by A.P. Kotlobye.

[17] LG Electronics Inc. Us6172347, microwave oven having halogen lamps, January 2001. Inventors: Lee, Kwan-Ho.

[18] Tecktron Inc. Us3591751 browning apparatus for microwave oven, July 1971. Inventor: Goltsos, Costas E.

[19] S.L.M. Junqueira and J.L. Lage. The fluid effect on the effective attenuation coefficient of a fully saturated porous medium under laser radiation. *Experimental Heat Transfer*, 12:157–174, 1999.

[20] Optronic Laboratories. A9:improving integrating sphere design for near-perfect cosine response. Internal Publication, Orlando, F:, USA, August 1995. .

[21] M.F. Modest. *Radiative Heat Transfer*. McGraw-Hill, New York, 1 edition, 1993.

[22] P. Navarri, J. Andrieu, and A. Gevaudan. Studies on infra-red and convective drying of non hygroscopic solids. *Drying 92*, pages 685–695, 1992.

[23] S.O. Nelson, Jr., W.R. Forbus, and K.C. Lawrence. Microwave permittivities of fresh fruit and vegetables from 0.2 to 20 ghz. *Transactions of theASAE*, 37(1):183–189, 1994.

[24] A.K. Ni, H.and Datta and K.E. Torrance. Moisture transport in intensive microwave heating of biomaterials: a multiphase porous media model. *International Journal of Heat and Mass Transfer*, 42:1501–1512, 1999.

[25] A.; Banga J.R.; Canto E.B.; Galt S.; Idebor M.; Phlsson T.; Saa J.; Sanchez I.; Scheerlinck N.; Sigter H.; Van Impe J.; Wappling-Raaholt B. Nicolai, B.M.; Alonso. Optimal control of micorwave combination ovens for food heating. *ASAE Meeting Presentation*.

[26] US Department of Energy web site. Energy savers - appliances. www.eere.energy.gov, 2003. Consulted by the author on February 10, 2003.

[27] K.T. Ojala and M.J. Lampinen. *Modeling, Measurements and Efficiencies of Infrared Dryers for Paper drying*, volume 2 of *Handbook of Industrial Drying*, pages 931– 976. Marcel Dekker, Inc., 1995. edited by Mujumbar, A.S.

[28] M. Peterson and S. Stenstrom. Modeling of an electric infrared heater at transient conditions- part i: model and validation. *International Journal of Heat and Mass Transfer*, 43:1209–1222, 2000.

[29] M. Petterson and S. Stenstrom. Absorption of infrared radiation and the radiation transfer mechanism in paper. part i: Theoretical model. *Journal of Pulp and Paper Science*, 24(11):349–355, 1998.

[30] Moulinex S.A. Us6002120 electric microwave oven with improved energy distribution, December 1999. Inventor:De Matteis, Michel.

[31] H. Sato, K. Hatae, and A. Shimada. Effect of heating system on the evaporation process of food: Radiation and convection. *Journal of the JApanese Society for Food Science and Technology - Nippon Shokuhin Kagaku Kogaku Kaishi*, 46(8):508–513, 1999.

[32] S. Shibukawa, K. Sugiyama, and T. Yano. Effect of heat transfer by radiation and convection on browning of cookies. *Journal of Food Science*, 54(3):621–624,699, 1989.

[33] R. Siegel and J.R. Howell. *Thermal Radiation and Heat Transfer*. Hemisphere Pub. Corp., Washington, 2 edition, 1981.

[34] C. Skjoldebrand and C. Andersson. A comparison of infrared bread baking and conventional baking. *Journal of Microwave Power and Electromagnetic Energy*, 24(2):70–75, 1989.

[35] E.M. Sparrow and J.P Abraham. Heat transfer coefficients and other performance parameters for variously positioned and supported thermal loads in ovens with/without water-filled or empty blockages. *International Journal of Heat and Mass Transfer*, 45:3597–3607, 2002.

[36] W.F. Talburt and O. Smith. *Potato Processing*. The Avi Publishing Co, Inc., 1959.

[37] Y.S. Touloukina. Thermophysical properties of matter; the tprc data series; a comprehensive compilation of data.

[38] J.R. Turner, I.W.; Puiggali and W. Jomaa. A numerical investigation of combined microwave and convective drying of a hygroscopic porous material: a

study based on pine wood. *Trans IChemE*, 76(part A):193–209, February 1998.

[39] H. Zhang. *Electromagnetic and Thermal Studies of Microwave processing of foods*. PhD thesis, Cornell University, 2000.

[40] H. Zhang and A.K. Datta. Coupled electromagnetics and heat transfer of microwave oven heating. *Journal of Microwave Power and Applied Energy*, 35(71), 2000.

[41] T.H. Zhang, Q.; jackson and A. Ungan. Numerical modeling of microwave induced natural convection. *International Journal of Heat and Mass Transfer*, 43:2141–2154, 2000.

[42] E.; Mehinger D. andMueller G.A. Zohm, H.; Kasper. Thermal processing of silicon wafers with microwave co-heating. *Microelectronic Engineering*, 54(3-4):247–253, Dec 2000.